Dynamics of Colloids in Polymer Solutions

Paul Michael Golz

Thesis submitted for the degree of Doctor of Philosophy

Department of Physics and Astronomy

University of Edinburgh

1999

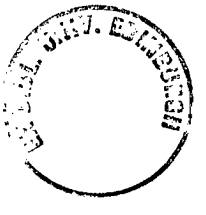

The soft overcomes the hard.
The slow overcomes the fast.
Let your workings remain a mystery.
Just show people the results.
LAO TSU

Abstract

The dynamics of a dilute suspension of colloids diffusing in a simple liquid are well understood and are characterised by the Stokes-Einstein equation. However the validity of this equation for describing diffusion through a polymer solution has been questioned. In this work on a well characterised model system, the motion of dilute poly(methylmethacrylate) spheres diffusing through a solution of flexible polystyrene polymers has been studied. Dynamic light scattering was used to measure the self-diffusion of the spheres and the diffusion coefficient for this motion was found to exhibit time dependence. At short times the colloid moves faster than expected from a simple 'polymer solution as a continuum' assumption whereas at longer times this assumption appears valid.

This behaviour can be explained within a Smoluchowski formulation in terms of the diffusional modes of the colloid-polymer mixture. At short times the dominant diffusional mode is of a colloid 'trapped' in a cage of polymers interacting only through hydrodynamics. At longer times the cage structure of the polymer relaxes and direct interactions between the species become significant. A hydrodynamic factor $H(Q)$ is defined as ratio of the short time diffusion coefficient of the colloids in a polymer solution D^S to its infinite dilution limit D_0^S. This quantity is compared to its value in a system of concentrated hard spheres and it is found that the hydrodynamic interaction for a colloid with polymers is less than with other colloids.

Solutions with polymer concentrations up to half the overlap concentration were investigated: the ratio of short to long time diffusion D^S/D^L was found to increase with the concentration. The effect of changing the quality of the solvent from theta to good was also investigated and no qualitative difference was found between the two.

In these experiments it was found that the effect of scattering from the polymer was more significant than originally expected. In particular, the presence of *cross scattering*, in which the electric field scattered from the colloid is correlated with that from the polymer, can be as high as 30%, despite the polymer scattering being only a few percent. A method for calculating, and measuring, the magnitude of the cross scattering has been described, and an experimental methodology proposed that obtains only the scattering from the colloids.

Acknowledgements

I wish to thank all the people who have helped and supported me during the writing of this thesis. On the academic side, none of this work would have been possible without the advice, support and seemingly endless patience of Peter Pusey - one day I'll plot a graph in the way he would like. I would also like to extend my gratitude to Wilson Poon who, despite his self-admitted ignorance of light scattering, has managed to provide guidance over the course of this work. I have also profited from many useful conversations and collaborations with others, both at Edinburgh and elsewhere. I am indebted to the EPSRC for funding both me and my project for three years.

On a personal front I would like to thank all my friends in Edinburgh for enduring my endless attempts to conquer the world, solve crosswords and run a martial arts club. Your help in all of these was appreciated. I am also very much indebted to endless phone calls, emails and visits from my friends in both Durham and Canada.

Needless to say, I am eternally grateful to my family for the enduring support and pride they have shown me over the past three years.

This thesis is dedicated to Claire, an uke goshi in a world of hiza gurumas:
'You gave me hope when hope was gone, you gave me strength to carry on.'

Contents

List of Figures

List of Tables

Notation

The following symbols and abbreviations occur frequently throughout this work. For symbols taking more than one meaning, or that appear in the text with subscripts, the exact meaning will be made clear in the adjacent text.

Abbreviations

PMMA	Poly(methylmethacrylate)
PHSA	Poly-12-hydroxystearic acid
decalin	Decahydronapthalene
tetralin	Tetrahydronapthalene
PBD	Poly(butadiene)
DMF	N,N-dimethylformamide
PIP	Poly(isoprene)
HPC	(Hydroxypropyl)cellulose
PVME	Poly(vinylmethylether)
SLS	Static Light Scattering
DLS	Dynamic Light Scattering
TCDLS	Two Colour Dynamic Light Scattering
PMT	Photomultiplier Tube
PAD	Pulse Amplifier Discriminator
TTL	Transistor-transistor logic
AMU	Atomic mass units

Sample Properties

η	Viscosity
$[\eta]$	Intrinsic viscosity
ρ	Density
m, M	Mass
n	Refractive index
ε	Dielectric constant
R, R_c	Colloid particle radius
σ_c	Colloid particle diameter
ϕ, ϕ_c	Colloid volume fraction
v_c	Colloid volume
R_g	Polymer radius of gyration
M_w	Weight averaged polymer molecular weight
c, c_p	Polymer concentration
c^*	Polymer overlap concentration
ϕ_p	Polymer concentration normalised by c^*
T_θ	Polymer-solvent theta temperature
ξ	Colloid-polymer size ratio
α	Free volume fraction
D	Diffusion coefficient
D_0	Diffusion coefficient for free diffusion
D^L	Long time diffusion coefficient
D^S	Short time diffusion coefficient
ΔD	Change in diffusion coefficient
M	Mobility constant
ξ	Friction coefficient
τ	Timescale

Thermodynamic Quantities

E,ε	Energy
U	Potential Energy
K	Interfacial energy parameter
F	Helmholtz free energy
f	Helmholtz free energy density
Ω	Grand potential
Z	Canonical partition function
Ξ	Semi-grand partition function
T	Temperature
β	Thermal energy
λ_T	Thermal length
P	Pressure
Π	Osmotic Pressure
V	Volume
μ	Chemical potential
a_p	Polymer activity
N	Number of particles
ρ	Number density of particles

Statistical Quantities

$P(x)$	Probability of being in state x
$P(x \mid y)$	Conditional probability of being in state x given condition y
$f(\ldots)$	Probability density
$g(r)$	Radial distribution function
$h(r)$	Total correlation function
$c(r)$	Direct correlation function

Light Scattering

λ	Wavelength
$\mathbf{k}$	Wavevector
θ	Scattering angle
$\boldsymbol{Q}$	Scattering vector
Q	Scattering vector amplitude
$\mathbf{E}$	Electric field strength
I	Intensity
$P(Q)$	Particle form factor
$b(Q)$	Scattering amplitude
$S(Q)$	Structure factor
$H(Q)$	Hydrodynamic factor
$< \ldots >$	Ensemble average
τ	Decay time
r	Centre of mass position
$g^{(2)}(Q,\tau)$	Intensity correlation function
$f(Q,\tau)$	Dynamic structure factor
β	Correlation factor
n	Count rate
Γ	Decay constant
μ_n	n'th moment of the decay constant

Fundamental constants and functions[1]

$N_A = 6.022 \times 10^{23}\text{mol}^{-1}$	Avogadro's constant
$k_B = 1.380 \times 10^{-23} JK^{-1}$	Boltzmann's constant
$h = 6.626 \times 10^{-34} Js$	Planck's constant
$g = 9.807 ms^{-2}$	Acceleration due to gravity
$\pi = 3.142$	Pi
$e = 2.718$	Exponential constant
∞	Infinity
$\delta(\ldots)$	Delta function

[1]Values from National Institute of Standards and Technology, U.S.

Chapter 1

Introduction

One of the basic assumptions in the calculation of many of the *static* properties of colloid-polymer mixtures is the 'polymer solution as a continuum' assumption, in which the degrees of freedom of the polymer are integrated out and replaced with some mean field property, e.g. an osmotic pressure [1]. In a calculation of the *dynamic* properties of colloids in polymer solutions, this approximation would replace the degrees of freedom of the polymers by a macroscopic viscosity. The colloids would then diffuse through a continuum with a viscosity equal to that of the polymer solution. The accuracy of this model has been investigated experimentally [2–14], and its validity challenged. There are reports of the colloid diffusing faster than expected [10, 13, 14], slower than expected [9–12], and even some polymer-concentration-dependent behaviour [5].

The aim of this work was to investigate the dynamics of colloids suspended in a polymer solution. Of particular interest is the accuracy of the 'polymer solution as a continuum' assumption for describing these dynamics. Should this assumption fail, it was my aim to provide an alternative model. Apart from the intrinsic interest in verifying the accuracy of a well established model of diffusion when two macroscopic species are present instead of one, this model can be regarded as fundamental in several other aspects. The Asakura Oosawa model [15] treats

the colloids as hard spheres and the polymers as freely interpenetrable coils. The centre of the polymer coil is, however, excluded from a region around the colloid. If we define the interaction radius ρ_α for these species as the separation at which the inter-coil potential becomes infinite, then for the polymer-polymer inter-coil potential $\rho_p = 0$, for the colloid-colloid inter-particle potential $\rho_c = 2R_c$, where R_c is the radius of the colloids, and for the colloid-polymer particle-coil potential $\rho_x = (R_c + R_p)$ where R_p is the radius of gyration of the polymers. This system is therefore an example of a *non-additive hard sphere* mixture, defined as

$$\rho_{12} \neq \frac{\rho_{11} + \rho_{22}}{2} \tag{1.1}$$

Self-diffusion has been measured in a concentrated system of colloids, which is essentially a special case of tracer diffusion through an additive hard sphere mixture, and a model proposed to explain the observed behaviour [16]. It is interesting to see how well this model works when a significant amount of non-additivity is introduced to the system.

Colloid-polymer mixtures are known to show a wide range of phase behaviour [1]. There is currently considerable interest in the dynamics of both the phases and phase transitions for colloid-polymer mixtures [17,18]. This study focuses on the colloid dynamics in the simplest phase and may well provide a basis for models of these more complex systems.

In this chapter I will provide a brief reminder of the colloid and polymer state and introduce the specific system under study.

1.1 Colloids

A colloidal suspension is a dispersion of microscopic particles in a liquid [19]. These particles may be regarded as colloids if they have radii, R, in the range $1nm < R < 500nm$, though these are not absolute limits [20]. The lower limit

comes from the requirement that the particles are significantly larger than the molecules of the suspending medium and the upper limit from the requirement that the particles' Brownian motion can keep them in suspension against gravity. This definition means that the colloidal suspension is in essence a thermodynamic system [21]. The typical relaxation time for a fluid material τ_R may be considered as the time taken for a particle in that fluid to diffuse its own radius .

$$\tau_R \approx \frac{R^2}{D} \tag{1.2}$$

where D is an appropriate self-diffusion coefficient of a particle. For the suspending medium this is typically of the order of $10^{-11}s$ whereas for the suspended particles (often just called 'the colloid') it is typically $10^{-2}s$ [20]. Thus the suspending medium may be considered a continuum for all measurements on the colloidal timescale.

1.2 Polymers

A polymer is a large number of chemically-bonded units (known as monomers) which do not dissociate under experimental conditions. The links between the monomers are covalent and commonly these monomers are organic and identical (*homopolymers*). A polymer molecule is formed when the condition required to add one monomeric unit to a system is almost independent of its size. If one has a polymer consisting of n monomeric units of (A), then the energy required to go from $(A)_n \rightarrow (A)_{n+1}$ is the same as the energy required to go from $(A)_{n+1} \rightarrow (A)_{n+2}$ [22]. This criterion leads to polymers consisting of at least several hundred, but more commonly several thousand, monomeric units.

In this work the only types of polymers considered are *linear polymers*, which have a carbon backbone and consist of a long single chain of mononmers. When placed in solution, the segments along the polymer chain can come into close proximity to

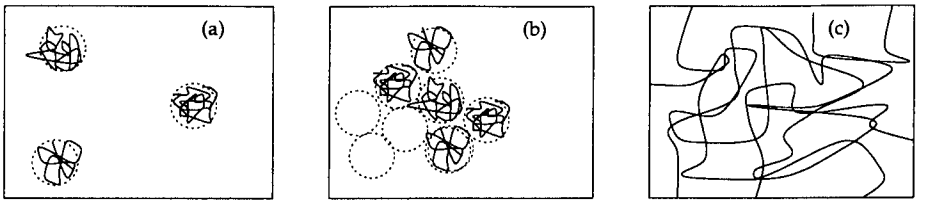

Figure 1.1: The topolgy of the three different concentration regimes for a polymer solution: (a) shows the dilute regime in which the polymers coils do not touch, (b) the overlap regime where the coils fill all space and (c) shows the semi-dilute regime in which there is significant overlap between polymers.

other segments further along the chain. The solvent mediated interaction of these segments controls the spatial size of the polymer coil [22]. For example, if it is energetically unfavourable for the polymer segments to be near each other, the coil swells and becomes highly solvated (a typical coil contains a large volume fraction of solvent). This solvent mediated segment-segment interaction is temperature dependent and the size of the coil changes as the solvent temperature changes. At a certain temperature, known as the theta temperature, the attractive and repulsive forces between segments cancel and the coil can be described by a simple (non-self avoiding) random walk. Solvents for polymers are therefore classified into 'good', 'theta' and 'poor' [22].

As the concentration of a polymer solution is increased from zero, three different concentration regimes are seen: dilute, overlap and semi-dilute [23]. Figure 1.1 shows the topology of these regimes in more detail. The dilute regime refers to a system in which the polymer coils do not overlap, each polymer occupying a spherical region of radius R_g. In this regime the polymer-polymer interaction is minimal. As the concentration increases further, at some *overlap concentration* c^* the polymer fills all available space. This occurs at roughly

$$c^* = \frac{3M_W}{4N_A\pi R_g^3}\,, \tag{1.3}$$

where M_W is the molecular weight, R_g the radius of gyration and N_A Avogadro's number. At even higher concentrations, individual polymer segments from dif-

ferent chains come into close proximity and it is no longer sensible to refer to a particular polymer coil.

1.3 Our system

Poly(methylmethacrylate) spheres in either *cis*-decalin or *trans*-decalin and linear polystyrene form a well established model system on which much work has been performed [20].

1.3.1 The colloid

PMMA spheres are well known in the field of colloid physics and are widely used in the research carried out at the University of Edinburgh and elsewhere. These spheres consist of an essentially solid core of poly(methylmethacrylate) with a mono-layer of poly-12-hydroxystearic acid (PHSA) grafted to the surface [24] (see figure 1.2). Typically this grafted layer is of the order of 10-15nm thick with

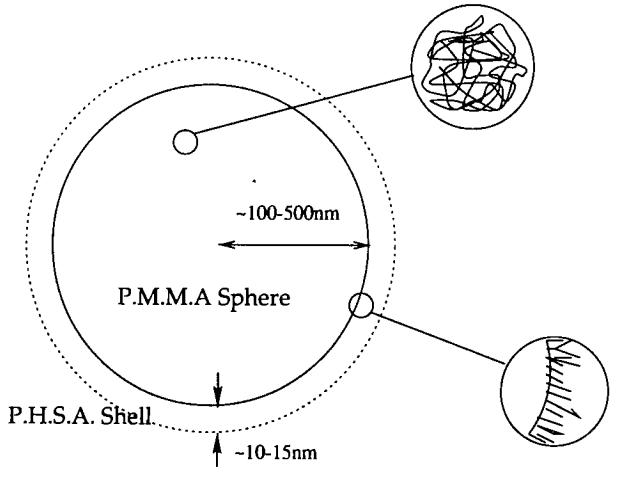

Figure 1.2: Schematic of colloidal sphere. The PMMA core is highly coiled and the PHSA brush is at a higher density than shown, covering nearly 100% of the surface.

a very high surface coverage (approaching 100%). The particles are suspended in any of *cis*-decalin, *trans*-decalin, or dodecane. These liquids are poor solvents for the PMMA which ensures low solvation of the core (see section 1.2), but good solvents for PHSA hairs which therefore adopt an extended structure. As two spheres are brought together, the PHSA layers either interpenetrate or compress. Both interpenetration and compression of the hairs are highly thermodynamically unfavourable and the result is an almost hard sphere interparticle potential [25].

The exact form of the inter particle repulsion has not been measured precisely, but preliminary work by Cairns *et al.* [26] indicated that it is strong and short ranged. Segrè *et al.* [16] performed measurements on the diffusion of these spheres, the property of the most relevance to the work presented here, and found that the short-time diffusion coefficient as a function of volume fraction agreed very well with both theory and simulation for hard spheres. Several other authors [27, 28] have considered the problem using different approaches and so far there is no evidence for any other than hard-sphere behaviour.

Light scattering is a useful tool for the study of colloidal properties. While there have been significant advances in obtaining useful data from multiply scattering systems, for the majority of techniques discussed in this thesis it is useful for the refractive index difference between the particles and solvent to be small. Table 1.1 gives the refractive indices of the more common used materials found in this work.

1.3.2 The polymer

The polymer used is linear polystyrene of high molecular weight (of the order of millions of atomic mass units) which does not interact chemically with either PMMA or PHSA. The concentrations investigated were below the overlap concentration, though this was more governed by the presence of phase boundaries than through any deliberate decision. If we define the size ratio (ξ) of the system

Species	Refractive Index
PMMA	1.484 (a)
PHSA	1.51 (b)
Particles	1.495 – 1.505 (c)
polystyrene	1.59 – 1.60 (a)
cis-decalin	1.481 (d)
trans-decalin	1.4695 (d)
tetralin	1.5413 (d)
dodecane	1.4216 (d)

Table 1.1: Refractive indices of polymers and solvents. (a) indicates that the measurement was made at $25°C$ at a wavelength of $589nm$ [29], (b) indicates the measurement was made by myself using a Abbe refractometer at $25°C$, (c) indicates the value was found by myself by refractive index matching and (d) indicates the measurement was made with the d-band of sodium light at a temperature of $25°C$ [30].

as the ratio of polymer radius of gyration to colloid radius, then all experiments were performed around $\xi = 0.3$. This ratio was chosen to allow for easy detection of the effect of the polymer relaxation on the dynamics of the colloid:

$$\frac{\tau_R^p}{\tau_R^c} \sim \xi^3 . \tag{1.4}$$

The polymer relaxes roughly two orders of magnitude faster than the colloid - a timescale easily accessible by dynamic light scattering.

1.4 Colloid-polymer mixtures

The addition of enough free polymer to an otherwise stable colloidal suspension causes phase separation. The earliest explanation for this phase separation was due to Asakura and Oosawa [15], who treated the colloids as hard spheres and the polymers as freely interpenetrable coils. The centre of the polymer coil is,

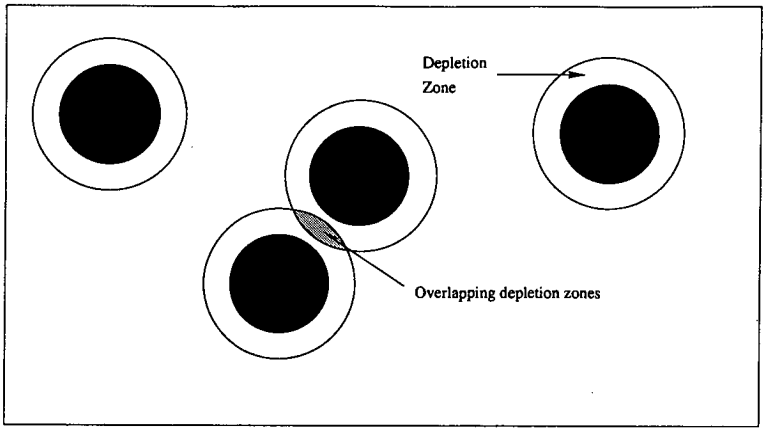

Figure 1.3: Polymers are excluded from a region around the colloid. When two of these regions overlap there is an unbalanced osmotic pressure on the colloids resulting in a net attraction between them.

however, excluded from a region around the colloid (the depletion zone). If, through thermal motions, two depletion zones overlap then the *free volume* (volume accessible to the polymers) increases as does the entropy of the polymers (see figure 1.3). At high concentrations of either component this effect leads to phase separation into colloid rich and colloid poor phases. A colloid-polymer mixture may therefore show 'crystal', 'liquid'-like or 'gas'-like phases [1]. If too much polymer is added then the strong forces between the colloids result in a temporary non-equilibrium structure known as a gel [31].

1.5 Evolution of work

For clarity, the layout of this thesis does not follow a historical route. In particular, much time was spent attempting to overcome the problems associated with *cross-scattering*, which can lead to spurious results in light scattering experiments. While I have discussed some of the routes taken to overcome these problems, the majority of the experimental chapter is concerned with the methodology and results of the final set of experiments in which cross-scattering had been minimised.

In this section I will give a brief, historically accurate, perspective on the work.

My initial aim was to attempt to adapt existing theories of diffusion to create a model for the diffusion of colloids in a colloid-polymer mixture. I worked on the governing equations obtained by Prof. W. C. K. Poon and Dr. P. Warren for a Cahn-Hilliard model of diffusion in a colloid-polymer mixture. My work has explained these results in terms of physical concepts. In addition I have included the effects of hydrodynamic interactions for a limited range of colloid and polymer concentrations. It became clear that this model was restricted both by the clumsy way in which hydrodynamics had to be included, and by the inability to solve the equations away from the low scattering vector limit. The Smoluchowski formalisation overcomes both these problems, but is considerably harder to solve and a quantitative solution for diffusion in a colloid-polymer mixture is not likely to be found in the immediate future. Nevertheless I made several qualitative predictions based on previous work on concentrated systems of hard-spheres.

To test these predictions I performed experiments on a well-characterised model system. These showed that the diffusion coefficient of the colloids was, as predicted, a function of time but did not appear to take the form expected from the Smoluchowski fomalisation. In addition, the data showed an unphysical dependence on the scattering vector.

To find the origin of this unphysical result, I looked carefully at some of the assumptions made in the light scattering experiment. To obtain the dynamic structure factor of the colloid alone, I had assumed that cross scattering (in which the light scattered from a colloid is correlated with that from a polymer) was negligible, and that the data needed to be corrected for the scattering from the polymer alone. This assumption was found to have no physical basis. I worked on trying to find the magnitude of this cross-scattering and arrived at a relatively simple method for estimating its magnitude. The results obtained by my method compared favourably with those obtained by a more complicated treatment recently

published by Dr. A. Louis *et al.* [32] Simultaneously I managed to find a way to measure this magnitude experimentally. Both theory and experiment showed the cross-scattering was likely to be significant in my previous experiments and I had to consider several methods to reduce it.

In neutron scattering it is common to use *contrast variation* to obtain scattering from one species only. For light scattering, contrast variation would involve changing the refractive index of either the solvent or one of the species. Tetralin was identified as having a suitable refractive index but previous work carried out in this department and elsewhere indicated that PMMA particles may swell when placed in tetralin. I decided to investigate whether this swelling was significant in our system. Through detailed light scattering experiments, it became clear that not only did the particles swell in tetralin, but there was also some complicated rearrangement of the tetralin within the particle that continued for several weeks. Tetralin clearly could not be used as a solvent. No other solvent or polymer could be found that would reduce cross-scattering, was safe to use and could be obtained in sufficient quantities.

Instead of using contrast variation, I attempted to measure the magnitude and form of the cross-scattering directly, with a view to then being able to correct the data previously obtained. I devised an experimental method for obtaining the form of the cross-scattering based on the scattering properties of the colloids. Unfortunately noise in the data and the size distribution of the colloid samples prevented an accurate measurement.

I then devised a new experimental methodology that allowed use of the scattering vector dependence as a check on whether cross-scattering was significant in the experiment. By changing the solvent and only considering data obtained at certain scattering vectors and colloid concentrations, the magnitude of the cross-scattering was reduced and shown to be negligible. Unfortunately multiple-scattering now became significant. The experiments had to be repeated using

two colour dynamic light scattering, which effectively removes multiple scattering. The majority of the work using two colour dynamic light scattering was performed in conjunction with Dr. A. Moussaïd. Finally I obtained data in which both cross-scattering and multiple scattering were negligible and which could be analysed to see whether the theoretical predictions were being followed.

1.6 Layout of thesis

Dynamic light scattering is a well established technique. However, as those who regularly work with it will know, it is extremely sensitive to alignment and stray light. The building of a reliable and accurate experimental set-up was fundamental to this work and a summary of the apparatus used, together with the experimental limitations of the equipment, are given in Chapter 2. A detailed description of the analysis techniques used is included here. Also included in Chapter 2 are the basic experimental techniques used to prepare and characterise the samples and a study designed to both illustrate the usefulness of light scattering techniques and to investigate the suitability of using tetralin as a solvent in this work.

Chapter 3 provides the theoretical background to diffusion in colloid-polymer mixtures. After summarising the basic thermodynamics of the system, an in depth study into a Cahn-Hilliard treatment of diffusion in this system is presented. The Cahn-Hilliard method was originally developed to explain a form of phase separation known as 'spinodal decomposition', but has been adapted to explain diffusion in non-phase separating samples. Initial work on this theory has been performed by Prof. W. C. K. Poon[1] and Dr. P. Warren[2], though their results are currently unpublished. Here their work is reviewed and new

[1]Department of Physics and Astronomy, University of Edinburgh
[2]Unilever Research, Port Sunlight

results presented. Using these results, a physical explanation for the diffusion in colloid-polymer mixtures at low scattering vectors is provided. Furthermore, a new model is presented which includes the effects of hydrodynamic interactions. The limitations of this model are also discussed.

Included in Chapter 3 is a summary of another theory of diffusion - the Smoluchowski model. This model is expected to have considerably more relevance to my work as it includes hydrodynamic interactions in a much more natural way. Both the model and the experimental work supporting it are reviewed and, based on this, a model for diffusion in this system proposed.

Chapter 4 contains the experimental investigation. Calculations carried out in collaboration with Dr. A. Louis and Prof. J. -P. Hansen[3] revealed that the scattering from the polymer introduces large errors into the measurements. Several new experimental directions were extensively investigated to overcome this problem. Eventually a methodology was found in which these complications could be minimised. The accuracy of this method was checked by use of the two colour dynamic light scattering equipment in collaboration with Dr. A. Moussaïd[4].

Chapter 5 contains a detailed, though not exhaustive, review of the current literature on colloids diffusing through polymer mixtures. Its late positioning in this thesis is because several of the authors appear to have had difficulties similar to those found by myself and reported in Chapter 4.

The last chapter contains the main conclusions of this thesis and presents suggestions for further work.

This work has been discussed with, and guided by, Prof. P. N. Pusey[5] and Prof. W. C. K. Poon.

[3]Department of Chemistry, University of Cambridge

[4]Department of Physics and Astronomy, University of Edinburgh

[5]Department of Physics and Astronomy, University of Edinburgh

Chapter 2

Experimental techniques

This chapter summarises the basic experimental procedures used to obtain and charcterise the samples. It also contains an overview of light scattering techniques, including the experimental apparatus designed and used in this work and a summary of the main analysis techniques used in dynamic light scattering. Also reported are the results of a study of some practical interest to those using PMMA particles, namely the effect of using tetralin as solvent.

2.1 Colloid stock preparation

2.1.1 Washing the colloid

The colloids were synthesised in the Department of Physics and Astronomy at the University of Edinburgh by Dr. A. Schofield. When supplied they are dispersed in dodecane, which is not an ideal solvent for the relevant experiments. The refractive index of dodecane differs strongly from the particles (see table 1.1) making multiple scattering effects important when using light scattering methods. To reduce multiple scattering, *cis*-decahydronapthalene (or *cis*-decalin for short) and

trans-decahydronapthalene (or *trans*-decalin) are used as solvents. The dodecane must therefore be replaced with either of these solvents and there is a standard procedure used to do this. The colloids are placed in either a glass or plastic cylindrical cell and centrifuged at high angular velocity. The colloids are denser than the solvent and move towards the base of the container. On settling the colloids adopt a random close packed structure at the bottom of the cell. The time taken for all the colloids to be part of this structure is dependent on the angular velocity chosen. The effective weight W of a particle is

$$W = \frac{4}{3}\pi R_c^3(\rho_c - \rho_s)\omega^2 r \ , \tag{2.1}$$

where R_c is the radius of the colloid, ρ_c the average density of the colloid, ρ_s the density of the solvent, ω the angular velocity and r the perpendicular distance of the colloid from the axis of the centrifuge which for the centrifuge used is 10cm. The upper limit to the centrifuge speed is given by the mechanical strength of the cells. In this centrifuge, glass is only capable of withstanding approximately 3000 revolutions per minute, whereas plastic can withstand over 10,000 revolutions per minute, which is the maximum attainable angular velocity. It is therefore roughly 10 times quicker to use a plastic container than a glass one. It is worth noting that at $20°C$ an isolated particle of radius 175nm will sediment about 0.5mm per day in *cis*-decalin under the earth's gravity.

After complete sedimentation is achieved, the supernatant dodecane can be removed and replaced with the desired solvent. The colloid is then redispersed using a mechanical shaker. The volume fraction of a close packed system of hard spheres is $\phi_{\rm rcp} \gtrsim 0.64$, with the exact value being dependent on the polydispersity[1] [33] and the slight compressibility of the particles. When the particles are redispersed, the solvent that was trapped in the sediment is freed. If we define a 'purity fraction' p_f as the ratio of the initial solvent (dodecane) to the total

[1]Real colloids have a distribution of sizes. The polydispersity is defined to be the standard deviation of the distribution normalised by the mean value.

amount of solvent (dodecane and either *cis*-decalin or *trans*-decalin), after one wash we find that

$$p_f = \frac{(1 - \phi_{\text{rcp}})\zeta}{1 - \phi_{\text{rcp}}\zeta} \tag{2.2}$$

where ζ is the ratio of the sediment volume to the total volume. Taking $\phi_{\text{rcp}} = 0.66$ (which assumes a polydispersity of about 5%) and $\zeta = 0.4$ gives a purity fraction of 18%. The whole process is repeated until the purity reaches an acceptable level. The number of washes required to approach a purity level of 0.01% is calculated from $p_f^n = 10^{-4}$, i.e. $n = 6$. Typically the wash is repeated seven times. To verify the purity after seven washes the refractive index of the discarded solvent is measured using an Abbe refractometer and compared to that of pure solvent. No difference was ever found to the level of accuracy of this device (0.05%).

2.1.2 Finding the volume fraction

It is perhaps suprising that one of the main experimental difficulties in working with PMMA colloids is the accurate determination of volume fraction. There are several methods available, but each makes an assumption about the system or particle which may be invalid.

One method is to find the mass fraction of the colloid and convert it to a volume fraction. The mass fraction may be found by drying a weighed amount of colloid and solvent in a vacuum oven at $50°C$ until all the solvent has evaporated. In practice one takes mass measurements every day until there is no additional weight change on further drying, which typically occurs after three days. To convert the mass fraction thus obtained to a volume fraction, the density of both particle and solvent must be known. Whilst the latter can be measured easily (see section 2.2.1), finding the density of the core-shell composite particle is not trivial. The PMMA core may be porous and have a different effective density to

the bulk material. In addition the PHSA layer is usually solvated to an unknown degree, affecting the density of the composite particle. If the volume fraction ϕ_f of a particular suspension were known in advance (by, for example, one of the methods discussed later in this section), then a single measurement of mass fraction provides the scaling constant.

$$\begin{aligned} \phi_f &= \frac{\rho_s m_c}{\rho_s m_c + \rho_c m_s} \\ &= \frac{m_c}{m_c + \beta m_s} , \end{aligned}$$

where

$$\beta = \frac{\rho_c}{\rho_s} ,$$

so

$$\beta = \frac{m_c}{m_s} \frac{1-\phi}{\phi} . \tag{2.3}$$

Having determined the scaling constant, this method may be used to determine subsequent volume fractions. This tends not to be a very popular method for two reasons: the scaling constant is different for different preparations, and once the volume fraction has been determined, the sample must be redispersed to be used in experiments, which can be difficult.

Other methods attempt to measure the volume fraction directly. As mentioned in section 2.1.1, on prolonged centrifuging the colloid adopts a close packed structure at the bottom of the cell. If the volume fraction of this sediment is known, then an easy way to determine the total volume fraction is to centrifuge the sample in a cell with a homogeneous cross-section. By measuring the heights of the sediment and solvent, the volume fraction may be determined

$$\phi_s = \frac{h_{\mathrm{RCP}}}{h_{\mathrm{tot}}} \phi_{\mathrm{RCP}} . \tag{2.4}$$

ϕ_s is the volume fraction of the suspension and ϕ_{RCP} that of the random close packed sediment, which for monodisperse hard spheres is known to be 0.64. For

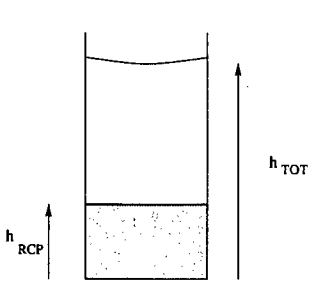

Figure 2.1: After centrifuging the sample cell contains a 'solid' region of random close packed colloids and a supernatant fluid. Measurement of the respective heights allows calculation of the volume fraction.

the definition of the other terms see figure 2.1. Schaertl and Sillescu [33] investigated the effect of polydispersity on this packing using computer simulation. They found that 5% polydispersity changes the volume fraction of random close packing to 0.66, whereas 10% increases it to 0.67. The error introduced by reasonable amounts of polydispersity is thus not large; however there are additional problems with this method. High speed centrifuging may well compress the particles, though if this deformation were not permanent it could be accounted for by measuring heights over a period of time. Transmission electron micrographs taken on colloidal suspensions that had been centrifuged at 3000 rpm and then redispersed revealed no significant shape polydispersity [21]. Furthermore I investigated the effect of centrifuge speed on the height of sediment by spinning down a sample at low speed until the sediment was formed, and then centrifuging again at much higher speeds (without redispersion). No height change was noted.

The most significant error in using this method to determine volume fraction is the uncertainty in the form of packing. Small particles (which achieve a lower sedimentation velocity) may have time to rearrange themselves into a structure with more efficient packing. It is known that the most efficient form of packing for hard spheres is a crystal with a volume fraction of 0.74, significantly more than that for random close packing. Even a mondisperse, non-compressing system of

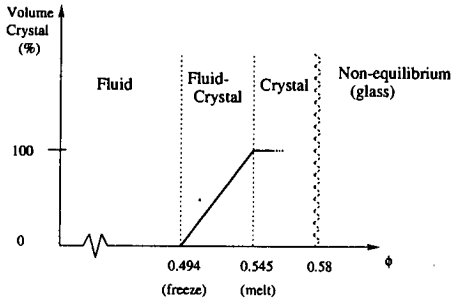

Figure 2.2: The phase diagram for hard spheres as a function of volume fraction ϕ.

hard spheres may have sediment with a volume fraction in the range $0.64 \leq \phi < 0.74$.

Another method for determination of the volume fraction is to exploit the phase diagram of the hard sphere system. Hoover and Ree [34] performed computer simulations on a monodisperse system and found that hard spheres undergo a 'freezing' transition at a volume fraction of 0.494 (ϕ_f) and a 'melting' transition at a volume fraction of 0.545 (ϕ_m). Between these volume fractions the system shows two coexisting regions, crystal and fluid (figure 2.2). This was seen experimentally by Pusey and van Megen [28]; however when they scaled their volume fractions to obtain freezing at ϕ_f, the melting transition was found at $\phi_m = 0.536$. Paulin and Ackerson also measured the phase diagram for PMMA spheres in a mixture of *cis*-decalin and tetralin. On scaling the freezing transition, they found the melting volume fraction to be 0.552 [35]. The reason for these discrepancies is very likely the effect of polydispersity. Two authors have attempted to calculate the phase diagram for polydisperse hard spheres based on density functional theory [36,37], but find different predictions and do not reproduce accurately the computer results for the monodisperse system. Polydispersity certainly affects crystallisation and there are various predictions for the *critical polydispersity* at which crystals cannot form. Experimentally it is found that in our system polydispersity greater than about 10% results in no crystallisation [20].

It is clear that for a fairly monodisperse system, taking the freezing transition at that predicted for hard spheres will not result in an error more than about 3%, and this is the best marker we have for calibrating a system. The aim is to put the colloid within the coexistence region and use figure 2.2 to determine the volume fraction. Experimentally we use a cell with a homogeneous cross-section and by assuming the spun-down sediment has a volume fraction of 0.64, we add or remove supernatant until the nominal volume fraction is 0.52 (using equation 2.4). If no crystals form, we can be sure that the volume fraction is greater than 0.545, since the estimate of 0.64 is a lower bound for the volume fraction of the sediment. More solvent is then gradually added until the system is brought into the coexistence region. When the crystals appear they nucleate throughout the sample and then sediment under gravity where they start to compress. Paulin and Ackerson [35] suggest a method for extrapolating the height of the various interfaces to zero time to obtain the initial height of crystals correctly. This can then be compared to figure 2.2 to obtain the volume fraction of the sample.

It is good practice to keep the stock solution, from which all dilutions are made, within the coexistence region so that it is easy to see if the volume fraction changes due to evaporation or handling. Evaporation is reduced considerably by using a tightly fitting cap which is then sealed with teflon tape. In a well sealed cell, evaporation typically changes the total mass by about 1% per month. In my experiments no samples were kept for longer than a month so the effect of evaporation can be neglected.

Having obtained the stock solution, it is necessary to dilute to appropriate concentrations. This is done according to the equation

$$\begin{aligned} \phi_n &= \frac{m_{ss}\phi_{ss}}{m_{ss} + \frac{\rho_{ss}}{\rho_d} m_d} \\ &= \frac{m_{ss}\phi_{ss}}{m_{ss} + (\phi_{ss}\beta + (1-\phi_{ss}))\, m_d} , \end{aligned} \tag{2.5}$$

where

$$\rho_{ss} = \phi_{ss}\rho_c + (1-\phi_{ss})\rho_d \, .$$

The subscript ss refers to stock solution and d refers to the added solvent. Once more we need the value β, which can be obtained from equation 2.3.

Using these various methods one can obtain clean colloid in a suitable solvent at known volume fraction. The last characteristic required for this work is the particle's radius. This can be obtained by light scattering and discussion of how this is obtained will be left to later sections.

2.2 Polymer stock preparation

For the purposes of this thesis, the polymer solution is characterised by its concentration, coil radius and viscosity. The polymer used is of very high molecular weight and can easily break if placed under high shear (for example by shaking vigorously). With this proviso in mind, the characterisation of the polymer solution is considerably more straightforward than that of the colloid.

2.2.1 Concentration and density

The polymer is obtained in powder form and is made into solution by dissolving a known mass in a known mass of solvent. The mixture is then tumbled slowly until fully homogenised. Any undissolved polymer can be seen as a glassy 'blob' within the solution. The concentration c_p is given by the mass of the polymer divided by the volume of the solvent (which relies on a value for the density of the solvent ρ_d - see below). The polymers contribute negligibly to the volume of the solvent, but the density of the solution ρ_{ps} becomes

$$\rho_{ps} = \rho_d + c_p \, . \tag{2.6}$$

It will become important in later sections to know the density of the polymer solution accurately. Densities can be measured experimentally by the following

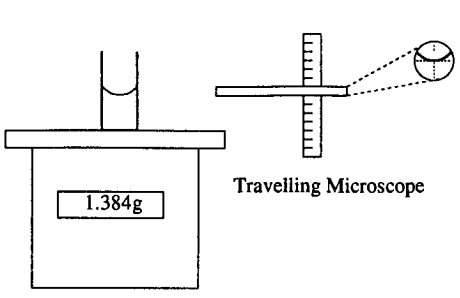

Figure 2.3: Schematic for measuring the density of solutions.

method. A cell with constant area (square based) is filled with increasing amounts of solvent. Each time the mass of the cell and solvent is measured. The height of the base of the meniscus is also measured using a travelling microscope (figure 2.3). A plot of height h against total mass m_T has as its slope the density ρ_d multiplied by the average cross-section of the cell A_{cell}:

$$m_T = h\rho_d A_{\text{cell}} + m_{\text{cell}} \,. \tag{2.7}$$

The cross-sectional area is found by performing this experiment with a solvent of known density. Using this method we could measure density differences down to as little as $2mgcm^{-3}$. Typical results are shown in figure 2.4, and we noticed no deviation from equation 2.6.

It is often convenient to write the polymer concentration in terms of the overlap concentration, defined in Chapter 1, to give an 'effective polymer volume fraction' and this will turn out to be a useful quantity in later chapters.

2.2.2 Polymer radius

In order to find the overlap concentration, we need the radius of the polymer coil (equation 1.3). This is controlled by the molecular weight M_W of the polymer and the temperature T of the solution. Berry [38] performed a comprehensive study on the behaviour of linear polystyrene in decalin (both *cis*-decalin and *trans*-

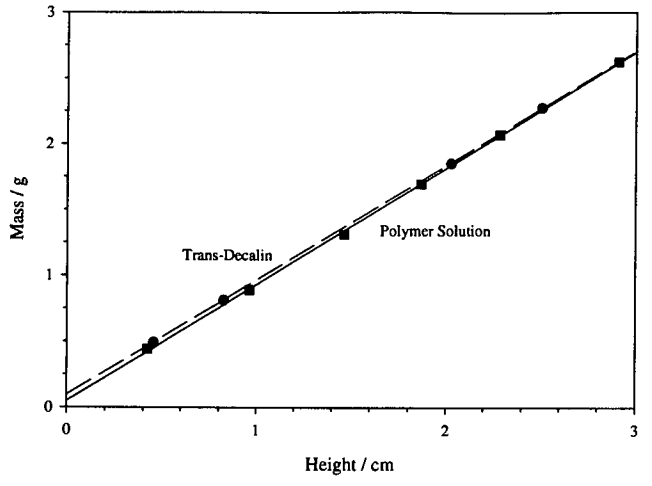

Figure 2.4: Typical results for density measurements. The circles are results for *trans*-decalin, and the dashed line is the linear regression best fit. The squares represent measurements on a polymer solution of concentration $18.2mgcm^{-3}$ with the solid line being the linear regression best fit. Using this method, we can detect density differences down to as little as 1%.

decalin). His results were consistent with the assumption that the expansion of the radius above the theta temperature T_θ is a function of a single variable, the Fixman parameter z. For decalin solutions of linear polystyrene, the Fixman parameter is given by

$$z = 0.00975 M_W^{\frac{1}{2}} \left[1 - \frac{T_\theta}{T}\right] . \tag{2.8}$$

Having calculated this parameter, the expansion of the coil $\left\langle R_g^2 \right\rangle / \left\langle R_g^2 \right\rangle_\theta$ can then be read off figure 12 in reference [38]. In the same paper Berry showed that, at the theta point, the radius of gyration (in nm) is given by

$$\sqrt{\left\langle R_g^2 \right\rangle_\theta} = 0.0276 \sqrt{M_W} . \tag{2.9}$$

A knowledge of the theta temperature and the molecular weight is therefore all that is needed to obtain the radius at any temperature above the theta point. Theta temperatures may be obtained from the Polymer Handbook ($12.5°C$ for *cis*-decalin, $20.4°C$ for *trans*-decalin) [29]. When the polymer is supplied, it comes with a data sheet providing the weight-averaged molecular mass M_W and the

ratio of moments which is this mass divided by the number averaged molecular mass M_n. For my polymers, this ratio was less than 1.05 which indicates a polydispersity of about 5%. Following Berry I have used M_W to calculate the radii.

2.2.3 Viscosity

Polymer solutions of high molecular weight or concentration show a type of non-Newtonian behaviour known as *shear thinning*. The polymer coils orientate themselves along flow lines where they interfere less with the flow of solvent. Thus the apparent viscosity decreases. On the other hand the coils also are deformed by the flow (in polymer solutions this is synonymous with elongation in the flow direction) causing the particles to interact more with the liquid and to increase the viscosity. The two partially cancel, but the orientation effect dominates and the viscosity decreases [39]. The onset of shear thinning is expected at Pe ≈ 1, where Pe is the Peclet number which characterises the amount of distortion of structures in shear flow [17]. It is given by

$$\mathrm{Pe} = \frac{\dot{\gamma} R_p^2}{2D_p}\,, \tag{2.10}$$

where $\dot{\gamma}$ is the shear rate, and R_p, D_p the radius and diffusion coefficient of the polymer coil respectively. For a typical polymer used in my experiments this gives the onset of shear thinning at a shear rate of $\dot{\gamma} \approx 50s^{-1}$.

For the case of a colloid diffusing in a polymer solution, the motion of both species is driven by the thermal energy of the suspending fluid. For size ratios smaller than 1 (i.e. a larger colloid), equation 1.2 results in a more intense thermal motion for the polymers than the colloid. Consequently the shear stress acting upon the polymers is weak and slowly changing as compared to the polymer diffusion [7] and shear thinning is not likely to be significant in the colloid-polymer mixture.

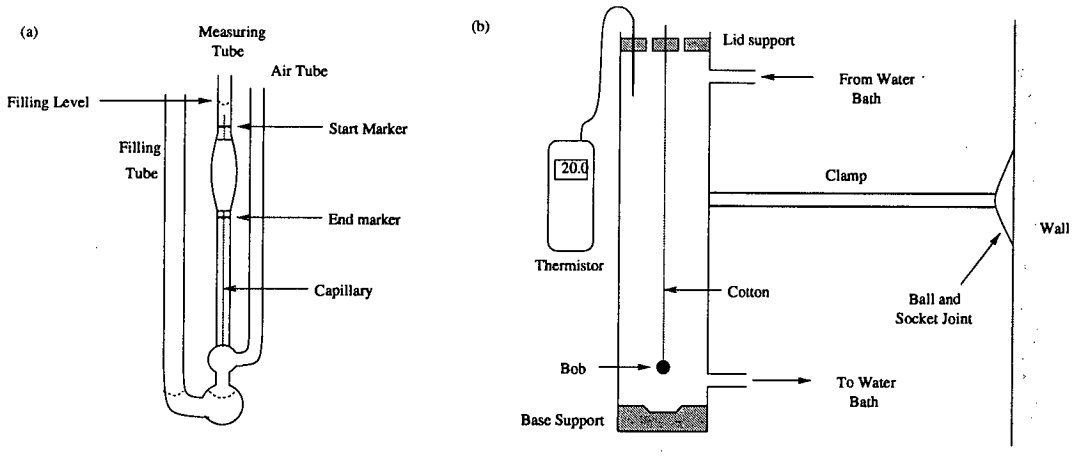

Figure 2.5: A schematic illustration of the Ubbelohde viscometer. Figure (a) shows the actual viscometer and (b) shows the holder which is designed to keep the viscometer at constant temperature, free from vibrations and vertical.

The viscosity of the polymer solutions was measured with an *Ubbelohde* viscometer. The measuring principle is based on the Poiseuille equation relating the volume flow $\dot{V}$ of a liquid through a capillary with radius a and length l to the viscosity of the liquid η and the pressure difference ΔP between the ends of the capillary that is causing the flow:

$$\dot{V} = \frac{\pi a^4 \Delta P}{8\eta l} . \tag{2.11}$$

The pressure difference is caused by gravity. A schematic of the apparatus is shown in figure 2.5a. The polymer solution is introduced through the filling tube. It is then sucked up through the capillary to the measuring bulb. The fluid is then allowed to flow under the action of gravity through the capillary and the flow time t is measured between the moments the miniscus passes the two markers. The pressure difference is given by $h\rho g$ which is substituted into equation 2.11 to give

$$t = K\frac{\eta}{\rho} , \tag{2.12}$$

where K is a constant dependent on the particular apparatus and is determined by a measurement on a known solvent. In the above treatment I have neglected

the correction for the kinetic energy gained by the fluid as it leaves the tube which for a well designed viscometer is negligible.

The flow field for Poiseuille flow is well known (see for example [40]). The maximum shear rate of the fluid is given by

$$\dot{\gamma}_{\max} = \frac{\Delta P a}{2\eta} . \tag{2.13}$$

This results in typical shear rates of $0.05s^{-1}$, ensuring that shear thinning will not be detected.

The precision of an Ubbelohde viscometer is remarkable. Typical efflux times of 400s are measured with a stop watch to an accuracy of ± 0.1s. To obtain this level of precision, the measuring environment needs to be strictly controlled; for example viscosity is a strong function of temperature with a fluctuation of 1K leading to an error of about 2%. Furthermore, the Ubbelohde needs to be kept vertical (to within half a degree) and vibration free. Commercial holders are available at not inconsiderable costs, but the apparatus in figure 2.5b shows a home-made alternative. The viscometer is held within a glass tube and protected against vibrations by a tight fitting base plate and cap. Water from a temperature-controlled bath is circulated within the glass holder maintaining the temperature to within 0.1K (as measured by a thermistor). Circulation rates are kept low to avoid turbulence. A plumb line is included within the tube and alignment is made possible by use of a ball hinge at the wall. This has the added advantage of suspending the viscometer away from further sources of vibrations.

Typical measurements on the concentration dependence of polystyrene in *trans*-decalin at 28.6°C are shown in figure 2.6. A *Carrimed* cone and plate rheometer was also used on these samples. This rheometer is considerably less accurate than the Ubbelohde for these low viscosities, but has the advantage of an adjustable shear rate. It was used primarily to verify that shear thinning was not observed. More details of this kind of rheometer can be found in the literature (e.g. [40]).

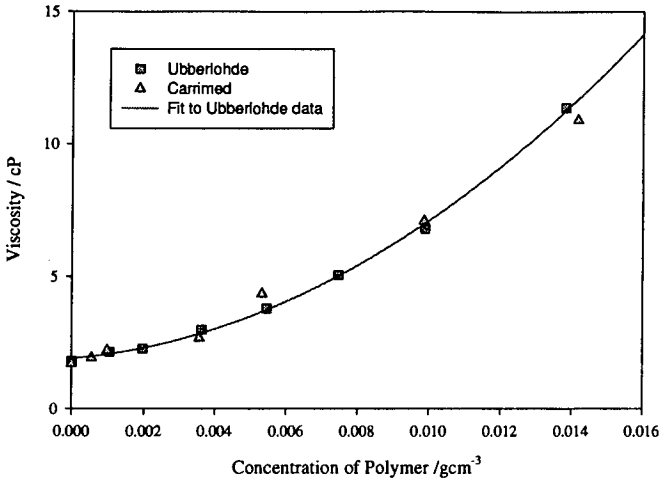

Figure 2.6: Concentration dependence of viscosity for polystyrene (2 million molecular weight) in *trans*-decalin. Squares represent the data obtained by the Ubbelohde viscometer with the curve being a quartic best fit, triangles are data obtained from a carrimed rheometer.

2.3 Light scattering

Light scattering is an immensely useful tool for studying colloids. Almost all visible objects scatter light [41]; the optical appearance of coloured objects (such as leaves and flowers) come from strong scattering combined with significant absorption bands in the visible spectrum. The blue colour of the sky (in everywhere except Edinburgh where it is more usually grey) is a result of the strong dependence on wavelength of the scattering from the atmosphere. Light scattering reveals information about the *structure* and *dynamics* of systems. The advances in removing low order multiple scattering (by, for example, using two colour dynamic light scattering) and obtaining useful information from heavily multiply-scattering systems (through diffusive wave spectroscopy) [41] open up the application of these techniques to stronger scatterers and more concentrated systems. However, in this work I shall mainly be considering systems where

multiple scattering is not significant. The theory behind light scattering is well understood and may be found in many texts (e.g. [20,42]). Here I will review the basic principles.

2.3.1 Fundamentals

Light with an electric field amplitude $\boldsymbol{E_0}$ linearly polarised along the $\boldsymbol{x}$ axis is incident along $\boldsymbol{z}$. This electric field induces a dipole moment inside the particle, which in turn radiates an electromagnetic dipole field. If the linear size of the scatterer R is significantly smaller than the wavelength of the light λ Maxwell's equations can be solved to give the following relation between the intensity of the scattered light I_s, the distance from the scatterer r, and ϕ - the angle between the scattering direction $\boldsymbol{r}$ and the direction of polarisation $\boldsymbol{x}$:

$$I_s = \frac{16\pi^4\alpha^2 E_0^2}{r^2\lambda^4}\sin^2\phi\,. \tag{2.14}$$

α is the polarisability of the scatterer. We have assumed in this derivation that the scattering is *elastic* - i.e. there is no energy absorbed or emitted by the scatterer. If we consider only scattering within the plane perpendicular $\boldsymbol{x}$, then from equation 2.14 we see that the light is scattered equally in all directions.

An extended object for which the Rayleigh limit ($R \ll \lambda$) does not hold can be treated as a series of small volume elements each scattering as above. The total scattered field is expressed as the coherent sum of the fields scattered from volume elements located at $\mathbf{r}_i$. As long as the incident plane wave front is not distorted by the presence of the other volume elements (the Rayleigh-Gans-Debye criterion), the phase factor between any two volume elements is simply $e^{-i\mathbf{Q}\cdot(\mathbf{r}_i-\mathbf{r}_j)}$ (see figure 2.7). $\boldsymbol{Q}$ is the scattering vector defined as the difference between the scattered and incident wave vectors (see figure 2.7). Since the scattering is elastic

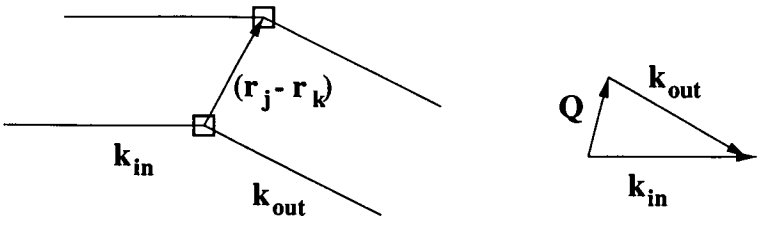

Figure 2.7: The phase difference between two scattering volume is given by the scalar product of the scattering vector Q and their radial separation, $\mathbf{r}_j - \mathbf{r}_k$.

$k_i = k_s$ and the magnitude of the scattering vector is given by

$$Q = \frac{4\pi n_s}{\lambda_0} \sin\left(\frac{\theta}{2}\right) , \tag{2.15}$$

where λ_0 is the *in vacuo* wavelength of the incident light and θ the angle between the incident and scattered wavevectors.

If the extended object is homogeneous (and infinite) then the scattering from each small volume is identical and the total scattered electric field averages to zero ($\int_V e^{-i\mathbf{Q}.(\mathbf{r}_i - \mathbf{r}_j)} = 0$). If there are optical inhomogeneities within the medium, cancellation does not occur. Consider such an inhomogeneity: using the theory of polarisation of dielectrics, we can relate the contribution to the total scattering from this inhomogeneity to the *excess* dielectric constant ($\Delta\epsilon = \epsilon_i - \epsilon_0$) of this region [39]. If $\delta\mathbf{E}_s{}^j$ is the contribution to the total scattering from a scattering volume v_s at $\mathbf{r}_j$ then it is related to the excess dielectric constant of that volume $\Delta\epsilon_j$ by

$$\delta\mathbf{E}_s{}^j = \frac{\pi v_s \Delta\epsilon_j}{\lambda_0^2} \frac{\mathbf{E}_0}{r} e^{-i\mathbf{Q}.\mathbf{r}_j} . \tag{2.16}$$

Integrating these contributions, we find that the total electric field is the Fourier transform of the excess dielectric constant. To obtain useful results for a system of colloidal particles we must now make some approximations. Firstly we assume that the suspending solvent contains insignificant inhomogeneities and so the excess polarisability in the system is entirely due to the particle. This is not necessarily true and must be checked experimentally in each case, particularly when

solvent *mixtures* are involved as these can give large compositional fluctuations. Further, we will only consider the light detection in the far field which allows use of the Fraunhofer approximation. The Rayleigh-Gans-Debye criterion (RGD) for this system places the following restriction on the radius of the particles R, the wavevector of the incident light k, and the ratio of the refractive indices of object and solvent n_c/n_s

$$kR\left|\frac{n_c}{n_s}-1\right| \ll 1 \,. \tag{2.17}$$

In this work this is realised by choosing a solvent of a similar refactive index to the scattering object.

The total dielectric constant ϵ_T of a system of particles and solvent is, to a good approximation, simply the volume average of the dielectric constants of the particles ϵ_p and solvent ϵ_s [43].

$$\epsilon_T = \Phi\epsilon_p + (1-\Phi)\epsilon_s \,, \tag{2.18}$$

where Φ is the total volume fraction of the scatterers, *not* the scattering particles.[2] Thus the excess polarisability is given by

$$\Delta\epsilon \equiv \epsilon_p - \epsilon_s = \frac{d\epsilon_T}{d\Phi} = \frac{M_W}{N_A V_p}\frac{d\epsilon_T}{dc} \,, \tag{2.19}$$

where c is the concentration (mass/volume) of the particles, V_p the scattering volume of a particle and M_W the molecular weight of the particle. For most substances the dielectric constant is related to the refractive index n by (see e.g. [39])

$$\epsilon = n^2 \,, \tag{2.20}$$

leading to an expression for excess polarisibility of

$$\Delta\epsilon = 2\frac{M_W}{N_A V_p} n_T \frac{dn_T}{dc} \,, \tag{2.21}$$

[2]This distinction is necessary as a polymer coil is not a solid entity.

where n_T is the total refractive index. In the limit of small refractive index differences, this expression may be expanded to give

$$\Delta\epsilon = 2n_s(n_c - n_s) = 2n_s\delta n \ . \tag{2.22}$$

The excess dielectric constant in equation 2.16 is therefore related to the refractive index difference between the solvent and the particle at position r_j ($\delta n(r_j)$) by a system specific constant, so that the total magnitude of the scattered light E_s in the far field is:

$$E_s(\mathbf{Q},t) = \sum_j \delta n(\mathbf{r}_j(t))e^{i\mathbf{Q}\cdot\mathbf{r}_j(t)} \ , \tag{2.23}$$

where we have neglected the prefactors for clarity. In general the inhomogeneities may move relative to the background medium, hence the inclusion of the time dependence in equation 2.23.

2.3.2 The form factor

Let us first consider the case of a single, orientationally symmetric, solid particle. The sum in equation 2.23 is now only over scatterers within one particle. Going to the continuum limit we find:

$$E_s(\mathbf{Q}) = \int_{V_c} \delta n(r)e^{i\mathbf{Q}.\mathbf{r}}dV \ , \tag{2.24}$$

where the integral is over the volume of the particle V_c. This quantity (which is in general a complex quantity) is known as the scattering amplitude of the particle, and is usually written $b(\mathbf{Q})$. For a solid, isotropic particle we can drop the temporal dependence of equation 2.23. The scattering amplitude for a homogeneous sphere of refractive index n_c and radius R, is found by performing the integral to give

$$b(Q,R) = 4\pi R^3(n_c - n_s)\left(\frac{\sin QR - QR\cos QR}{(QR)^3}\right) \ . \tag{2.25}$$

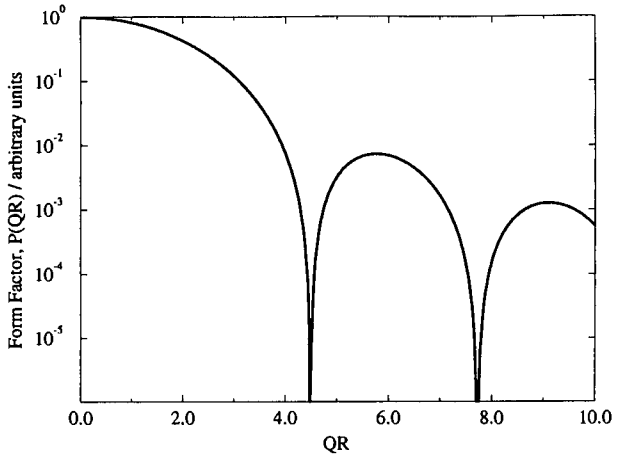

Figure 2.8: Theoretical form factor for a homogeneous sphere.

A more useful quantity to consider is the *form factor* which is the normalised intensity scattered by a single particle, defined as

$$P(Q,R) = \frac{|b(Q,R)|^2}{|b(0,R)|^2}\,, \tag{2.26}$$

which for a homogeneous sphere has the form

$$P(QR) = 9\left(\frac{\sin QR - QR\cos QR}{(QR)^3}\right)^2\,. \tag{2.27}$$

This is plotted in figure 2.8. The minima occur whenever $QR = \tan QR$, which has solutions at $Q^n_{\min}R = 4.493, 7.725, 10.904, \ldots$.

The form factor of a random walk polymer can be obtained by assuming that the separation of scatterers along the chain has a Gaussian distribution. For a polymer with radius of gyration R_g the form factor is given by [44]

$$P(QR_g) = \frac{2}{(Q^2R_g^2)^2}\left(Q^2R_g^2 - 1 + e^{-Q^2R_g^2}\right)\,. \tag{2.28}$$

2.3.3 The structure factor

As the concentration is increased we have to consider correlations between the light scattered from different particles. It is convenient to rewrite the position

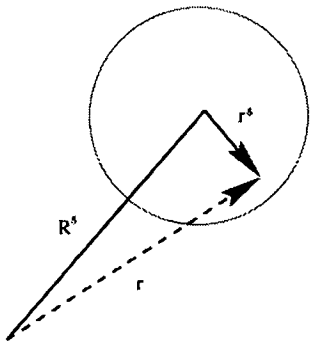

Figure 2.9: Schematic showing redefintion of $\boldsymbol{r}$ in the calculation of the structure factor for a spherical particle.

of the j'th scatterer relative to the centre of the particle it is contained in, i.e. $\mathbf{r}_j(t) = \mathbf{R}_j^s(t) + \mathbf{r}_j^s$ where $\mathbf{R}_j^s(t)$ is the position at time t of the center of the particle containing the j'th scatterer and $\mathbf{r}_j^s$ is the position of the scatterer relative to that sphere (see figure 2.9). The sum in equation 2.23 now becomes separable:

$$\begin{aligned} E_s(\mathbf{Q},t) &= \sum_j \delta n(\mathbf{r}_j) e^{i\mathbf{Q}\cdot\mathbf{r}_j(t)} \\ &= \sum_j \sum_k \delta n(\mathbf{r}_j) e^{i\mathbf{Q}\cdot\mathbf{r}_j^s} e^{i\mathbf{Q}\cdot\mathbf{R}_k^s(t)} \\ &= \sum_k b(\mathbf{Q},R_k) e^{i\mathbf{Q}\cdot\mathbf{R}_k^s(t)} , \end{aligned} \tag{2.29}$$

where $b(\mathbf{Q},R_k)$ is the scattering amplitude of the k'th particle. The time-averaged intensity[3] $< I(Q) >$ is related to the electric field by

$$\begin{aligned} < I(Q) > &= < E^*(\mathbf{Q},t) E(\mathbf{Q},t) > \\ &= \left\langle \sum_j \sum_k b^*(\mathbf{Q},R_j) b(\mathbf{Q},R_k) e^{-i(\mathbf{Q}\cdot\mathbf{R}_j^s(t) - \mathbf{Q}\cdot\mathbf{R}_k^s(t))} \right\rangle . \end{aligned} \tag{2.30}$$

If we now assume that all the particles are identical, then this can be rewritten as

$$< I(Q) >= N \left| b(0,R) \right|^2 P(Q,R) S(Q) , \tag{2.31}$$

[3]All systems considered will be *ergodic*, for which the time-average and ensemble average are equal.

with the structure factor $S(Q)$ being defined as

$$S(Q) = \frac{1}{N}\sum_{j=1}^{N}\sum_{k=1}^{N}\left\langle e^{i\mathbf{Q}\cdot(\mathbf{R}_j^s(t)-\mathbf{R}_k^s(t))}\right\rangle . \tag{2.32}$$

The structure function is a useful quantity as it gives information in reciprocal space on the relative positions of the particles [45]. It is related to the radial distribution function which gives similar information in real space. To show this relation we now split the double sum into two parts $j = k$ and $j \neq k$.

$$\begin{aligned} S(Q) &= \frac{1}{N}\left\langle \sum_{j=k} \exp i\mathbf{Q}\cdot(\mathbf{R}_j^s(t)-\mathbf{R}_k^s(t))\right\rangle + \frac{1}{N}\left\langle \sum_{j\neq k} \exp i\mathbf{Q}\cdot(\mathbf{R}_j^s(t)-\mathbf{R}_k^s(t))\right\rangle \\ &= 1+\frac{1}{N}\left\langle \sum_{j\neq k}\int\int e^{i\mathbf{Q}\cdot(\mathbf{r}-\bar{\mathbf{r}})}\delta(\mathbf{r}-\mathbf{R}_j^s(t))\delta(\bar{\mathbf{r}}-\mathbf{R}_k^s(t))d\mathbf{r}d\bar{\mathbf{r}}\right\rangle \\ &= 1+\frac{1}{N}\int\int e^{i\mathbf{Q}\cdot(\mathbf{r}-\bar{\mathbf{r}})}\left\langle \sum_{j\neq k}\delta(\mathbf{r}-\mathbf{R}_j^s(t))\delta(\bar{\mathbf{r}}-\mathbf{R}_k^s(t))\right\rangle d\mathbf{r}d\bar{\mathbf{r}} . \end{aligned} \tag{2.33}$$

We define $g(\mathbf{r}-\bar{\mathbf{r}})$, the radial distribution function as:

$$g(\mathbf{r}-\bar{\mathbf{r}}) = \left\langle \delta(\mathbf{r}-\mathbf{R}_j^s(t))\delta(\bar{\mathbf{r}}-\mathbf{R}_k^s(t))\right\rangle / V^2 , \tag{2.34}$$

with V the total accessible volume. Equation 2.33 becomes:

$$\begin{aligned} S(Q) &= 1+\frac{(N-1)}{V^2}\int\int e^{i\mathbf{Q}\cdot(\mathbf{r}-\bar{\mathbf{r}})}g(\mathbf{r}-\bar{\mathbf{r}})d\mathbf{r}d\bar{\mathbf{r}} \\ &= 1+\frac{N}{V}\int g(\mathbf{r})e^{i\mathbf{Q}\cdot\mathbf{r}}d\mathbf{r} , \end{aligned}$$

where we have assumed N to be large and $g(\mathbf{r}-\bar{\mathbf{r}})$ to have radial symmetry. This equation is more usually written to show the straight-through beam at zero angle explicitly:

$$S(Q) = 1+\frac{N}{V}\int (g(\mathbf{r})-1)e^{i\mathbf{Q}\cdot\mathbf{r}}d\mathbf{r}+\frac{N}{V}\delta(\mathbf{Q}) .$$

2.3.4 Measuring particle radii

In the dilute limit $g(\mathbf{r}) \to 1$, as therefore does $S(Q)$. When this occurs the Q-dependence of equation 2.31 is entirely contained within $P(Q)$. We would

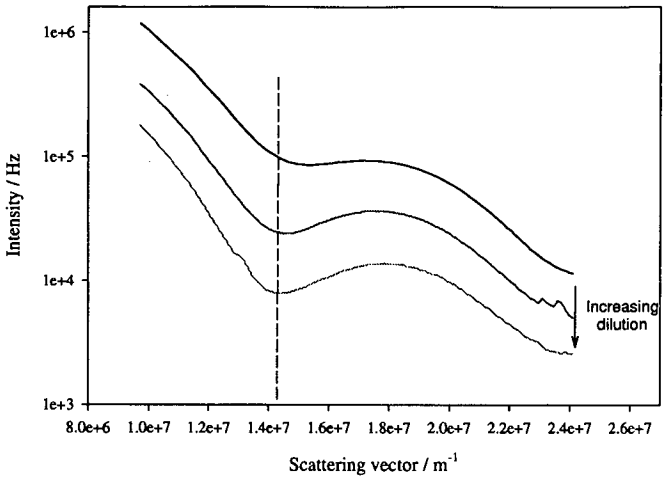

Figure 2.10: To find the form factor the solution is diluted until the position of the minima do not change on further dilution. Identifying the 1st minimum as $Q^1_{\min}R_c = 4.493$ gives a radius of 313nm, whereas the Pusey-van Megen method gives a mean radius of 310nm and a polydispersity of 11%.

expect a plot of intensity against angle for such a system to show minima at $Q^n_{\min}R = 4.493, 7.725, 10.904, \ldots$ (see section 2.3.2). This can be exploited to determine the radius of spherical colloidal particles. The intensity as a function of angle is measured using *static light scattering*, which is a well documented technique (see e.g. [21]). The dilute limit is reached when the position of the intensity minimum does not change on further dilution of the solution. The radius is then given by $R_c = 4.493/Q^1_{\min}$ (see figure 2.10).

This method of determining the radius makes two critical assumptions - that the particles are *homogeneous*, and *identical*. Neither assumption is likely to be correct. As discussed in chapter 1, the particles have a 'core-shell' structure. The relative sizes of the core and the shell can be found by fitting the form factor obtained to that calculated for such a structure, having as free parameters the total radius and the size of either the core or shell. Dingenouts and Ballauff [46] have suggested another method for finding the radius of the particle. They considered a spherically symmetric particle with radial variations in refractive index,

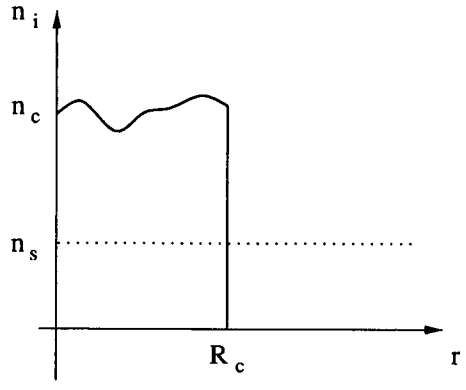

Figure 2.11: Refractive index profile for a radially optically inhomogeneous sphere.

an example of which is sketched in figure 2.11. By rewriting the refractive index at radius r as $n_{\mathrm{T}}(r) = n_c + \Delta n(r)$ where the first term is a fixed reference value, equation 2.24 now includes a term containing information about the internal optical structure of the particle:

$$b(Q, R_c) = 4\pi R_c^3 (n_c - n_s) \left(\frac{\sin QR_c - QR_c \cos QR_c}{(QR_c)^3} \right) + \frac{4\pi}{Q} \int_0^R r \Delta n(r) \sin Qr \; dr \; . \tag{2.35}$$

The second term is independent of the refractive index of the solvent and only reveals information on the internal structure of the particle. We exploit the dependencies of the two terms on n_s by varying this refractive index (usually by addition of small amounts of a similar solvent with a close refractive index e.g. tetralin added to *cis*-decalin) and finding the iso-scattering point where the resultant form factors cross. The intensity at this point is a constant and represents the scattering from the internal structure only. When this occurs the first term of equation 2.35 is zero i.e. we are at the minimum in the form factor. This occurs at $QR_c = \tan QR_c$. Thus the radius of the particle can once more be found. Figure 2.12 is taken from reference [21] to illustrate the method.

The assumption of identical particles is also likely to be wrong. The method by which these particles are synthesised results in a polydisperse sample - a range of particle sizes are present. The effect of polydispersity can be taken into

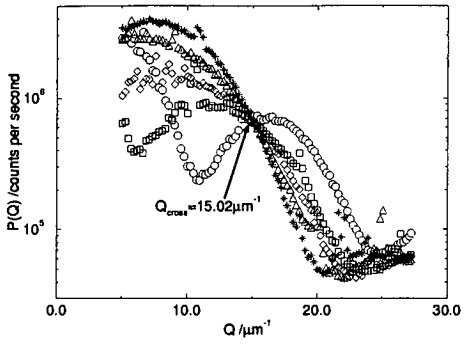

Figure 2.12: Form factors showing crossing point for a sample in which solvent refractive index n_s is varied. This procedure enables the radius R_{cross} to be determined to be $4.4934/Q_{\text{cross}} = 299 \pm 2nm$, which agrees with the fitted form factor value of $R_{\text{ff}} = 300\text{nm}$. Reproduced from [21].

account in two ways. The more accurate method is to calculate the theoretical form factor for a particular size distribution and refractive index profile of the particles and fit it to the experimental result. The free parameters for such a fit are the polydispersity, shape of distribution, core and shell thickness. In practice this is a very time consuming method [47]. A simpler method of measuring the polydispersity was developed by Pusey and van Megen [48]. They neglected the effect of any optical inhomogeneities in the particles and expanded the analytic expression for the intensity around the first minimum. They found that a small enough polydispersity σ can be estimated from the relative heights of the first minimum I^1_{min} and secondary maximum I^2_{max}:

$$\sigma^{-2} = 57.337 \frac{I^2_{\text{max}}}{I^1_{\text{min}}} - 15 \,, \tag{2.36}$$

and the mean radius is now given by

$$\overline{R_c} = 4.4934 \left(1 - \sigma^2\right) / Q_{\text{min}} \,. \tag{2.37}$$

The validity of some of the assumptions made in this method have been challenged [49] though it is expected that for polydispersities less than about 5% it should give reliable results.

As neither the radius, nor the polydispersity are crucial parameters in my work, I

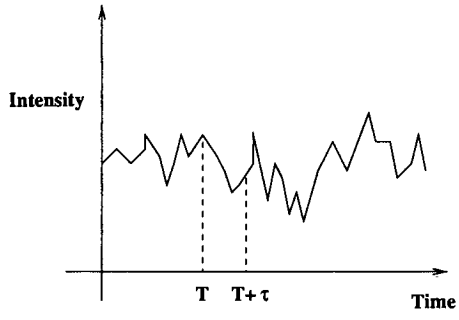

Figure 2.13: Intensity fluctuations due to moving scatterers. It is the temporal correlation of these fluctuations that are of interest.

used the Pusey-van Megen for obtaining both. Since the particles used crystallise, the polydispersity is unlikely to be too high (see section 2.1.2).

2.3.5 Dynamic structure factor

Previously we have considered the time averaged intensity; however there is considerable information to be gained from the time dependence of the intensity. The intensity at a particular time is given by

$$I(Q,t) = \left\langle \sum_j \sum_k b^*(\mathbf{Q}, R_j) b(\mathbf{Q}, R_k) e^{-i(\mathbf{Q}\cdot\mathbf{r}_j(t) - \mathbf{Q}\cdot\mathbf{r}_k(t))} \right\rangle , \qquad (2.38)$$

(see equation 2.30) - essentially a sum over the phases of the scattered electric fields. As the scatterers move, these phases change and the total intensity fluctuates about some mean value (see figure 2.13). The time correlation of these intensity fluctuations evidently contains information on the dynamics of the system. This is the basis of dynamic light scattering.

Consider the simplest example of a dilute[4] suspension of identical, hard spheres. The electric field scattered by this system at some scattering vector Q and time t is $\mathbf{E}(Q,t)$. Since the motion of the colloids is essentially random, the electric

[4]Here dilute means that the typical inter-particle spacing is such that the spatial correlations may be ignored.

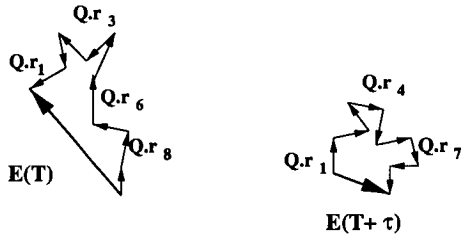

Figure 2.14: The electric field is essentially a random walk in two dimensions.

field can be represented by a two dimensional random walk of N steps, where N is the number of spheres (see figure 2.14). As N$\rightarrow \infty$ the probability distribution $P(\mathbf{E})$ becomes Gausssian [50]. Thus the probability distribution of the intensity $P(I =\mid \mathbf{E} \mid^2)$ is exponential in I:

$$P(I) = \frac{1}{< I >} e^{-\frac{I}{<I>}} . \tag{2.39}$$

Consider the statistics of such a system. Clearly the ensemble averaged electric field $< \mathbf{E}(Q,t) >$ is zero. The average intensity is given by

$$\begin{aligned} \langle I(Q,t) \rangle &= \left\langle \sum_j \sum_k e^{-i(\mathbf{Q}\cdot\mathbf{r}_j(t) - \mathbf{Q}\cdot\mathbf{r}_k(t))} \right\rangle \\ &= \left\langle \sum_{j=k} 1 \right\rangle + \sum_{j\neq k} \left\langle e^{-i(\mathbf{Q}\cdot\mathbf{r}_j(t))} \right\rangle \left\langle e^{-i(\mathbf{Q}\cdot\mathbf{r}_k(t))} \right\rangle \\ &= N , \end{aligned}$$

where the prefactors have been dropped as all the relevant quantities will turn out to be normalised. Next we consider the time correlation of the intensity $\langle I(Q,t)I(Q,t+\tau)\rangle = \langle I(Q,0)I(Q,\tau)\rangle$ if ergodic:

$$\begin{aligned} \langle I(Q,0)I(Q,\tau)\rangle &= \sum_j \sum_k \sum_l \sum_m \left\langle e^{-i(\mathbf{Q}\cdot\mathbf{r}_j(0) - \mathbf{Q}\cdot\mathbf{r}_k(\tau) + \mathbf{Q}\cdot\mathbf{r}_l(0) - \mathbf{Q}\cdot\mathbf{r}_m(\tau))} \right\rangle \\ &= \underbrace{N^2}_{j=k,l=m} + \underbrace{\sum_j \sum_k}_{j=m,k=l} \left\langle e^{-i(\mathbf{Q}\cdot\mathbf{r}_j(0) - \mathbf{Q}\cdot\mathbf{r}_j(\tau))} \right\rangle \left\langle e^{i(\mathbf{Q}\cdot\mathbf{r}_k(0) - \mathbf{Q}\cdot\mathbf{r}_k(\tau))} \right\rangle \\ &= N^2 + N^2 \mid \left\langle e^{-i(\mathbf{Q}\cdot\mathbf{r}(0) - \mathbf{Q}\cdot\mathbf{r}(\tau))} \right\rangle \mid^2 \\ &= < I(Q) >^2 + \mid \langle E(\mathbf{Q},0)E^*(\mathbf{Q},\tau)\rangle \mid^2 . \end{aligned} \tag{2.40}$$

We now define $g^{(2)}(Q,\tau)$ as the normalised intensity correlation function and the dynamic structure function $f(Q,\tau)$ as the normalised electric field correlation function, so that

$$g^{(2)}(Q,\tau) = 1 + f^2(Q,\tau) \,, \tag{2.41}$$

the so-called *Seigert* relation [43].

2.3.6 Dynamic light scattering

When viewed on a screen in the far field, the intensity variation of the scattered light manifests itself as an assembly of bright and dark regions known as speckles. The bright regions correspond to partly constructive interference of the scatterers, and the dark regions are where the interference is destructive. The aim of dynamic light scattering is to measure the intensity variation of this pattern with time. Ideally we would like to consider the intensity at one point only. Consider an infinitely small pinhole: at zero time delay the dynamic structure factor becomes $\langle E(Q,0)E^*(Q,0)\rangle / I(Q) = 1$. Thus the intensity correlation function evaluates as 2. For a pinhole of finite size we are taking a part-ensemble average as well as a time average and this manifests itself as a drop in this value (though it must always be greater than 1). This effect is often referred to as the *dynamic contrast* of the system. Including this contrast in the Seigert relation gives

$$g^{(2)}(Q,\tau) = 1 + \beta^2 f^2(Q,\tau) \,. \tag{2.42}$$

For the maximum contrast (and therefore the maximum useable data) β needs to approach unity. This is achieved by detecting at most a single speckle [51]. The linear size of a speckle l_{speckle} depends on the scattering volume V_s, the distance between the detector and the scattering volume l_d, the wavevector of the incident radiation k and the detection angle θ [43]:

$$l_{\text{speckle}} = 2\pi \frac{l_d}{V_s^{1/3} k \sin\theta} \,. \tag{2.43}$$

Good resolution is therefore achieved by using a small detection pinhole and a small scattering volume. The size of the scattering volume is controlled by imaging the centre of the sample onto an adjustable slit, and detecting in the far field from this slit. These are marked in figure 2.15 - the focusing lens is lens F, the detection pinhole is pinhole D and the scattering volume slit is slit S. Competing with the desire for a small pinhole and a small scattering volume is the need for a detectable photon flux. A photomultiplier tube has a 'dark count', a random output voltage even in the absence of light due to thermionic emission from the photo-cathode, and the detected signal needs to be significantly above this value. Any random noise has the effect of reducing the value β. To increase the signal to noise ratio, the laser beam is tightly focused (lens I) onto the middle of the cell. Since the cell and bath are both curved, there is an additional focusing effect from these. Noise from stray light is also a significant problem for light scattering. The laser beam is 'cleaned' using pinhole C, stray light is further removed by pinhole E and the light shield. Reflections from the cell surfaces are reduced by immersing the cell in a bath containing a tetralin-decalin mixture, arranged to have a refractive index similar to glass ($n_{\text{glass}} \sim 1.5$). Both the cell and the bath are made from high quality glass to minimise stray reflections. A neutral density beam stop is placed *within* the bath on the back wall to remove the reflection from the glass/air interface. Further, we only make measurements in the range $(0^+ \ldots \pi^-)$ on one side and a piece of black anodised aluminium is placed in the bath covering the other half to remove the scattering to that side. With these precautions we can regularly obtain a value for β of 0.96.

2.3.7 Detection and correlation

The detection system for a light scattering experiment consists of two parts: the photomultiplier tube (PMT) and a pulse amplifier discriminator. Their aim is to equate a single photon incident at the detection pinhole with a pulse that can be

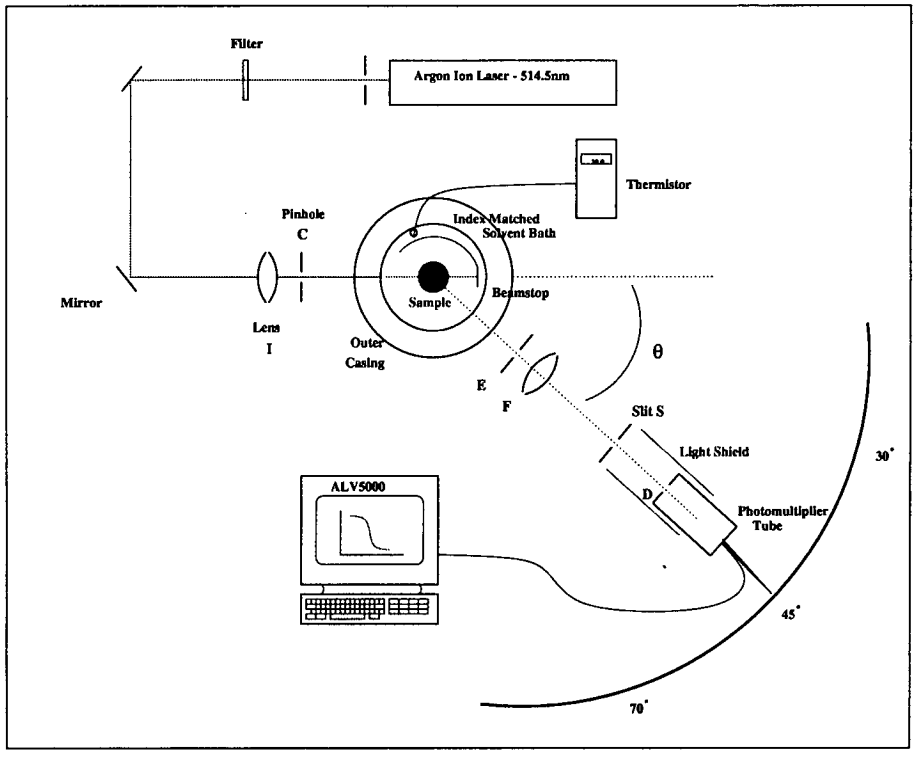

Figure 2.15: Schematic showing dynamic light scattering apparatus. The laser beam is cleaned by a pinhole and steered by two mirrors. It is focused by lens I onto the centre of a cell. The middle of the cell is imaged (at some angle θ) by lens F onto slit S, the size of which controls the effective scattering volume. The photomultiplier tube is in the far field from slit S and has a fixed radius pinhole D which controls the part of the speckle pattern sampled. The photomultiplier tube is connected to a pulse amplifier discriminater and a correlator, the output of which is fed into a computer. The sample cell is contained within an index matching solvent bath and contains a beamstop, a piece of black anodised aluminium to remove scattering to one side, and a thermistor probe (kept behind the aluminium to remove reflections). Pinhole C and E are added to minimise any stray light.

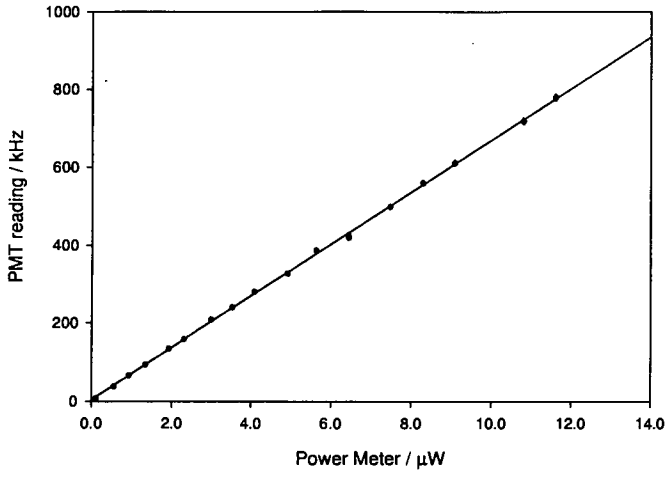

Figure 2.16: Characterisation of the dead time of the PMT. Within the range studied the transmitted laser power and the measured count rate were linearly dependent, implying that dead time effects can be neglected.

used by a correlator. The exact workings of a PMT can be found in a wide variety of texts (e.g. [52]) and here I mention only a few experimental considerations. All photomultipliers have an inherent dead time τ_D which is the time for the electron cascade to travel through the tube. Another photon arriving in this time will not be detected. Clearly the number of missed photons will be higher the greater the incident flux. A simple treatment assumes that if the incident flux is n then the number missed in the dead time is $n\tau_D$. The relationship between the measured flux n_c and the incident flux is therefore

$$n_c = \frac{n}{1 + n\tau_D} . \tag{2.44}$$

The incident flux at the pinhole can be found (to within a factor) by measurement of the transmitted laser intensity. The detected count rate at the PMT was found to be a linear function of this intensity within the range of count rates studied (to 800kHz - see figure 2.16) implying a dead time of much smaller than $\tau_D^{\max} \sim 1\mu$s. The effect of the dead time can therefore be neglected for correlations as low as

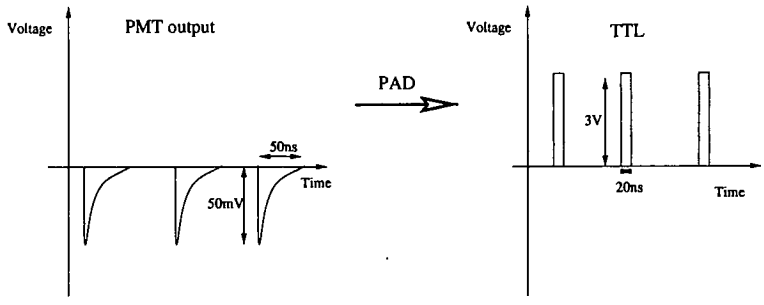

Figure 2.17: PMT-produced pulses and TTL pulses. The PAD converts between the two.

$\tau_D^{\max}$.

The output from the photomultiplier is small, short, negative pulses whereas we require TTL pulses for the correlator (figure 2.17). A pulse-amplifier discriminator (PAD) is used to convert between the two. Photomultiplier tubes often produce *afterpulses* caused by a positive ion that was generated during an electron cascade returning to the cathode (or early dynode) initiating a second electron pulse [52]. It is important that the PAD does not detect these pulses or an artificial correlation will be seen. The coupling between the PAD and the correlator must also be matched to avoid reflected pulses. After spending much time attempting to build a suitable PAD, it was decided to buy one specifically built for our application.

The output from the PAD is fed into a *correlator*, a device capable of obtaining the correlation function of an electronic signal. A schematic is shown in figure 2.18. The correlator contains a shift register and the total number of pulses arriving in a period is passed down the register. In addition it possesses a 'correlation function memory' (channel) which keeps a running total of the correlation between any two registers, i.e. the first channel contains $\sum_{i=1}^{M} n(t_i)n(t_{i-1})$ where M is the total number of sample times. In general

$$< I(0)I(mT) >= \frac{1}{M}\sum_{i=1}^{M} n(t_i)n(t_{i-m}) \; . \tag{2.45}$$

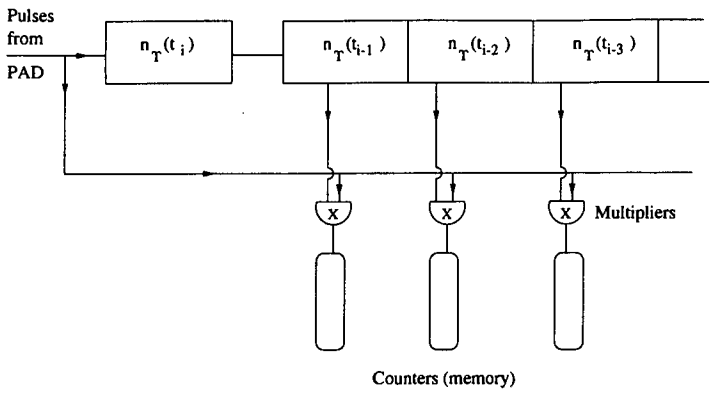

Figure 2.18: Schematic of a correlator.

Often logarithmically spaced channels are used. The correlator used in this work has 250 channels which allows correlations on scales from $10^{-7} - 10^{3}$ seconds.

2.3.8 Temperature control

Diffusion is dependent on temperature so it is necessary to know the temperature within the sample cell. Further, it is highly desirable to be able to adjust this temperature; we know, for example, that the size of the polymer is temperature dependent. Temperature control in my DLS apparatus is maintained by circulating water through the metal holder (see figure 2.20a). By heating the holder from above and below we partially eliminate convective effects within the solvent bath. However the bath has a thin coupling layer of silicone oil on its base providing better thermal contact from below, so it is inevitable that convection cannot be neglected completely. Whilst convection within the solvent bath will not significantly affect the results, convection within the *cell* can easily corrupt the data. To reduce this effect, the cell is immersed within the solvent to above the level of the sample, but large temperature differences between the bath and the environment should still be avoided. Experimentally we find no unexpected temperature effects within the range $15 - 30°C$. The sample should however be given at least three minutes to equilibrate before measurements are taken. Having

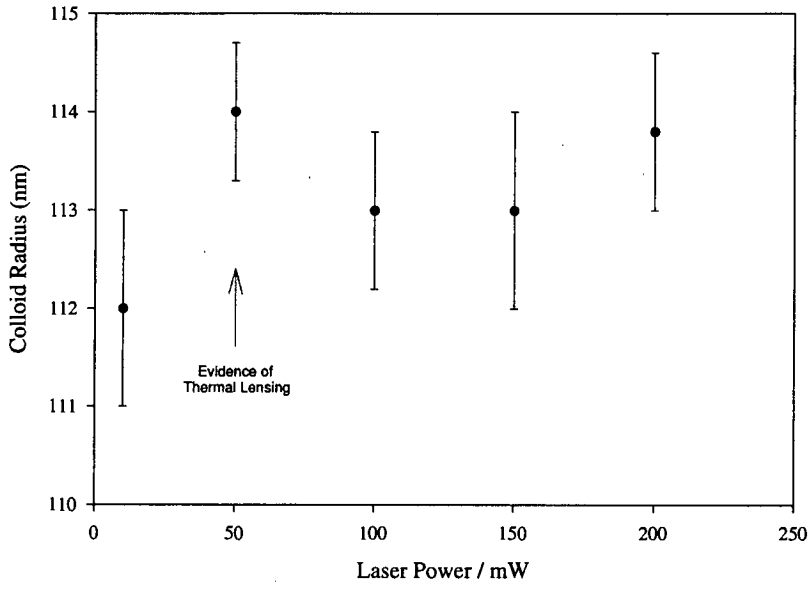

Figure 2.19: Plot of measured radius against incident laser power for a well characterised test sample. Thermal lensing was seen to occur at 50mW, though the data remains uncorrupted at intensities up to 200mW.

reached equilibrium the temperature of the sample is within $0.1°C$ of the bath[5] and the latter is recorded by a thermistor.

Convection can also be caused within the sample by *thermal lensing*. As the laser passes through the sample it heats it, changing the local refractive index. Experimentally this is seen as a widening of the straight through beam when the laser is first incident. To test the importance of this effect, measurements were made on a well characterised test sample at varying laser powers up to 200mW. At laser powers above 50mW, thermal lensing was seen to occur; however, as the results in figure 2.19 show, this did not affect the results obtained. Nevertheless, the laser power was kept as low as possible, and always under 80mW.

[5]This is found by several measurments over time of the temperature within a test sample cell using a thermistor.

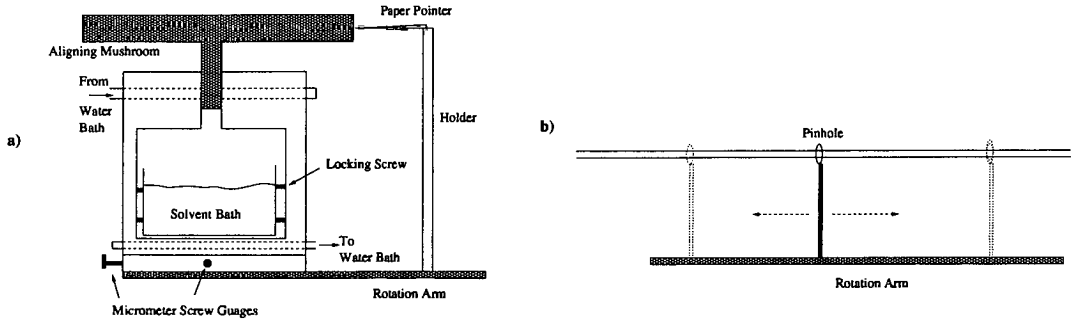

Figure 2.20: Schematic of cell holder and alignment procedure. a) A paper point is placed just touching a metal 'mushroom', the position of the holder is adjusted using the two micrometer screws gauges until the paper remains in contact at all angles.b) A pinhole is slide along the detection arm in the beam stop position to check the vertical alignment of the beam.

2.3.9 Angular range

Dynamic light scattering should be able to measure the dynamic structure function over a wide range of angles (theoretically from just greater than zero degrees to just less than one hundred and eighty); the dependence on angle can be used to obtain information even on a dilute system (e.g. polydispersity [48]). However to obtain reliable data over a range of angles requires precise alignment of the apparatus. The alignment procedure is mainly concerned with ensuring the centres of the cell, the solvent bath and the rotation arm are coaxial. The alignment takes roughly one day to complete according to the following procedure:

- The rotation arm is centred on the cell holder - A metal 'mushroom' is placed in the position of the cell and a paper pointer attached to the rotation arm (see figure 2.20a). The whole holder array is mounted on a moveable plate whose position is controlled by two perpendicular screw gauges and it is moved until the paper pointer registers no deflection when the rotation arm is moved throughout its entire range.

- The solvent bath is centred on the cell holder - The solvent bath is placed

within the holder and locked into place by three sets of screws. A similar procedure to above is used to check that the solvent bath is coaxial with the rotation arm.

- The laser is centred on the cell holder - The mushroom is replaced with a metal pin and the laser steered by adjustable mirrors until hitting the pin. Lens I is added to focus the beam onto the pin. The deviation from horizontal is measured by placing a pinhole at various distances on the far side (figure 2.20b).

- The detection arm is aligned - A strongly scattering sample is placed in the equipment and the rotation arm swung away from zero degrees. Lens F is placed on the detection arm and the light focused on slit S. This slit should be at the centre of the focused image at all angles, which can be used as a good check of the previous steps. The PMT is added and the detection pinhole centred on the scattered beam.

- The detection pinhole is optimised - On the PMT used the detection pinhole was a fixed size. The length between the pinhole and slit S is adjusted until the best intercept is seen (here we use a typical sample). This optimisation is a balance between minimising the amount of speckle and maximising the amount of light received. For each angle and sample the incident flux changes. Rather than move the pinhole each time, the PMT is fixed in position and the width of slit S changed to increase (or decrease) the size of the scattering volume. Measurements show that, as expected, this only changes the intercept β and not the shape of the dynamic structure factor.

The 'quality' of the alignment can be checked by two methods; obtaining a high intercept and, more importantly, checking the Q^2-dependence of a dilute sample. The exact details of this dependence will be discussed later, but for 'standard' samples the diffusion coefficient obtained at all angles should be the same. Figure

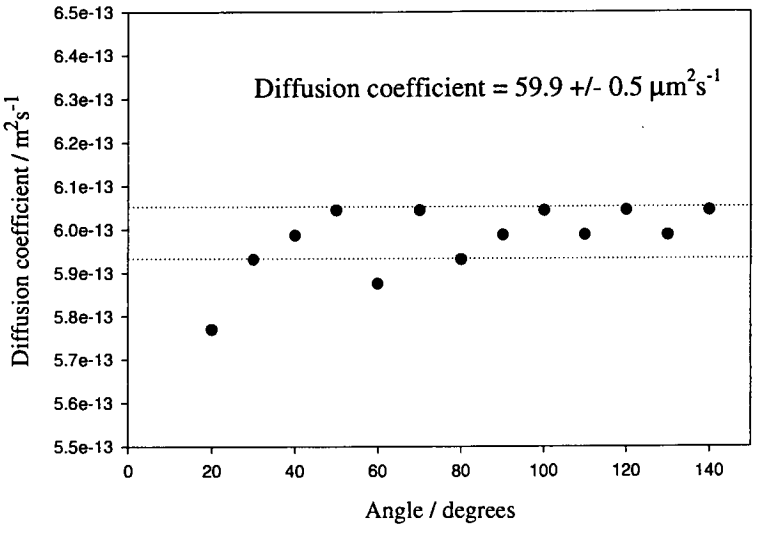

Figure 2.21: Test of alignment of DLS apparatus. The equipment is found to give consistant results within the range $30° - 140°$. The accuracy of a single measurement within this range is roughly 1%.

2.21 shows typical results and indicates the usuable angular range, and accuracy, of the equipment. It is found that for an accuracy of 1% a single measurement of at least 3 minutes is needed, though for weakly scattering samples this can increase up to several hours. For samples with a low scattered intensity, better results are obtained by averaging multiple runs than from one long run. The alignment is checked by this method every month and is found to remain constant over a period of up to four months.

2.3.10 Multiple scattering

Dynamic light scattering gives useful data only if the sample is relatively transparent. For more concentrated samples, or samples with a poor index match, multiply-scattered light contibutes to the intensity received at the pinhole. The

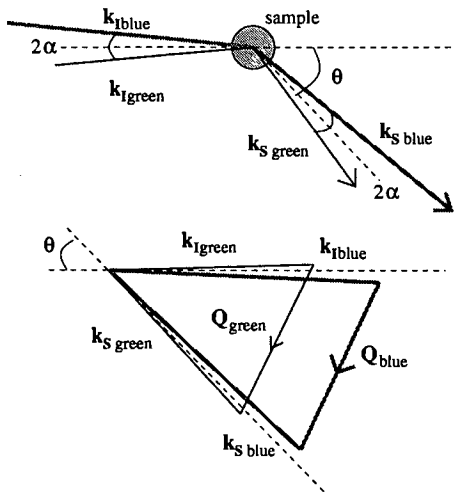

Figure 2.22: Scattering vector diagram for two colour dynamic light scattering. For every angle θ there corresponds an angle α such that the intermediate scattering wavevectors $\mathbf{Q}_{\text{Green}}$ and $\mathbf{Q}_{\text{Blue}}$ are equal. Reproduced from [51].

relations between this intensity and the properties of the medium are complex [51]. Two colour dynamic light scattering was developed to overcome this problem by selecting only singly-scattered light for correlation. This technique is described in detail in [51]. The basic idea is to illuminate the sample with two laser beams (green and blue) and to arrange two detectors so that the scattering vector for each beam-detector pair is identical (figure 2.22). The *cross*-correlation of the two beams is then recorded. For singly-scattering light the electric field of the scattered light at time t is proportional to the amplitude of the $\mathbf{Q}^{\text{th}}$ spatial Fourier component of the refractive index variation in the medium (equation 2.23). If we have the same scattering vector for both beams then the *auto*-correlation of each as well as the cross-correlation should be identical.

However the same is not true of multiply-scattered light. As figure 2.23 shows, although the total scattering vectors are the same in each case, the intermediate scattering vectors are in general different. Thus the detectors are probing different Fourier components of the refractive index profile of the sample. It can be shown that different spatial Fourier components are statistically independent

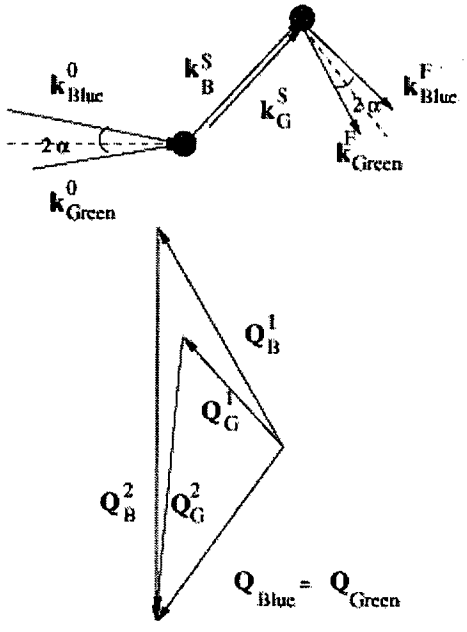

Figure 2.23: Scattering vector diagram for a double scattering event. Although the total intermediate scattering wavevectors are equal ($\mathbf{Q}_{\mathrm{Green}} = \mathbf{Q}_{\mathrm{Blue}}$), their retrospective components differ resulting in uncorrelated signals between the two detectors. Reproduced from [51].

and undergo uncorrelated temporal fluctuations, so the cross-correlation of the doubly scattered light both with itself and with the singly-scattered light is independent of time and contributes only to the 'baseline'. Higher order scattering is also removed from correlation by a similar principle.

We can derive this quantitatively if we define the total electric field of the scattered blue/green light as $\mathbf{E}_{\mathrm{B/G}}(\mathbf{Q},t)$, and that of singly/multiply-scattered light as $\mathbf{E}^{s/m}_{\mathrm{B/G}}(\mathbf{Q},t)$ where $\mathbf{Q}$ is the *total* scattering vector. The quantity we measure (or hope to measure) in dynamic light scattering in this terminology is

$$f(\mathbf{Q},\tau) = \left\langle \mathbf{E}^s_{\mathrm{B/G}}(\mathbf{Q},t)\mathbf{E}^s{}_{\mathrm{B/G}}(\mathbf{Q},t)\right\rangle \ . \tag{2.46}$$

The cross correlation of the singly-scattered light becomes

$$\frac{\langle I^s_B(0)I^s_G(\tau)\rangle}{\langle I^s_B\rangle\langle I^s_G\rangle} = 1+\beta^2_{\mathrm{ov}}\beta^2[f(\mathbf{Q},\tau)]^2 \ . \tag{2.47}$$

The additional factor β^2_{ov} comes from the incomplete overlap of the scattering

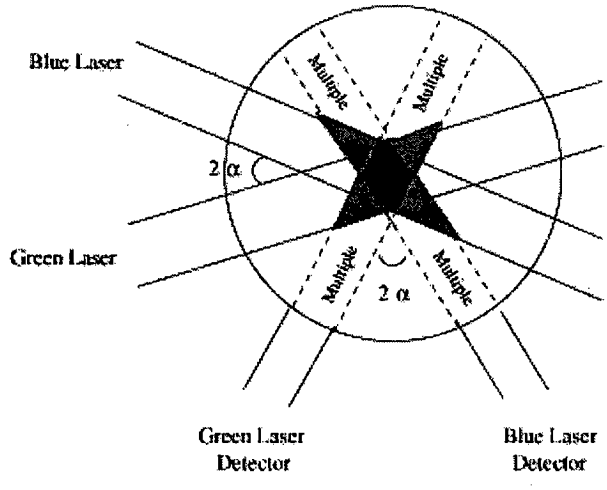

Figure 2.24: Scattering and overlap volumes in two colour dynamic light scattering. Each pinhole receives light only from between the broken lines connecting to it. The medium shaded areas either (i) scatter from only one laser or (ii) are viewed by only one detector. The darkest region is illuminated by both laser beams and seen by both detectors. The areas marked 'multiple' are sampled by the PMTs but are not directly in the incident beams so light detected from these areas has been multiply-scattered. The drawing is not to scale, in particular the overlap region is much larger. Reproduced from [51].

volumes of blue and green light (figure 2.24). In autocorrelation, light is received from either grey region whereas for cross correlation light is only received from the overlap of these two regions. β_{ov} has the form

$$\beta_{\text{ov}} = \frac{\left\langle I^s_{\text{B,OV}} \right\rangle \left\langle I^s_{\text{G,OV}} \right\rangle}{\langle I^s_B \rangle \langle I^s_G \rangle} , \tag{2.48}$$

where $\left\langle I^s_{\text{B,OV}} \right\rangle$ is the intensity of light scattered from the overlap volume.

When the cross correlation of the total scattered light $g^{(2)}_C(\mathbf{Q}, \tau)$ is considered one finds a similar form:

$$g^{(2)}_C(\mathbf{Q}, \tau) = 1 + \beta^2_{\text{ms}} \beta^2_{\text{ov}} \beta^2 [f(\mathbf{Q}, \tau)]^2 , \tag{2.49}$$

where

$$\beta^2_{\text{ms}} = \frac{\langle I^s_B \rangle \langle I^s_G \rangle}{\langle I_B \rangle \langle I_G \rangle} \tag{2.50}$$

gives the intensity of singly-scattered light to total scattered light. Consider a dilute sample: far from the form factor minimum there should be little multiply-scattered light and so $\beta_{\rm ms}^2 \approx 1$. A measurement of the intercept of the cross correlation function gives a value for $\beta_{\rm ov}^2\beta^2$ which is typically about 0.5-0.6. Repeating the experiment for the sample of interest allows calculation of $\beta_{\rm ms}^2$ for that sample (if it lies within the experimentally accessible range of 0.01 to 1). From equation 2.50 we have that

$$\begin{aligned} \beta_{\rm ms}^2 &= \frac{[\beta_{\rm ms}^2\beta_{\rm ov}^2\beta^2]^{\rm concentrated}}{[\beta_{\rm ov}^2\beta^2]^{\rm dilute}} \\ &\approx \left[\frac{\left\langle I_G^{\rm single}\right\rangle}{\left\langle I_G^{\rm total}\right\rangle}\right]^2 , \end{aligned} \tag{2.51}$$

where the approximation is due to the λ^{-4} scattering causing slight differences between the intensities of the blue and green light. Using TCDLS we can obtain both the magnitude of the multiple scattering and the correlation function of the singly-scattered light.

2.3.11 TCDLS - experimental setup

To achieve the requirement that the 'detector to input' scattering vector is the same for both green and blue light, the apparatus shown in figure 2.25 is used. The blue and green laser beams enter the sample separated by an angle 2α, which is generally of the order of 1°, and are then detected in directions also separated by 2α. If the midpoint angle is θ (see figure) then the requirement for identical **Q** is that

$$\frac{\sin\left(\frac{\theta_G}{2}\right)}{\lambda_G} = \frac{\sin\left(\frac{\theta_B}{2}\right)}{\lambda_B} \tag{2.52}$$

and

$$\tan\alpha = \left(\frac{\lambda_G - \lambda_B}{\lambda_G + \lambda_B}\right)\tan\frac{\theta}{2} . \tag{2.53}$$

A mirrored prism is used to reflect the lasers onto a lens. As the prism is moved along the direction shown in figure 2.25 the beams change their linear separation

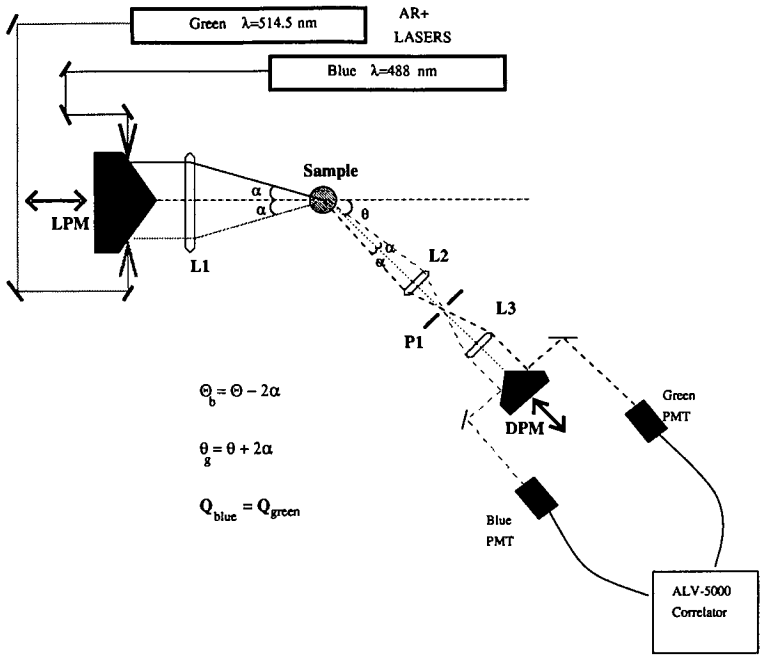

Figure 2.25: Schematic of two colour dynamic light scattering apparatus. LPM and DPM are moveable prisms and L1, L2 and L3 are lenses.

on the lens and therefore their angle separation at the sample. Another prism is used on the detection arm. Alignment of the TCDLS apparatus is difficult and a complete alignment takes several weeks [53].

2.4 Interpreting dynamic light scattering data

The aim of dynamic light scattering is to relate the dynamic structure function to some property of the medium. The interpretation of the data obtained by this method is not a trivial affair; in general one must consider interactions between particles due to both the inter-particle potential and *hydrodynamic* forces carried through the suspending fluid. Consider first a dilute system of spherical colloids with negligible hydrodynamic interactions. Each particle only interacts with the suspending fluid. This interaction can be broken into two parts: a rapidly varying force due to the random collisions of solvent molecules on the colloid and a

systematic frictional force on the colloid due to its motions. For large particles (with respect to the solvent molecules) this systematic force may be calculated assuming the suspending medium to be a continuum (see for example [54]). For low Reynolds numbers it is found to be directly proportional to the velocity of the Brownian particle, and the constant of proportionality is called the *friction coefficient.* For a sphere with stick boundary conditions the friction coefficient is given by $\zeta_0 = 6\pi\eta R$ where η is the viscosity of the suspending medium and R the radius of the colloid.

The characteristic timescale for Brownian motion is given by $\tau_B = M/\zeta_0$ where M is the mass of the colloid. At times short compared to this time the motion of the colloid is *ballistic*, whereas for times long compared to this time the momentum coordinate of the colloid is in equilibrium with the solvent [43]. For a typical colloid the Brownian time is approximately 10^{-9}s whereas with dynamic light scattering we typically probe timescales on the order of microseconds. Thus only the diffusive motion of the Brownian particles should be detected.

At times long compared to the Brownian time regime the particle's motion describes a random walk in three dimensions. The *diffusion coefficient* D_0 for non-interacting particles is defined by

$$< \Delta r^2(t) >= 6D_0 t \,, \tag{2.54}$$

where $< \Delta r^2(t) >$ is the mean square displacement after time t. The dynamic structure function may now be written as

$$\begin{aligned} f(Q,\tau) &= \left\langle e^{i\mathbf{Q}\cdot(\mathbf{r}(0)-\mathbf{r}(\tau))} \right\rangle \\ &= \int e^{i\mathbf{Q}\cdot\mathbf{\Delta r}} P(\mathbf{\Delta} r) d^3(\mathbf{\Delta} r) \,, \end{aligned} \tag{2.55}$$

where $P(\mathbf{\Delta} r)$ is the probability that a particle will be displaced by a distance $\mathbf{\Delta} r$ in a time t. Since $\mathbf{\Delta} r$ is a Gaussian quantity this integral becomes

$$f(Q,\tau) = e^{-\frac{Q^2 < \Delta r^2(t) >}{6}} \,, \tag{2.56}$$

and substituting in equation 2.54 gives

$$f(Q,\tau) = e^{-Q^2 D_0 t} . \tag{2.57}$$

The diffusion coefficient for a dilute system is given by the Stokes-Einstein equation

$$D_0 = \frac{k_B T}{\zeta_0} = \frac{k_B T}{6\pi\eta R} , \tag{2.58}$$

where k_B is Boltzmann's constant and T the temperature. This forms the basis of yet another method for characterising the radii of particles. A log-linear graph of the dynamic structure factor against time has a slope of $Q^2 D_0$ from which the radius can be calculated. This is the *hydrodynamic* radius, which characterises the drag on the particle.

2.4.1 Method of cumulants

As mentioned in section 2.3.4, all real colloids are polydisperse implying a range of diffusion coefficients present in the sample. In a dilute sample the dynamic structure factor is a sum of exponentials weighted by the scattering intensity of each species.

$$f(Q,\tau) = \int_0^\infty d\Gamma G(\Gamma) e^{-\Gamma\tau} . \tag{2.59}$$

$\Gamma = Q^2 D$ is the decay constant. Ideally to obtain the distribution $G(\Gamma)$ we would measure the dynamic structure factor and apply a Laplace inversion. In general though even small amounts of noise in the measurement convert to large uncertainty in the distribution [55]. Another method for determining information about the system is based on expanding the exponential in equation 2.59 about the mean value $\bar{\Gamma}$ defined as

$$\bar{\Gamma} = \int_0^\infty d\Gamma G(\Gamma)\Gamma . \tag{2.60}$$

Thus

$$e^{-\Gamma\tau} = e^{-\bar{\Gamma}\tau} e^{-(\Gamma-\bar{\Gamma})\tau}$$

$$= e^{-\bar{\Gamma}\tau}\left(1-(\Gamma-\bar{\Gamma})\tau+\frac{(\Gamma-\bar{\Gamma})^2\tau^2}{2!}-\frac{(\Gamma-\bar{\Gamma})^3\tau^3}{3!}+\ldots\right) \quad (2.61)$$

and the equation 2.59 becomes

$$\ln[f(Q,\tau)] = 1-\bar{\Gamma}\tau+\frac{1}{2!}\left(\frac{\mu_2}{\bar{\Gamma}^2}\right)(\bar{\Gamma}\tau)^2-\frac{1}{3!}\left(\frac{\mu_3}{\bar{\Gamma}^3}\right)(\bar{\Gamma}\tau)^3\,, \quad (2.62)$$

where

$$\frac{\mu_n}{\bar{\Gamma}^n} \equiv \frac{1}{\bar{\Gamma}^n}\int_0^\infty (\Gamma-\bar{\Gamma})^n G(\Gamma)d\Gamma \quad (2.63)$$

are the normalised moments about the mean of $G(\Gamma)$ and are known as the cumulants of the expansion. Of particular interest is the second cumulant which gives information on the variance of the diffusion coefficient.

This expansion is exact if all terms in the expansion are kept; however it is rather laborious to fit all orders and for narrow, symmetric distributions it is found that three-term analysis is sufficient to describe the data over a wide range. The two chosen end points of the fit can affect the value of the cumulants obtained and the following procedure is observed to minimise any effect of noise.

- Find the first data point for which the decay is evident above noise (t_{start}). For a logarithmic correlator of the type used in these experiments, the initial channels are close together (10^{-6}s) and the correlation function will not have decayed significantly between channels (see inset in figure 2.26).
- Now apply a linear, quadratic and cubic fit to all the remaining data points to obtain the cumulants.
- Fit to successively less and less points by changing the final endpoint (t_{end}), e.g. if the original fit was over channels 7-120, then the successive fits might be 7-100, 7-80 and so on (figure 2.26). The linear fit has less parameters so will be the most stable as the number of data points is reduced.

The last step is labour intensive and is usually left to a computer to do. A plot of the parameters obtained provides information on the system. Consider the following cases:

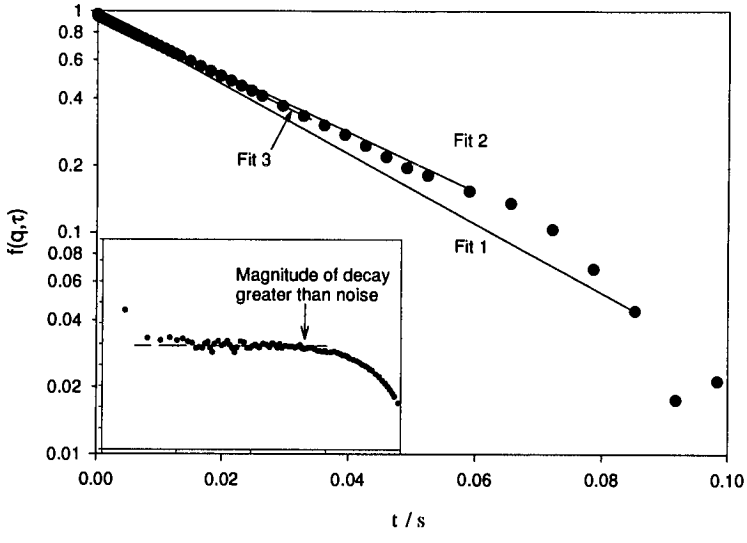

Figure 2.26: Method for obtaining low order cumulants. When fitting the data, two end-points must be chosen for the fit. The lower (t_{start}) is selected as the point where the magnitude of the decay is greater then noise (see inset). The upper point (t_{end}) is initially taken as the last data point available and then progressively stepped to shorter times.

- Monodisperse data (figure 2.27). The linear fit should provide a first cumulant that does not vary as the number of fitting points is changed. The second and third cumulants obtained by higher order fits should be zero.

- Polydisperse data (figure 2.28). The first cumulant obtained from the linear fit will vary as the number of fitting points is reduced whereas that obtained from the quadratic and cubic fits should be constant. The second cumulant from these fits should now be constant over the range.

This procedure works very well for non-interacting systems. In an interacting system the diffusion coefficient may well be a function of time. In this case the method can still be used, but the cumulants should be extrapolated to their value at t_{start}. By varying t_{start} the cumulants can be found as a function of time. This technique is known as a *stepped cumulant fit.*

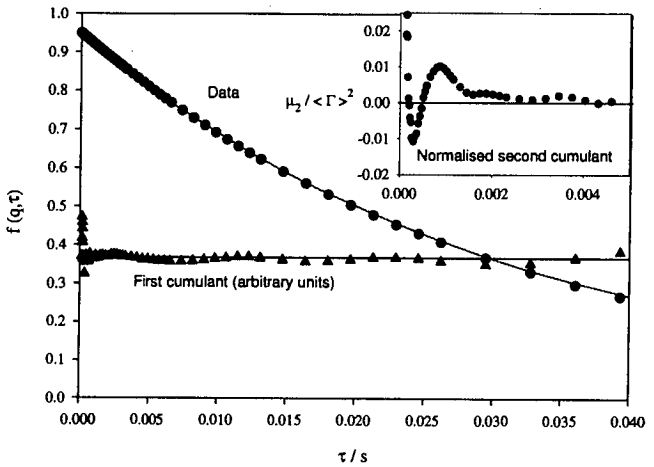

Figure 2.27: Cumulants for monodisperse spheres. The circles represent the dynamic structure factor, the triangles are the first cumulants from a linear fit which do not vary significantly whatever value for t_{end} is used. The average value is used to calculate the line that runs through the circles. The inset contains the normalised second cumulant obtained from a quadratic fit. Its average value is close to zero implying little polydispersity. The second cumulant is significantly more susceptible to noise than the first cumulant obtained from a linear fit.

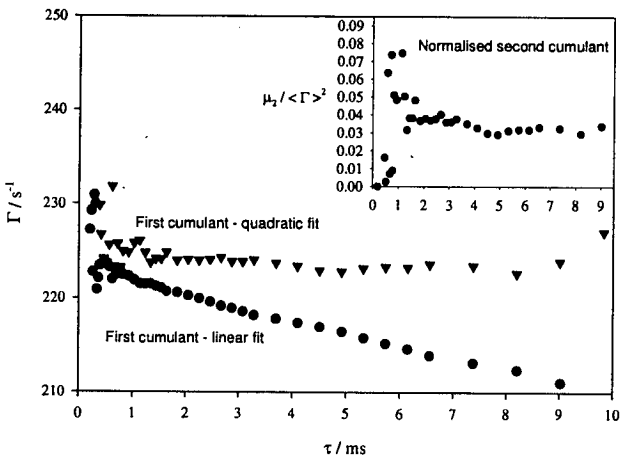

Figure 2.28: Cumulants for polydisperse spheres. The circles represent the first cumulant of a linear fit which are directly proportional to t_{end}. The triangles are the first cumulant of the second order fit and do no show any dependence on t_{end}. The decay constant for this sample is 225s^{-1}. The normalised second cumulant is (inset) 0.04. The data (not shown) is clearly well described by its first two cumulants.

2.5 The swelling of PMMA particles by tetralin

As mentioned in section 2.1 PMMA spheres are usually synthesised in dodecane and then placed in *cis*-decalin for experimental use. The refractive index match, while good, is sometimes not enough for some purposes. At volume fractions of >1% the suspension starts to look milky, implying significant multiple scattering is occuring. For this reason tetralin is often added to the solvent to contrast match the colloid and suspensions with volume fractions up to 50% can appear transparent. It is known that the tetralin can be absorbed into the PMMA spheres (tetralin is a good solvent for PMMA), but there is suprisingly little published work on the effect of this absorbtion. Manoharan heated PMMA particles to 80°C in mixtures of various compositions and used DLS to study the radius of the particle after 2.5 hours. He found that the particles swell by as much as 70% in pure tetralin [56], though saw no noticeable swelling at the index match ratio of roughly 1/3 tetralin. Martelozzo studied the apparent shift in the melting volume fraction as the solvent was changed from pure *cis*-decalin to an index matching *cis*-decalin/tetralin mixture. She found that the radius increased by 1% over a period of several weeks [57]. In my study I decided to measure the effect of tetralin on the PMMA over short times (minutes and hours as opposed to months and years) using both static and dynamic light scattering.

2.5.1 Experimental procedure

Three sets of PMMA spheres were characterised in *cis*-decalin by both static and dynamic light scattering (see table 2.1). To study the short time dynamics of the swelling, a drop of the colloid in *cis*-decalin was added to a volume of tetralin ($\sim$ 2cm^3) and shaken rapidly. Lavery *et al.* [58] found that mixing solvents in this manner can lead to an effect in which the PMMA sphere becomes 'coated' in a thin layer of the original solvent. This layer changes the boundary conditions

Name	DLS	SLS
P4	112nm	-
P5	144nm	134nm
P6	175nm	166nm

Table 2.1: Radii of three sets of PMMA latices characterised by static (SLS) and dynamic (DLS) light scattering. The two methods measure different radii; SLS measures the scattering radius and DLS measures the hydrodynamic radius. P4 shows no form factor minimum within the angular range accessible by SLS so its radius cannot be determined by this method.

between the spheres and the solvent which modifies the Stokes-Einstein relation (equation 2.58).

$$D_{\text{coated}} = \frac{k_B T}{\alpha \pi \eta R}, \tag{2.64}$$

where α is a number between 4 and 6. This is seen as an increase in the diffusion coefficient measured by dynamic light scattering which, if not accounted for in this way, could be mistakenly interpreted as a decrease in the particle's radius. The coating appears to form instantly on the mixing of the solvents, and desorbs from the particle over a period of several weeks. In our system, measurements of the radius immediately after mixing showed no variation from their values in *cis*-decalin, indicating that the Lavery effect was not significant in this work. To avoid any concentration-dependent effects, the initial volume fractions of the particles in tetralin were ensured to be the same for each of the three sets of particles used. Furthermore, for each set of particles two volume fractions were used - dilute ($\varphi \approx 0.01\%$) and concentrated ($\varphi \approx 0.1\%$). The refractive index difference between the particles and tetralin is high (at least initially, as the tetralin enters the particles the difference decreases) so for the concentrated samples the effect of multiple scattering cannot be ignored.

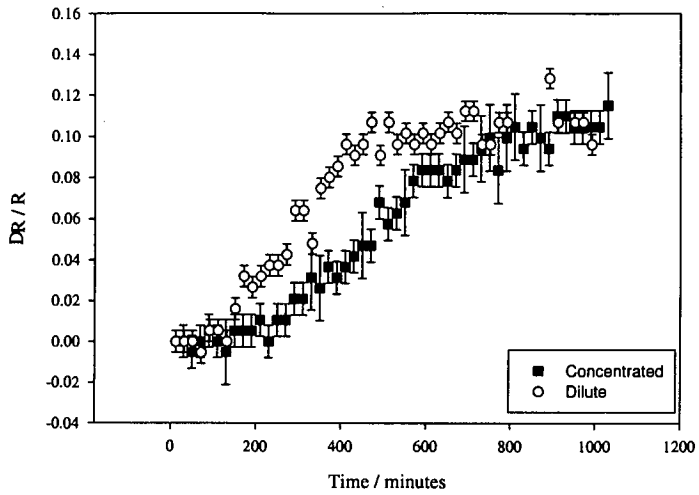

Figure 2.29: Change in radius DR of PMMA spheres by tetralin as measured by DLS. The results for concentrated (black squares) and dilute (white circles) show similar behaviour. These results were obtained from measurements on P6, though both P4 and P5 showed similar behaviour.

2.5.2 Results - dynamic light scattering

Dynamic light scattering was performed at an angle of 50 degrees (corresponding to a scattering vector of $Q = 15.9 \times 10^6 \mathrm{m}^{-1}$) at five minute intervals for 17 hours. The results were interpreted using a cumulant analysis and it was found that a linear fit to the data was appropriate (i.e. polydispersity was not significant). As figure 2.29 shows both the concentrated and dilute samples gave similar results. All sets of particles showed an increase in radius with time and a final radius R_{final} was reached typically 10% larger than the original radius (figure 2.29). The time taken for R_{final} to be reached (t_{final}) varied from sample to sample. A summary of the radius change and the time taken to reach it is shown in table 2.2.

Experiments were then performed on a daily basis for a period of 12 days. No further swelling was seen.

Sample	$R_{\text{final}}/R_{\text{start}} - 1$	t_{final}
P4	10%	16.7 hours
P5	6%	5 hours
P6	10%	10 hours

Table 2.2: The swelling of PMMA spheres in tetralin as measured by dynamic light scattering. $R_{\text{final}}/R_{\text{start}}$ is the ratio of final to original radii. t_{final} is the time taken for the final radius to be reached which varies considerably from sample to sample.

2.5.3 Results - static light scattering

Static light scattering was performed on the sample over the range: $5.4\times10^{6}\text{m}^{-1} < Q \leq 3.8 \times 10^{7}\text{m}^{-1}$. One angular sweep took roughly 90s. Successive angular sweeps occured at five minute intervals for a period of 7 hours. The results are considerably harder to interpret than those from dynamic light scattering. P4 is the smallest particle and its radius cannot be found by SLS as the form factor minimum cannot be seen within this Q-range. The time evolution of the form factor on addition of tetralin is shown in figure 2.30. The intensity of scattered light decreases with time, from which we can infer that tetralin is entering the particle reducing the refractive index difference between it and the solvent. Figure 2.31 shows the evolution of the form factor for P6. The form factor minimum moves from $Q = 4.49/R_{\text{unswollen}}$ to higher Q and simultaneously the minimum is smeared out. The form factor continues to evolve throughout the experiment. Work on P5 in both concentrated and dilute solutions showed similar behaviour. Additional experiments monitored the form factor over a 12 day period and further evolution was seen throughout this period.

As the tetralin soaks into the particles it changes the refractive index profile and a core-shell structure is likely to occur in which the tetralin has only reached a radius r_s after time t. Some progress in understanding this profile may be made if we assume a two step function - figure 2.32. This model neglects the existence

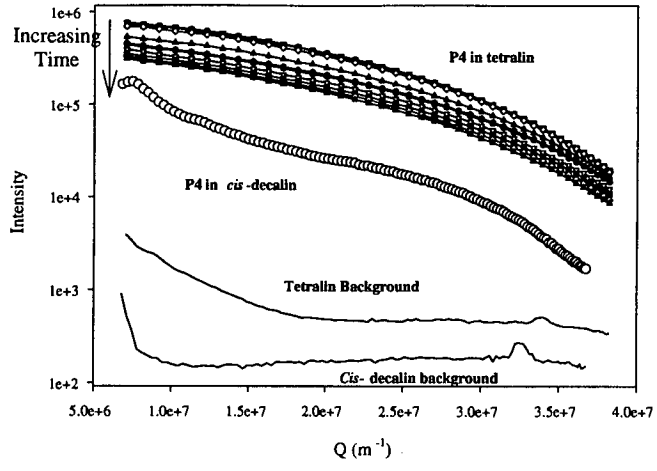

Figure 2.30: The static structure factors for P4 in tetralin (represented by small black and white symbols) are shown at 25 minute intervals. The reduction in intensity is due to the tetralin entering the particles and reducing the refractive index difference. Also shown is the form factor for P4 in *cis*-decalin (white circle), and the intensity scattered by the solvents (black lines, no symbols).

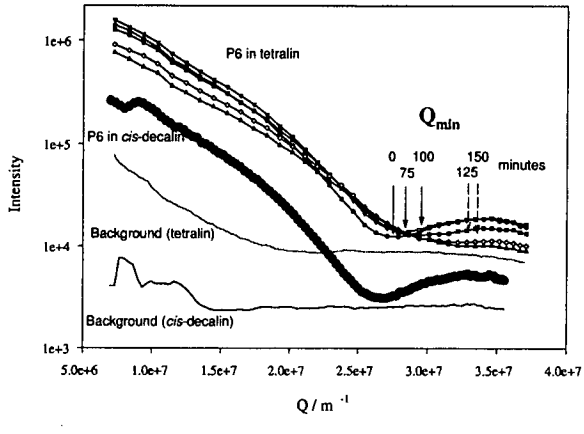

Figure 2.31: The static structure factors for P6 in tetralin (represented by small black and white symbols) show a minimum that moves to higher Q. This minimum is also smeared out and at times greater than about 125 minutes cannot easily be seen. Also shown is the form factor for P6 in *cis*-decalin (black circles), and the intensity scattered by the solvents (black lines, no symbols).

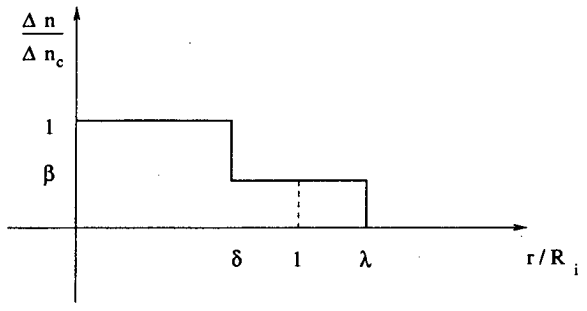

Figure 2.32: Core-shell refractive index profile for a particle in tetralin. R_i is the initial radius and Δn_c the initial (and core) refractive index difference between the particle and the solvent. When placed in tetralin, the particle swells and has a final radius of λR_i. The tetralin enters the swollen particle to a depth δR_i. The refractive index difference of the shell with the solvent is related to that of the core and the solvent by $\beta \Delta n_c$.

of the PHSA shell and assumes that as the tetralin penetrates the particle it both swells it and decreases its refractive index. The refractive index profile of the particle is thus characterised by three parameters: β - the ratio of refractive index difference between the core and the solvent to the refractive index difference between the shell and the solvent, δ - the ratio of core radius to initial radius, and λ - the ratio of total final radius to initial radius. The form factor for such a particle is given by

$$P(z) = 9\frac{[(1-\beta)\delta^3(\sin(z\delta) - z\delta\cos(z\delta)) + \beta\lambda^3(\sin(z\lambda) - z\lambda\cos(z\lambda))]^2}{z^6((1-\beta)\delta^3 + \beta\lambda^3)^2} . \quad (2.65)$$

Consider first a particle which does not swell, i.e. $\lambda = 1$. For a fixed core radius/shell radius ratio, i.e. δ =constant, decreasing β moves the minimum of the form factor to higher Q (figure 2.33). In essence, more of the scattering is coming from the core of the particle, and the scattering radius appears to decrease. If instead we fix β, and decrease δ, then the minimum of the form factor moves to higher Q until the experimentally determined value of $\delta = 0.64$. After this the minimum moves to lower Q again, with $\delta = 0$ corresponding to a minimum of $QR_i = 4.49$ where R_i is the initial radius (figure 2.34). Physically, this value of 0.64 indicates when the scattering from a shell of outer radius R_i

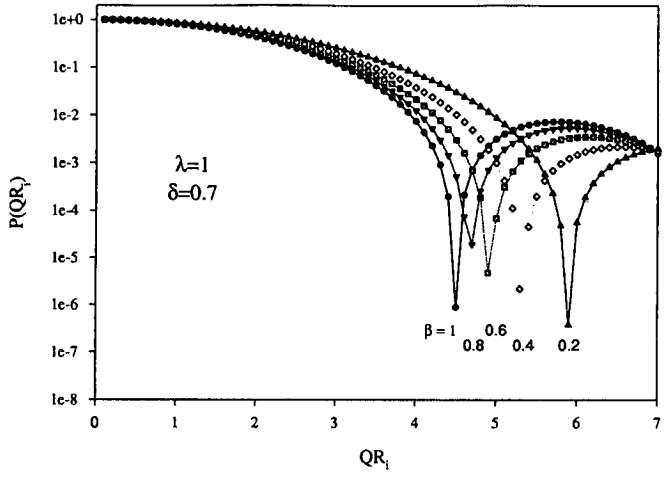

Figure 2.33: Effect of reducing the contrast between the shell and solvent in a core-shell model. The core/shell size ratio is fixed. The minimum moves to higher QR_i. For explanation of terms see text.

and inner radius δR_i is equal to the scattering from a solid sphere of radius δR_i, i.e. the scattering from the core and shell are equal. For $\delta > 0.64$ scattering from the core dominates and when $\delta < 0.64$ scattering from the shell dominates[6].

The case of fixing β and reducing δ is equivalent to assuming that the amount of tetralin is constant throughout the shell, but that its range of penetration may vary. By fixing δ and allowing β to vary we assume the tetralin concentration in the shell varies, but its progression into the particle is limited. In practice both scenarios are unlikely, the tetralin concentration is likely to have a smoothly varying profile that, in time, penetrates right to the centre of the particle.

We now consider the case of a swelling particle. The absolute magnitude of the swelling is known from DLS and we can use this information and figure 2.31 to obtain information on the magnitude of β and δ. Specifically, as the particle swells the form factor minimum would be expected to move to lower Q. Experimentally

[6]As the inner radius of a shell approaches zero, the minimum of its form factor moves to higher Q.

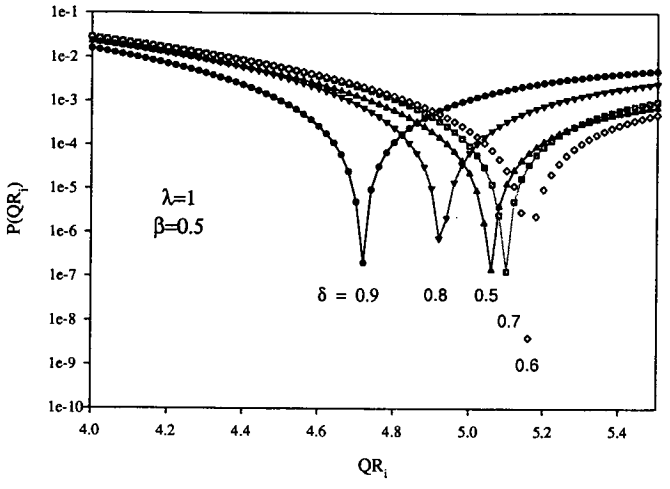

Figure 2.34: Effect of reducing the core size between the shell and solvent in a core-shell model. The contrast between the core and shell is fixed. The minimum moves to higher Q until the experimentally determined value of $QR_i = 0.64$. Further increasing δ moves the minimum to smaller Q until the limit of $QR_i = 4.49$ is reached at $\delta = 0$. For explanation of terms see text.

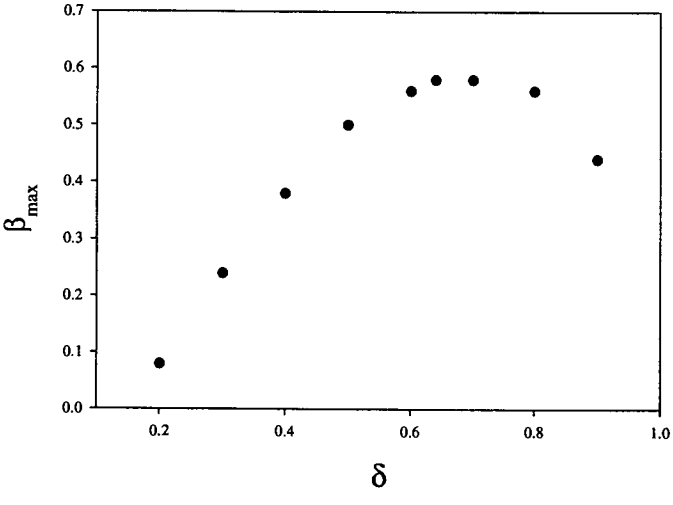

Figure 2.35: Plot of the maximum value of β for each δ that results in a form factor minimum greater than $QR_i = 4.49$. λ is fixed at 1.1 - the result obtained by DLS. See text for explanation of terms.

this is not observed, indicating that the total swollen core-shell refractive index profile still results in a $Q_{min} > 4.49$. Figure 2.35 shows the maximum value of β for each value of δ that allow this to occur, when $\lambda = 1.1$ as obtained by DLS. The refractive index of the shell is always reduced by at least 42%, indicating that at least this volume of the shell is taken up with tetralin. The PMMA particle is thus rather permeable to tetralin.

2.5.4 Conclusions

Static light scattering experiments conclusively show that tetralin is entering the PMMA particles, seen as a reduction in scattering intensity with time at low Q. DLS reveals that the particles swell by about 10% over a period of 5 to 20 hours. Using this value and assuming a core-shell model, we have shown that the shifting of the form factor minimum obtained in SLS to higher Q indicates that the shell is roughly 50% by volume tetralin. The smearing out of the form factor indicates a heterogeneity in the scattering from the particles. This could be a size polydispersity (unlikely considering the DLS data was well described by the first cumulant only) or a refractive index profile polydispersity.

Whilst no further swelling is seen by DLS over a period of 12 days, the refractive index profile continues to change (seen as an evolution in the form factor). This changing profile could be due to the further absorption of tetralin without swelling or a rearrangement of the tetralin already contained within the particle. It is suprising that no further swelling occurs. It is conceivable that it is the PHSA layer which prevents further swelling, being able to only bear a certain amount of strain, or that it is energetically unfavourable for the PMMA coils themselves to expand beyond some fixed radius.

Another suprise is the relatively small amount of swelling in an index-matching solution of tetralin and *cis*-decalin. If a linear relation were assumed then a radial

increase of about 3% would be expected. Manoharan found that the relationship between swelling and tetralin volume fraction was not linear for his particles [56], and it would be interesting to perform measurements in this system at several other tetralin concentrations.

The suitability of a core-shell model for the particle in tetralin could certainly be questioned. It seems more likely that a smoothly varying profile would occur; however the model used here provides useful insights into the system with only a few parameters.

Chapter 3

Theoretical treatment of diffusion

3.1 Introduction

In a non-interacting system of colloids the diffusion follows the Stokes-Einstein relation (equation 2.58). The presence of interactions due to either the inter-particle potential, hydrodynamics or both can cause very different behaviour. In this chapter I will discuss some theoretical ideas relating to the diffusion of colloids through polymer solutions. After giving an overview of the thermodynamics of the system, I will discuss two different descriptions of diffusion: the *Cahn-Hilliard* theory, which is based on a phenomenological approach, and the *Smoluchowski* approach which follows the evolution of the particle spatial probability function.

Poon and Warren [59] used a Cahn-Hilliard approach to find the governing equations for diffusion in a colloid-polymer mixture obeying the Asakura Oosawa potentials. In this chapter I will discuss these equations in terms of a new diffusional mode analysis and will show how this treatment yields an intuitive physical picture of the diffusion. I will also make predictions for the form of the dynamic structure factor obtained at low Q. Further, I have attempted to include the effects of hydrodynamic interactions into these equations, with some success.

Hydrodynamics are included in a much more natural way in the Smoluchowski equation. Unfortunately this equation has not yet been solved for the system under study, but here I make several qualitative predictions on the basis of theories previously derived for systems of hard spheres that have been confirmed by experiment.

3.2 Statistical mechanics of colloid-polymer mixtures

3.2.1 Thermodynamic concepts

Statistical Mechanics[1] concerns itself with predicting the macroscopic behaviour of systems with very many particles. In a large enough system, variables such as pressure, temperature and energy may be defined as 'constant' when the system is in a state of thermal equilibrium. Here 'constant' means either unchanging in time, or with fluctuations small compared to the mean value. For a single species there are only three independent state variables on which all the others depend. In a particular experiment we must choose to fix one from each of temperature and energy, pressure and volume, chemical potential and number of particles. In statistical mechanics, the choice of the fixed variables defines an *ensemble.* For a one component system table 3.1 gives the definitions of the common ensembles.

A particular macrostate of a system usually corresponds to very many *microstates* (complete atomistic specifications). The probability of a specific microstate occuring can be formulated (but sadly rarely calculated) in terms of its thermodynamic variables. For example, the probability of a particle being in an energy state E_i

[1]For a good introduction to statistical physics see, for example, Mandl [60].

Name	Fixed Variables	Fluctuating Variables
Microcanonical	E, V, N	None
Canonical	T, V, N	E
Grand Canonical	T, V, μ	E, N

Table 3.1: Definition of statistical mechanical ensembles. E is the energy, T the temperature, N the number of particles, V the volume and μ the chemical potential.

is, within the canonical ensemble

$$p_i = \frac{e^{-\beta E_i}}{Z} , \tag{3.1}$$

where $\beta = 1/k_B T$ and Z is the normalising factor given by

$$Z = \sum_i e^{-\beta E_i} , \tag{3.2}$$

called the partition function. The partition function itself contains useful information on the system. For each ensemble there is an associated 'free energy' or potential which is minimised by the system. For the canonical ensemble the appropriate potential is the Helmholtz free energy $F(T, V, N)$, whereas for the grand canonical ensemble it is the grand potential $\Omega(T, V, \mu)$. These ensembles have an associated partition function from which they may be calculated, e.g.

$$F = -k_B T \ln Z . \tag{3.3}$$

3.2.2 Perfect gas

A perfect gas is one in which the constituents do not interact with each other. Polymer solutions are often treated as perfect gas - an approximation which is expected to have some validity at the theta temperature. This approximation is particularly useful as the perfect gas has a partition function that can be evaluated

precisely [60]. Consider a single particle with a translational kinetic energy ϵ_i. The partition function for this particle is

$$Z_1 = \sum_i \exp(-\beta\epsilon_i) \; . \tag{3.4}$$

According to classical mechanics the translational centre-of-mass energy is related to its momentum $\mathbf{p}$ by

$$\epsilon = \frac{1}{2m}p^2 \; . \tag{3.5}$$

Classically the momentum may assume any value, but according to quantum mechanics a particle confined in a box can only have discrete values for its momentum. For a volume V the density of states $f(p)$ within the range p to $p+dp$ is given by

$$f(p)dp = \frac{V}{h^3}4\pi p^2 dp \; , \tag{3.6}$$

where h is Planck's constant. The partition function for the single particle now becomes

$$\begin{aligned} Z_1 &= \int_0^\infty f(p)\exp(-\beta\epsilon(p))dp \\ &= V\left(\frac{2\pi m k_B T}{h^2}\right)^{\frac{3}{2}} \\ &= \frac{V}{\lambda_T^3} \; , \end{aligned} \tag{3.7}$$

where $\lambda_T = \sqrt{(h^2/2\pi m k_B T)}$ is the thermal length. For indistinguishable particles, the N-particle partition function is therefore

$$Z_N = \frac{1}{N!}\left(\frac{V}{\lambda_T^3}\right)^N \; . \tag{3.8}$$

Having obtained the partition function, the Helmholtz free energy can be calculated according to equation 3.3:

$$\begin{aligned} F &= -k_B T \ln\left[\frac{1}{N!}\left(\frac{V}{\lambda_T^3}\right)^N\right] \\ &= N k_B T\left[\ln\left(\frac{N\lambda_T^3}{V}\right) - 1\right] \; , \end{aligned} \tag{3.9}$$

where we have used Stirling's approximation for large N. From the Helmholtz free energy we can obtain the equation of state of a perfect gas:

$$P = -\left(\frac{\partial F}{\partial V}\right)_{T,N} \tag{3.10}$$

$$\frac{\beta P}{\rho} = 1\,, \tag{3.11}$$

where ρ is the number density.

3.2.3 Hard spheres

A collection of hard spheres is arguably the paradigmatic non-ideal system [21]. The particles have infinite repulsion when touching and no interaction when their separation is greater than their diameter. Even with this simple potential, an exact solution for the equation of state is, as yet, unavailable. On the other hand, considerable progress has been made in obtaining the lower order terms in the virial expansion which expresses the equation of state as a power series expansion in the density of the fluid. The first three virial coefficients (B_{2-4}) may be obtained exactly, and Ree and Hoover [61] numerically computed B_5, B_6 and B_7. Carnahan and Starling derived a very useful heuristic equation of state based on Ree and Hoover's result [62]. They obtained an expression for B_n, the n'th virial coefficient, which allowed the virial expansion to be summed giving

$$\frac{\beta P}{\rho} = \frac{1+\phi+\phi^2-\phi^3}{(1-\phi)^3}\,. \tag{3.12}$$

ϕ is the volume fraction. This equation of state agrees remarkably well with simulation results obtained by Hoover and Ree [34] and with recent experimental measurements by Phan and colleagues [27] over the whole fluid range. Using this result and equation 3.10 we can obtain the excess Helmholtz free energy for a hard-sphere fluid:

$$\frac{\beta F^{\text{ex}}}{N} = \frac{\phi(4-3\phi)}{(1-\phi)^2}\,. \tag{3.13}$$

3.2.4 Colloid-polymer mixtures

Having obtained the equation of state for both ideal polymer solutions and hard sphere colloids, we now turn our attention to the properties of the mixture. In the Asakura Oosawa model [15] defined in Chapter 1, the relevant potentials are given by:

$$\begin{aligned} U_{cc}(r) &= \begin{cases} 0 & r > 2R \\ \infty & r \leq 2R \end{cases} \\ U_{cp}(r) &= \begin{cases} 0 & r > R(1+\xi) \\ \infty & r \leq R(1+\xi) \end{cases} \\ U_{pp}(r) &= 0 \ \forall \ r \end{aligned}$$

where R is the radius of the colloid and ξ the size ratio. Following the paper by Warren *et al.* [63], the thermodynamic potentials for such a system may be obtained within a mean field approximation. Let the colloids be at $\vec{r}_i$ where $i = 1 \ldots N_c$, and be referred to collectively as $\vec{r}_c = \{\vec{r}_i\}$. Similarly the polymers are at $\vec{r}_\mu$ where $i = 1 \ldots N_p$, and are referred to collectively as $\vec{r}_p = \{\vec{r}_\mu\}$. Working in the canonical ensemble the partition function is expressed as

$$\begin{aligned} Z &= \sum_{\text{microstates}} e^{-\beta E} \\ &= Z_c^{(\text{id})} Z_p^{(\text{id})} \int \frac{d^3\vec{r}_c}{V^{N_c}} e^{-\beta U_{cc}} \times \int \frac{d^3\vec{r}_p}{V^{N_p}} e^{-\beta U_{cp}} , \end{aligned} \tag{3.14}$$

where $Z_c^{(\text{id})}, Z_p^{(\text{id})}$ are the partition functions of a perfect gas of colloids and polymers respectively. To deal with the colloid-polymer interaction we introduce the void function

$$\varphi(\vec{r}_\mu; \vec{r}_c) = \Pi_i \, \theta\left[\mid \vec{r}_\mu - \vec{r}_i \mid -R(1+\xi) \right] , \tag{3.15}$$

where

$$\theta(x) = \begin{cases} 0 & x < 0 \\ 1 & x \geq 0 \end{cases} \tag{3.16}$$

The void function is zero if a polymer lies within the depleted region of any colloid centre ($r < R(1+\xi)$) and is unity otherwise. This clearly depends on the position of all the colloid particles which we assume to be fixed. This allows us to define a free volume fraction $\alpha(\vec{r}_c)$ as:

$$\alpha(\vec{r}_c) = \frac{1}{V}\int \varphi(\vec{r}_\mu;\vec{r}_c)d^3\vec{r}\,. \tag{3.17}$$

We can now rewrite $e^{-\beta U_{cp}} = \Pi_\mu\, \varphi(\vec{r}_\mu;\vec{r}_c)$, so

$$\begin{aligned} Z &= Z_c^{(\mathrm{id})} Z_p^{(\mathrm{id})} \int \frac{d^3\vec{r}_c}{V^{N_c}} e^{-\beta U_{cc}} \times \int \frac{d^3\vec{r}_p}{V^{N_p}} \Pi_\mu\, \varphi(\vec{r}_\mu;\vec{r}_c) \\ &= Z_c^{(\mathrm{id})} Z_p^{(\mathrm{id})} \int \frac{d^3\vec{r}_c}{V^{N_c}} e^{-\beta U_{cc}} \alpha(\vec{r}_c)^{N_p}\,. \end{aligned} \tag{3.18}$$

Consider a reservoir of pure polymer in osmotic equilibrium with the colloid-polymer mixture. Polymers may now be exchanged between the system and the reservoir. This could be actualised by connecting the system via a membrane with holes of radius r_m where $R\xi < r_m < R$. By so fixing the chemical potential μ_p of the polymers we are choosing to work in a semi-grand ensemble. The partition function for this ensemble is given by:

$$\begin{aligned} \Xi &= \sum_{N_p=0}^{\infty} e^{\beta N_p \mu_p} Z(N_p) \\ &= Z_c^{(\mathrm{id})} \int \frac{d^3\vec{r}_c}{V^{N_c}} e^{-\beta U_{cc}} \sum_{N_p=0}^{\infty} \frac{1}{N_p!} \left(\frac{V}{\lambda_p^3}\right)^{N_p} \alpha(\vec{r}_c)^{N_p} \exp(\beta N_p \mu_p) \\ &= Z_c^{(\mathrm{id})} \int \frac{d^3\vec{r}_c}{V^{N_c}} e^{-\beta U_{cc}} \exp\left[\frac{V}{\lambda_p^3}\alpha(\vec{r}_c)\exp(\beta\mu_p)\right]\,, \end{aligned} \tag{3.19}$$

where we have used equation 3.8 for the ideal part of the polymer partition function. For convenience we define the polymer *activity* as

$$a_p = \frac{e^{\beta\mu_p}}{\lambda_p^3}\,, \tag{3.20}$$

so that equation 3.19 becomes

$$\Xi = Z_c^{(\mathrm{id})} \int \frac{d^3\vec{r}_c}{V^{N_c}} e^{-\beta U_{cc}} \exp\left[V\alpha(\vec{r}_c)a_p\right]\,. \tag{3.21}$$

To progress in solving this equation, it is necessary to use a mean field approach, replacing $\alpha(\vec{r}_c)$ by its average value in the unperturbed (hard sphere) system, i.e.

$$\alpha(\vec{r}) \longrightarrow \langle \alpha(\vec{r}) \rangle_0 = \alpha(\phi) \, . \tag{3.22}$$

The semi-grand potential associated with this partition function is then given by

$$\begin{aligned} \Omega &= -k_B T \ln \Xi \\ &= \underbrace{-k_B T \ln Z_c^{(\mathrm{id})}}_{F_c^{(\mathrm{id})}} \underbrace{- k_B T \ln \int \frac{d^3\vec{r}_c}{V^{N_c}} e^{-\beta U_{cc}}}_{F_c^{(\mathrm{ex})}} - V k_B T a_p \alpha \, , \end{aligned} \tag{3.23}$$

where $F_c^{(\mathrm{id})}$ is the free energy of a perfect gas of colloids, given by equation 3.9 and $F_c^{(\mathrm{ex})}$ is the excess free energy of the hard-sphere colloids, given by 3.13.

The above treatment assumed the presence of a polymer reservoir. Experimentally it is much more likely that no reservoir will be present. In this case the chemical potential of the polymers is not fixed and we must work in the canonical ensemble. Using the same mean field approximation as in the semi-grand ensemble, equation 3.18 becomes

$$Z = Z_c^{(\mathrm{id})} Z_p^{(\mathrm{id})} \int \frac{d^3\vec{r}_c}{V^{N_c}} e^{-\beta U_{cc}} \alpha(\phi)^{N_p} \, . \tag{3.24}$$

The appropriate thermodynamic potential is the Helmholtz free energy. By the separability of the partition function this can be written

$$\begin{aligned} F_{\mathrm{TOT}} &= F_c^{(\mathrm{id})} + F_p^{(\mathrm{id})} - k_B T \ln \int \frac{d^3\vec{r}_c}{V^{N_c}} e^{-\beta U_{cc}} \alpha(\phi)^{N_p} \\ &= F_c + F_p^{(\mathrm{id})} - k_B T N_p \ln \alpha(\phi) \, , \end{aligned} \tag{3.25}$$

where F_c represents the *total* free energy of a system of colloidal spheres. Using equation 3.9, we can combine the final two terms in equation 3.25 so that the total free energy is given by:

$$\frac{F_{\mathrm{TOT}}}{k_B T V} = \rho_p \left[\ln \left(\frac{\rho_p \lambda_p^3}{\alpha} \right) - 1 \right] + \frac{F_c}{k_B T V} \, . \tag{3.26}$$

The depletion effect is accounted for by the increase in the polymer number density in the free volume.

Both equation 3.23 and 3.26 use a mean field approximation in which the free volume in a system with added polymer is replaced by that in a system with no polymer added. A closed-form expression for this quantity can be obtained through scaled particle theory results for hard-sphere mixtures [1,64]:

$$\alpha = (1-\phi)\exp\left[-A\gamma - B\gamma^2 - C\gamma^3\right] , \tag{3.27}$$

in which $\gamma = \phi/(1-\phi), A = 3\xi + 3\xi^2 + \xi^3, B = 4.5\xi^2 + 3\xi^3$ and $C = 3\xi^3$. Simulations performed by Meijer and Frenkel have shown that this expression is reasonably accurate even for dense fluid phases [65].

3.3 Cahn-Hilliard theory

The Cahn-Hilliard theory was created to explain *spinodal decomposition* in terms of thermodynamic arguments [2]. Spinodal decomposition refers to a type of fluid phase separation in which density fluctuations of some spatial wavelengths grow leading to a lowering of the free energy. In the Cahn-Hilliard approach the volume is divided into small elements which are internally in equilibrium. These volume elements are sufficiently large to contain many colloidal particles with negligible spatial correlations. On the other hand the volume elements should be small compared to the wavelengths of the density fluctuations that are unstable. Furthermore the relaxation time of fluctuations whose wavelengths are of a size comparable to the linear dimension of the volume element should be much less than the rate of demixing due to the unstable fluctuations [43]. This allows a thermodynamic description of each volume element. If these assumptions are met then the Helmholtz free energy takes a Landau-Ginzburg form:

$$F[\rho(\vec{r})] = \int d\vec{r}\left\{\frac{1}{2}K(\nabla\rho(\vec{r}))^2 + f(\rho)\right\} . \tag{3.28}$$

[2]For a good summary of Cahn-Hilliard theory see Dhont [43]

$\rho(\vec{r})$ is the number density at $\vec{r}$, K is a measure of the interfacial energy between high and low density regions and $f(\rho)$ is the local free energy density of a volume element.

Conservation of number of colloid particles leads to a continuity equation.

$$\frac{\partial \rho}{\partial t} = -\nabla \cdot \mathbf{j} \,, \tag{3.29}$$

where $\mathbf{j}(\vec{r}, t)$ is the number density flux which is assumed to be linearly proportional to the thermodynamic driving force - the gradient of the chemical potential μ:

$$\mathbf{j}(\vec{r}) = -M\nabla \cdot \mu \,, \tag{3.30}$$

where M is a mobility coefficient, assumed ρ-independent. The chemical potential is given by the functional derivative of the free energy with respect to density (see for example [43]):

$$\mu(\vec{r}) = \frac{\delta F[\rho(\vec{r})]}{\delta \rho(\vec{r})} \,. \tag{3.31}$$

Working in one dimension, combining equations 3.28, 3.29, 3.30 and 3.31 we obtain the Cahn-Hilliard equation:

$$\frac{\partial \rho}{\partial t} = M\frac{\partial^2}{\partial x^2}\left(-K\frac{\partial^2 \rho}{\partial x^2} + \frac{\partial f}{\partial \rho}\right) \,. \tag{3.32}$$

We wish to consider fluctuations in density, $\delta\rho(x,t) = \rho(x,t) - \bar{\rho}$ where $\bar{\rho}$ is the average density. This fluctuation in density may be expanded in terms of its Fourier components

$$\delta\rho(x,t) = \frac{1}{V}\sum \hat{\delta\rho}(Q,t)e^{iQx} \,, \tag{3.33}$$

where the sum is over wavevectors contained within the first Brillioun Zone. Fourier transforming equation 3.32 and expanding around the mean density gives the equation of motion for the Q-th component of the density fluctuation:

$$\frac{\partial \hat{\delta\rho}(Q,t)}{\partial t} = -MQ^2[KQ^2 + f_0'']\hat{\rho}(Q,t) \,, \tag{3.34}$$

where f_0'' is the value of $\partial^2 f/\partial\rho^2$ evaluated at $\bar{\rho}$. This has a solution

$$\hat{\delta\rho}(Q,t) = \hat{\delta\rho}(Q,0)e^{-D(Q)Q^2 t}\,, \tag{3.35}$$

where

$$D(Q) = M(KQ^2 + f_0'')\,. \tag{3.36}$$

The condition for density fluctuations to grow is clearly $f_0'' < 0$, in which case all fluctuations with wavevectors in the range $0 < Q < Q_c = (-f_0''/K)^{1/2}$ grow with time. The fastest growing fluctuation has wavelength $Q_m = Q_c/2$.

In the case of the free energy depending on *two* order parameters, $F[\rho_1(x), \rho_2(x)]$, equation 3.30 becomes:

$$\begin{aligned} j_1(\vec{r}) &= -M_1\nabla\mu_1 \\ j_2(\vec{r}) &= -M_2\nabla\mu_2\,. \end{aligned} \tag{3.37}$$

where μ_1, μ_2 are the functional derivatives of the free energy with respect to ρ_1, ρ_2 respectively. Working through a similar treatment to before leads to an equation of motion for each species:

$$\begin{aligned} \frac{\partial\hat{\delta\rho}_1(Q,t)}{\partial t} &= -M_1Q^2[K_1Q^2 + f_0''^{11}]\hat{\delta\rho}_1(Q,t) - M_1Q^2 f_0''^{12}\hat{\delta\rho}_2(Q,t) \\ \frac{\partial\hat{\delta\rho}_2(Q,t)}{\partial t} &= -M_2Q^2[K_2Q^2 + f_0''^{22}]\hat{\delta\rho}_2(Q,t) - M_2Q^2 f_0''^{21}\hat{\delta\rho}_1(Q,t)\,. \end{aligned} \tag{3.38}$$

In these equations $f_0''^{12} = \partial^2 f/\partial\rho_1\partial\rho_2$ evaluated at $(\bar{\rho}_1, \bar{\rho}_2)$ and similarly.

Cahn-Hilliard theory gives the equations of motion of density fluctuations of a particular wavelength. It contains a local free energy term and an interfacial energy term. The exact calculation of the latter is difficult. Dhont showed [66] that for a single species, the parameter K takes the form

$$K = \frac{2\pi}{15}\bar{\rho}\int_0^\infty dr\, r^5 \frac{dV(r)}{dr}\left(g^{\mathrm{eq}}(r) + \frac{1}{8}\bar{\rho}\frac{dg^{\mathrm{eq}}(r)}{d\bar{\rho}}\right)\,, \tag{3.39}$$

in which $V(r)$ is the inter-particle pair potential and $g^{\mathrm{eq}}(r)$ the equilibrium pair-correlation function for a homogeneous system. For a colloid-polymer mixture

at reasonable densities, a closed form for the pair-correlation is unavailable and, for this reason, only the $Q \longrightarrow 0$ limit will be discussed. This is also the limit in which the instability first sets in. It should also be mentioned that while the implicit assumption of small gradients in number density in equations 3.30 and 3.37 is unlikely to be valid for points at or beyond the spinodal line, this treatment should be valid for decaying density fluctuations.

We now apply the Cahn-Hilliard treatment to diffusion in colloid-polymer mixtures.

3.3.1 One species diffusion

The simplest case to consider is a colloid-polymer mixture attached to a polymer reservoir. The chemical potential of the polymer is thus fixed and the density fluctuations of the colloid may be adequately described by the one-body Cahn-Hilliard equation with the correct inter-particle potential[3]. Combining equations 3.9, 3.13, 3.23 and 3.34 gives

$$\frac{\partial \hat{\delta\rho}_c(Q,t)}{\partial t} = -M_c Q^2 \left[v_c \left(\frac{1}{\bar{\phi}_c} + \frac{2(4-\bar{\phi}_c)}{(1-\bar{\phi}_c)^4} \right) - v_c^2 \bar{\rho}_p \frac{\alpha''}{\alpha} \right] \delta\rho_c(\hat{Q},t) \ , \qquad (3.40)$$

where we have used the 'natural' units for the free energy - $k_B T$. v_c is the volume of a single colloidal sphere, $\bar{\phi}_c$ is the mean colloid volume fraction, $\bar{\rho}_p$ the mean polymer number density and a prime denotes differentiation with respect to ϕ_c. The identity $\alpha a_p = \rho_p$ has also been used. In the absence of polymer and at low colloid volume fractions we would expect to recover free diffusion of a single species. Equations 3.36 and 3.40 thus allow us to rewrite the mobility constant in terms of the free diffusion coefficient of the colloid D_c^0:

$$M_c = D_c^0 \frac{\bar{\phi}_c}{v_c} \ . \qquad (3.41)$$

[3]In the $Q \longrightarrow 0$ limit, only infinite wavelength density fluctuations are considered. Thus we may neglect the local Brownian motions of the polymers.

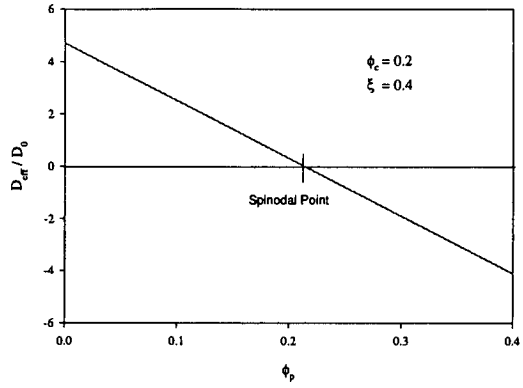

Figure 3.1: Colloid diffusion coefficient as a function of polymer reservoir concentration (in c^*). As polymer is added the density fluctuations die away more slowly until the spinodal point is reached. At polymer concentrations higher than this point, phase separation occurs. Data is shown for a colloid volume fraction of 0.2 and a size ratio of 0.4.

The change in the diffusion constant due to the presence of the polymer and the finite size of the colloidal particle ΔD is given by

$$\Delta D = \frac{D_{\text{eff}}(Q \to 0) - D_c^0}{D_c^0} = \bar{\phi}_c \left(\frac{2(4 - \bar{\phi}_c)}{(1 - \bar{\phi}_c)^4} - \frac{1}{\xi^3} \bar{\phi}_p \frac{\alpha''}{\alpha} \right) . \tag{3.42}$$

ξ is the size ratio and $\bar{\phi}_p$ is the mean effective volume fraction of polymers given by c/c^*. This equation represents the change in the diffusion coefficient due to interactions with other colloidal particles (figure 3.1). The hard sphere interaction causes the density fluctuations to relax quicker whereas the depletion interaction causes the density fluctuations to relax slower than those for a non-interacting system. At some polymer concentration the depletion interaction will balance the natural tendency for the fluctuations to decay away. This is the spinodal point. At higher polymer concentrations the density fluctuations grow and the system phase separates.

By a simple consideration of the dynamics of a colloid-polymer mixture, we have found the condition for spinodal decomposition (at zero Q) - that the second derivative of the free energy density is zero. This condition is equivalent to the thermodynamic definition of the spinodal point [43], namely that the osmotic

pressure of the system does not change as the number density increases.

$$\frac{d\Pi}{d\rho} \equiv \frac{d^2 f_{\mathrm{TOT}}}{d\rho^2} = 0 \tag{3.43}$$

3.3.2 Two species diffusion

In a system where no reservoir is present, gradients in both the colloid and the polymer potential exist and will drive diffusion. Equation 3.38 shows that a density fluctuation in one species drives diffusion in the other. Working in the $Q \longrightarrow 0$ limit, equation 3.38 and 3.41 combine to give an equation of motion for the two species:

$$\frac{\partial}{\partial t}\vec{R} = -Q^2 \mathbf{D}\vec{R}\,, \tag{3.44}$$

where the vector $\vec{R}$ is

$$\vec{R} = \begin{pmatrix} \hat{\delta\rho_c}(Q,t) \\ \hat{\delta\rho_p}(Q,t) \end{pmatrix}\,, \tag{3.45}$$

and $\mathbf{D}$ is a 2×2 matrix involving the second derivatives of the free energy:

$$D = \begin{pmatrix} D_c^0 \bar{\rho}_c f_0^{\prime\prime cc} & D_c^0 \bar{\rho}_c f_0^{\prime\prime cp} \\ D_p^0 \bar{\rho}_p f_0^{\prime\prime pc} & D_p^0 \bar{\rho}_p f_0^{\prime\prime pp} \end{pmatrix}\,, \tag{3.46}$$

where $f_0^{\prime\prime cp} \equiv \partial^2 f/\partial\rho_c\partial\rho_p$ evaluated at $(\bar{\rho}_c, \bar{\rho}_p)$, and so on. Substituting in the free energy (equation 3.26) gives:

$$D = \begin{pmatrix} D_c\phi_c\left[f''_{HS} - \frac{\phi_p}{\xi^3}\left(\frac{\alpha''}{\alpha} - \frac{\alpha'^2}{\alpha^2}\right)\right] & -D_c\phi_c\frac{\alpha'}{\alpha} \\ -D_p\frac{\phi_p}{\xi^3}\frac{\alpha'}{\alpha} & D_p \end{pmatrix}\,. \tag{3.47}$$

f_{HS} is the free energy density of a system of hard spheres. This matrix may be diagonalised to provide two uncorrelated diffusional modes which are linear combinations of ϕ_c and ρ_p:

$$\begin{aligned} \hat{\delta\rho_1} &= \hat{\delta\rho_c} + a \times \hat{\delta\rho_p} \\ \hat{\delta\rho_2} &= \hat{\delta\rho_p} + b \times \hat{\delta\rho_c}\,, \end{aligned} \tag{3.48}$$

which diffuse according to

$$\begin{aligned} \frac{\partial}{\partial t}\delta\hat{\rho}_1 &= \lambda_+ Q^2 \delta\hat{\rho}_1 \\ \frac{\partial}{\partial t}\delta\hat{\rho}_2 &= \lambda_- Q^2 \delta\hat{\rho}_2 \,, \end{aligned} \tag{3.49}$$

where λ_+, λ_- are the eigenvalues and $\delta\hat{\rho}_1, \delta\hat{\rho}_2$ the eigenvectors of $\mathbf{D}$. The spinodal point occurs when one of the eigenvalues is zero i.e. when

$$R = D_p D_c \phi_c \left[f''_{HS} - \frac{\phi_p}{\xi^3}\left(\frac{\alpha''}{\alpha} - \frac{\alpha'^2}{\alpha^2}\right)\right] - D_c D_p \frac{\phi_p}{\xi^3}\phi_c \left(\frac{\alpha'}{\alpha}\right)^2 = 0 \,, \tag{3.50}$$

which is satisfied by $f''_{HS} = \frac{\phi_p}{\xi^3}\frac{\alpha''}{\alpha}$ as obtained by the semi-grand canonical ensemble. Since the spinodal is a thermodynamic quantity it is independent of the ensemble used to calculate it.

At zero polymer concentration both ensembles give $D_{\text{eff}} = D_c \phi_c f''_{HS}$. As polymer is added (within the canonical ensemble), the eigenvalues obtained by solving equation 3.48 are related by

$$(\lambda_+ - \lambda_-)^2 = \left\{ D_c \phi_c \left[f''_{HS} - \frac{\phi_p}{\xi^3}\left(\frac{\alpha''}{\alpha} - \frac{\alpha'^2}{\alpha^2}\right)\right] + D_p \right\}^2 - 4R \tag{3.51}$$

$$= [A(\phi_c)\phi_p + B(\phi_c)]^2 + C(\phi_c)\phi_p + D(\phi_c) \,, \tag{3.52}$$

where A, B, C, D are functions independent of ϕ_p. These eigenvectors represent diffusion coefficients for each mode and as such must be real. Therefore the RHS of equation 3.52 must be positive for all ϕ_p, i.e. the quadratic is entirely contained within the upper quadrants (see figure 3.2) having at most one distinct root. Equivalently, it must take the form $\phi_p^2 + a\phi_p + b$ where $(a \leq 2\sqrt{b})$. By expansion of the equation 3.51 it is easy to show that this root may only occur at $\phi_p = 0$ (and then only if $D_p = D_c \phi_c f''_{HS}$). Thus within the positive quadrant the quadratic must be monotonically increasing with ϕ_p. This means that the eigenvalues on the LHS of equation 3.52 diverge as the polymer concentration is increased.

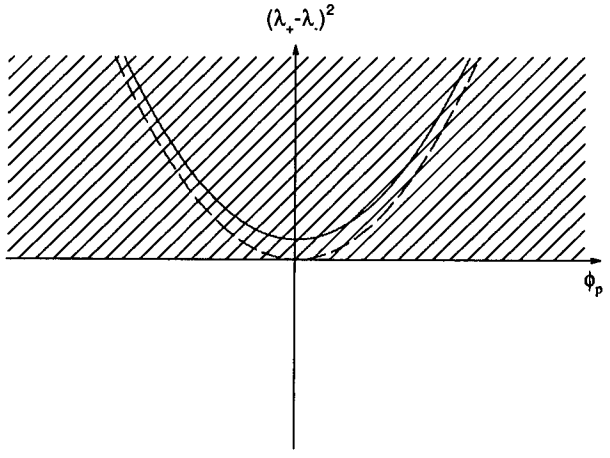

Figure 3.2: The quadratic given in equation 3.51 must be entirely contained within the upper quadrants (shaded area). The exact form is monotonically increasing throughout the positive quadrant with the zero polymer concentration value being dependent on the relative values of D_p and $D_c\phi_c f''_{HS}$

This results in a 'fast' mode and a 'slow' mode (see figure 3.3). The composition of these modes can be found by solving the eigenvector equation and it is found significant quantities of each species are present in each mode (figure 3.4). The physical interpretation of these modes is difficult. Pusey [67] considered a system of similar, yet distinguishable, hard spheres and showed that the two diffusive modes of this system may be thought of as a 'condensation' mode, for which the fluctuations are in the *total* density, and a 'demixing' mode, in which the fluctuations are in *species* density (figure 3.5). In our formalisation, a condensation mode would correspond to $a = 1$ and, since the decay involves relatively small motions of the bulk, would be the fast mode. Demixing corresponds to $b = -1$ this mode will take longer to decay as it involves relatively large scale motions of single particles. It is not easy to create an intuitive picture for the decays in a colloid-polymer mixture as condensation and demixing occur in both diffusive modes but, as expected, the fast mode remains dominated by condensation (figure 3.6).

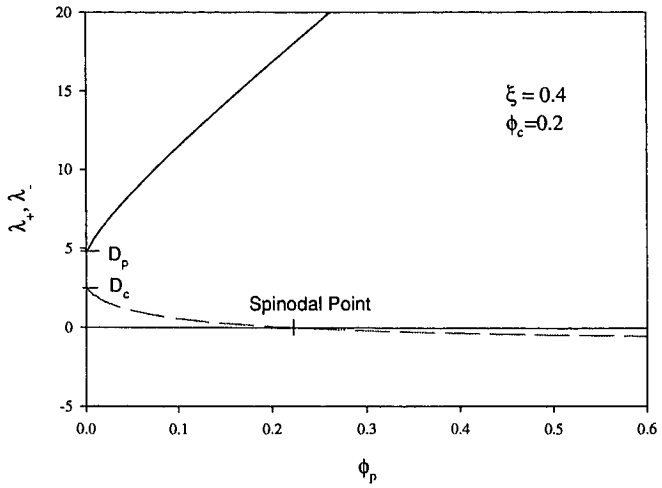

Figure 3.3: The eigenvalues of equation 3.49 with a size ratio of 0.4 and a colloid volume fraction of 0.2. These are the diffusion coefficients of the diffusive modes. As polymer is added the eigenvalues diverge resulting in a 'fast' and 'slow' mode. The predicted spinodal point agrees with that obtained from the semi-grand canonical ensemble.

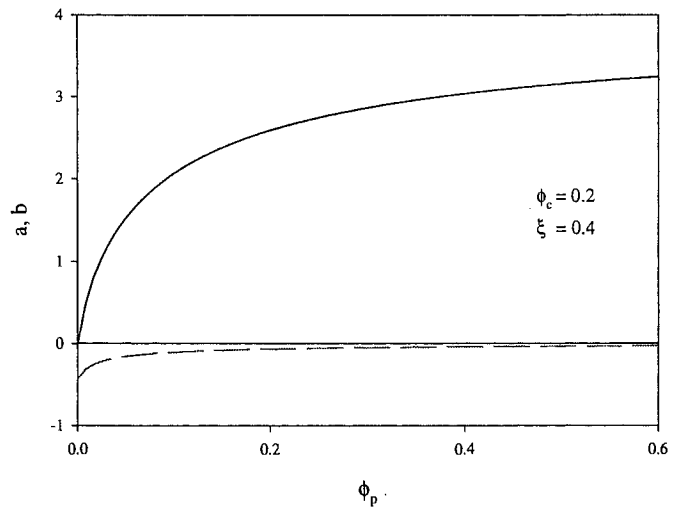

Figure 3.4: a (solid line) and b (dotted line) values of the eigenmodes as described in equation 3.48 with a size ratio of 0.4 and a colloid volume fraction of 0.2. $a = b = 0$ would imply the diffusion modes were pure polymer and colloid. In this system the modes contain a significant proportion of both species.

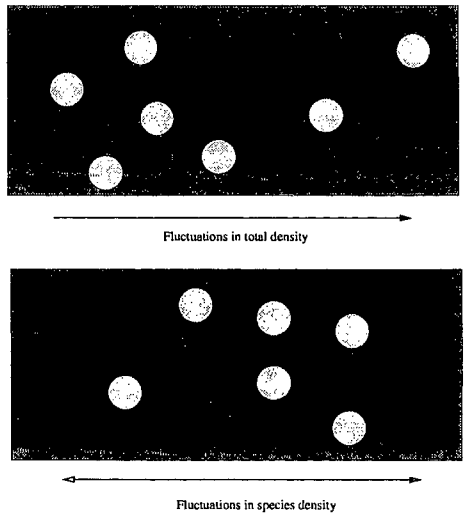

Figure 3.5: Condensation and demixing modes in a system of similar yet distinguishable hard spheres. In the upper diagram the fluctuations are in total density (corresponding to $a = 1$ or $b = 1$). This mode decays by relatively small movements of the bulk. The lower mode contains fluctuations in species density ($a = -1$ or $b = -1$) and decays by relatively large motions of single particles. This mode can therefore be identified as a 'slow' mode.

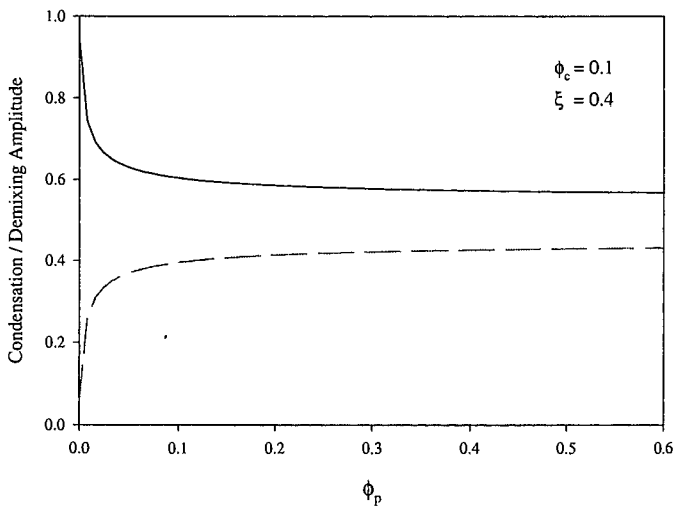

Figure 3.6: Condensation (dashed line) and demixing (solid line) amplitudes in the spinodally active mode. The spinodal decomposition is driven by demixing - a natural consequence of the slower timescale for this type of relaxation. The size ratio is 0.4 and the colloid volume fraction 0.1.

The divergence of the eigenvalues has the unusual consequence that only one mode becomes spinodally active. This implies that spinodal decomposition, which only occurs in the slow mode, is dominated by demixing. It is worth mentioning that this result is only true as $Q \longrightarrow 0$ and is not valid for a quench into the spinodal region, since this leads to spinodal decomposition that is dominated by the spatial wavelength $Q = (-f_0''/K)^{1/2}/2$. At these wavelengths the interfacial energy between the high and low density regions becomes significant.

3.3.3 Dynamic structure factor

The solution of equation 3.44 may be written as

$$\vec{R} = \vec{A_1} e^{-\lambda_+ Q^2 t} + \vec{A_2} e^{-\lambda_- Q^2 t} , \tag{3.53}$$

where $\vec{A}_1, \vec{A}_2$ are vector constants. Multiplying by $\hat{\delta\rho_c}(t=0) \equiv \hat{\delta\rho_c}^0$ and ensemble averaging gives

$$\begin{pmatrix} \langle \hat{\delta\rho_c}^t \hat{\delta\rho_c}^0 \rangle \\ \langle \hat{\delta\rho_p}^t \hat{\delta\rho_c}^0 \rangle \end{pmatrix} = B_1 \begin{pmatrix} 1 \\ a \end{pmatrix} e^{-\lambda_a Q^2 t} + B_2 \begin{pmatrix} b \\ 1 \end{pmatrix} e^{-\lambda_b Q^2 t} , \tag{3.54}$$

where a, b are given by equation 3.48. Either of the eigenmodes could be the spinodally active mode, so either $\lambda_a = \lambda_+$ and $\lambda_b = \lambda_-$ or vice versa. The constants B_1, B_2 are such that

$$\begin{aligned} \langle \hat{\delta\rho_c}^0 \hat{\delta\rho_c}^0 \rangle &= B_1 + bB_2 \\ \langle \hat{\delta\rho_p}^0 \hat{\delta\rho_c}^0 \rangle &= aB_1 + B_2 . \end{aligned}$$

Recalling the definition of the dynamic structure factor we may rewrite equation 3.54 in terms of the ratio $\aleph = \langle \hat{\delta\rho_p}^0 \hat{\delta\rho_c}^0 \rangle / \langle \hat{\delta\rho_c}^0 \hat{\delta\rho_c}^0 \rangle$:

$$f(Q,t) = \frac{\langle \hat{\rho_c^t} \hat{\rho_c^0} \rangle}{\langle \hat{\rho_c^0} \hat{\rho_c^0} \rangle} = \frac{1 - \aleph b}{1 - ab} e^{-\lambda_+ Q^2 t} + \frac{\aleph b - ab}{1 - ab} e^{-\lambda_- Q^2 t} . \tag{3.55}$$

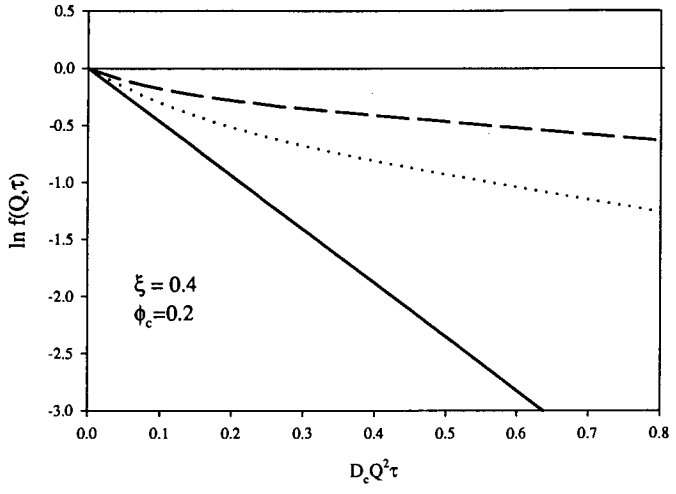

Figure 3.7: Colloid dynamic structure factor predicted by a 2 species Cahn-Hilliard treatment. The polymer concentrations (in c^*) are 0 (solid line), 0.05 (dotted line), 0.1 (dashed line). The size ratio is 0.4 and the colloid volume fraction 0.2. The dynamic structure factor is the weighted sum of two exponentials.

$\aleph$ may be easily calculated in terms of the free energy from the fluctuation theory result [68]:

$$\aleph = \frac{-\partial^2 F/\partial\rho_c\partial\rho_p}{\partial^2 F/\partial\rho_p^2} = \frac{\phi_p}{\xi^3}\frac{\alpha'}{\alpha}\,, \tag{3.56}$$

where F is the total free energy. Rewriting a and b in terms of the eigenvalues, equation 3.55 becomes

$$f(Q,t) = \Lambda e^{-\lambda_+ Q^2 t} + (1-\Lambda)e^{-\lambda_- Q^2 t}\,, \tag{3.57}$$

with

$$\Lambda = \frac{\lambda_- - \phi_c\left[f''_{HS} - \frac{\phi_p}{\xi^3}\left(\frac{\alpha''}{\alpha}\right)\right]}{\lambda_- - \lambda_+}\,. \tag{3.58}$$

The dynamic structure factor is piecewise exponential, representing the motion of the colloid in the various modes. An example of this expected form is shown in figure 3.7. If we were to apply the method of cumulants to obtain a diffusion coefficient, then we would find a time dependence $D(t)$. The initial diffusion coefficient would be measured as

$$D(t) \quad = \quad \frac{1}{Q^2}\frac{\partial}{\partial t} f(Q,t)$$

$$\longrightarrow \quad -D_c\phi_c\left[f''_{HS} - \frac{\phi_p}{\xi^3}\left(\frac{\alpha''}{\alpha}\right)\right] \text{ as } t \longrightarrow 0\,. \tag{3.59}$$

Interestingly this is the diffusion coefficient of colloids in the previous system where a polymer reservoir is attached. The initial diffusion coefficient is independent of the presence of the reservoir. At zero time the polymer chemical potential gradient is identical in the closed and open system and only changes in the former as the system evolves.

3.3.4 Hydrodynamics

The Cahn-Hilliard approach does not lend itself easily to the inclusion of hydrodynamic interactions. Only in the simplest case of single species diffusion can any real progress be made. However, in a colloid-polymer mixture there is the additional problem of hydrodynamic interactions between the diffusing colloid and the quasi-stationary polymer[4]. If the polymer concentration is sufficiently low, we may neglect these interactions and consider only the hydrodynamics between the colloids. Felderhof [69] considered the case of one species of spherically symmetric particles in a homogeneous background solvent with only two-body interactions. He found that the effective diffusion coefficient D_{eff} is related to the pure diffusion coefficient D_0 by

$$D = D_0[1 + \phi_c(C_V + C_O + C_D + C_S + C_A)]\,, \tag{3.60}$$

where C_V, C_O, C_D, C_S, C_A are the Virial, Oseen, Dipole, Short-Range and Angular coefficients respectively. These are complicated integrals given in terms of the unperturbed radial distribution function $g_0(r)$ of the particles, where

$$g_0(r) = \exp(-\beta U(r_{12}))\,, \tag{3.61}$$

[4]Since we are working in the $Q \longrightarrow 0$ limit, we may once more neglect the Brownian motion of the polymers.

and $U(r_{12})$ is the inter-particle potential. The Felderhof expansion is therefore only valid to the lowest order in density. In his treatment, the Virial coefficient is given by

$$C_V = -\int [g_0(\mathbf{r}) - 1] d\mathbf{r} \,, \tag{3.62}$$

which we identify as the double derivative of the free energy in equation 3.36. However the Cahn-Hilliard analysis given earlier uses the *exact* radial distribution function in equation 3.62. At low colloid and polymer concentrations, the approximation of $g(r)$ by $g_0(r)$ is valid and the two methods may be compared.

The effect of the polymers is to modify the form of the inter-particle potential. The polymer degrees of freedom may be integrated out to give an effective pair potential between the colloids [70]:

$$U(r) = \begin{cases} \infty & r \geq 2R_c \\ -\Pi_P V_{OV} & 2R_c < r \leq 2R_c(1+\xi) \\ 0 & r > 2R_c(1+\xi) \end{cases} \tag{3.63}$$

where $\Pi_P = n_p k_b T/\alpha$ is the osmotic pressure of the polymer and

$$V_{OV} = \left[1 - \frac{3r}{4R_c(1+\xi)} + \frac{1}{16}\left(\frac{r}{R_c(1+\xi)}\right)^3\right] v_c(1+\xi)^3 \tag{3.64}$$

is the volume of overlap. Substituting this potential into equation 3.61 and using equation 3.60, we obtain

$$\begin{aligned} \Delta D &= \frac{D_{\text{eff}}(Q \to 0) - D_0}{D_0} \\ &= \phi_c \left\{ A + \int_2^{2(1+\xi)} \exp\varsigma \left[1 + \frac{3x}{4(1+\xi)} + \frac{1}{16}\left(\frac{x}{1+\xi}\right)^3\right] \right. \\ &\quad \left. \times \left[3x - 3x^2 - \frac{15}{4}x^{-2} + \frac{27}{8}x^{-4} + \frac{75}{4}x^{-5}\right] dx \right\} \,, \end{aligned} \tag{3.65}$$

where $x = r/R_c$,

$$A = 1 + 8(1+\xi)^3 - 6(1+\xi)^2 + \frac{75}{256}(1+\xi)^{-4} + \frac{9}{64}(1+\xi)^{-3} - \frac{15}{8}(1+\xi)^{-1} \,, \tag{3.66}$$

and

$$\varsigma = \frac{(1+\xi)^3}{\xi^3}\frac{\phi_p}{\alpha} \,. \tag{3.67}$$

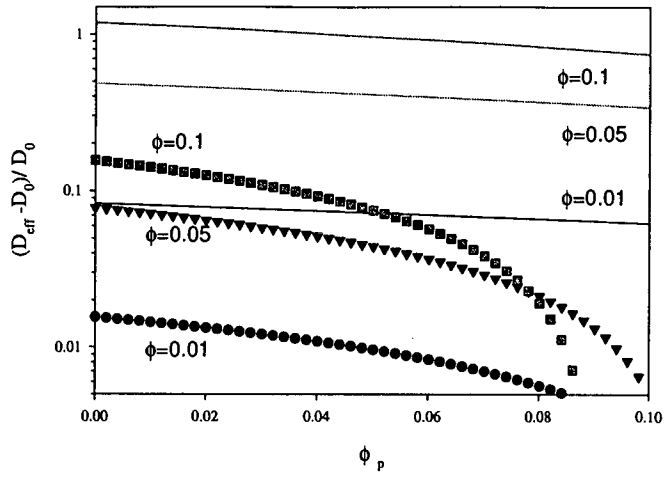

Figure 3.8: The change in diffusion coefficient as a function of polymer concentration (in c^*). The lines represent the results from the Cahn-Hilliard treatment and the symbols from the Felderhof treatment (with hydrodynamics). Three colloid volume fractions are shown: 0.1, 0.05 and 0.01, and the size ratio is 0.4.

These equations are solved by numerical integration and figure 3.8 compares this result with the one obtained without hydrodynamics (equation 3.42). Even at zero polymer concentration, the effect of the hydrodynamic interactions between hard-sphere colloids significantly damps out the increase in diffusion from the inter-particle interactions.

These results show the importance of hydrodynamics in the diffusion of colloid in a colloid-polymer mixture. However the numerical results should be treated with suspicion at anything other than the lowest polymer and colloid concentrations. Hydrodynamic interactions in pure colloidal systems are significant at volume fractions above ϕ_H =0.005 [20]. Assuming the colloid-polymer hydrodynamic coupling is of a similar order to colloid-colloid hydrodynamic coupling, hydrodynamic interactions between the colloid and polymer may only be ignored if the polymer concentration is below ϕ_H. The colloid volume fraction is limited by the approximation of the unperturbed radial distribution function, which breaks down in colloidal systems at a volume fraction of about $\phi_{\rm rdf}$ =0.01 [43]. Signifi-

cant deviation from this value is not expected when polymer is added whilst the effective polymer volume fraction remains lower than its hydrodynamic bound, ϕ_H. This gives a relatively narrow range of colloid and effective polymer volume fractions for which this treatment is valid.

3.4 The Smoluchowski equation

In the previous section I showed how inter-particle potentials lead to a non-singly exponential dynamic structure factor. Neither the short nor long time diffusion coefficient is expected to obey the Stokes-Einstein equation. The Cahn-Hilliard approach makes several assumptions about the system and introduces several phenomological constants (e. g. the square gradient constant which we avoided by working in the $Q \longrightarrow 0$ limit). A better starting point for formulating the dynamics of colloidal systems is the Smoluchowski equation, which requires no free energy functional. In addition this equation is a much more natural starting point for the inclusion of the second type of interactions in a colloidal system - hydrodynamics.

The most basic equation for the dynamical behaviour of a suspension is the Liouville equation which is the exact 6N-dimensional analogue of the usual 3D equation of continuity for an incompressible fluid [71]. It describes the dynamics of both the Brownian particles and the molecules of the suspending medium in terms of the probability density in phase space $f^{(N)}(\mathbf{r}^N, \mathbf{p}^N; t)$ where $f^{(N)}(\mathbf{r}^N, \mathbf{p}^N; t) d\mathbf{r}^N d\mathbf{p}^N$ is the probability of finding the system at time t in a microscopic state represented by a phase point lying within $d\mathbf{r}^N d\mathbf{p}^N$,

$$\frac{\partial f^{(N)}}{\partial t} = \left\{ H, f^{(N)} \right\} , \tag{3.68}$$

where the $\{\ldots\}$ represent Poisson brackets and H is the Hamiltonian for the system. This equation is far too complex to solve precisely so we use the fact that

the solvent molecules relax much quicker than the Brownian particles to integrate out their degrees of freedom. This leaves a description that is only valid on timescales $t > \tau_{\text{solvent}}$ - the Fokker-Planck equation. The degrees of freedom of the solvent are replaced by additional interactions between the Brownian particles, known as hydrodynamic forces.

$$\mathbf{F}_i^H = -\sum_{j=1}^{N} \zeta_{ij}\mathbf{v}_j \,, \tag{3.69}$$

with ζ_{ij} being a friction tensor that in general depends on the positions of all of the Brownian particles. Having neglected the momenta of the solvent molecules, the momentum density of the Brownian particles is not a conserved quantity. The momentum coordinates of the Brownian particles are relaxed to thermal equilibrium faster than their position coordinates due to the frequent collisions with the solvent molecules. The typical relaxation time for the momentum is given by $\tau_m = M/\zeta_0 \sim 10^{-9}s$ [71]. In this time the particle has not moved significantly. For times $t \gg \tau_m$ we can integrate out the momenta of the Brownian particles in equation 3.68 to leave the probability distribution $P(\mathbf{r}^N; t)$ of the macroparticles' positions. This is the famous Smoluchowski equation (for a derivation of this equation see [20]):

$$\frac{\partial}{\partial t}P(\mathbf{r}^N; t) = \sum_{i,j=1}^{N} \nabla_i \cdot \mathbf{D}_{ij}(\mathbf{r}^N) \cdot \left(\nabla_j + \frac{1}{k_B T}\nabla_j U(\mathbf{r}^N)\right) P(\mathbf{r}^N; t) \,, \tag{3.70}$$

where $U(\mathbf{r}^N)$ is the energy related to inter-particle potentials of the configuration $\mathbf{r}^N$, and $\mathbf{D}_{ij}(\mathbf{r}^N)$ is the diffusion tensor given by the reciprocal of ζ_{ij}

$$\mathbf{v}_i = \frac{1}{k_B T}\sum_{j=1}^{N} \mathbf{D}_{ij}\mathbf{F}_j \,. \tag{3.71}$$

In equilibrium, the left hand side can be set to zero and the distribution now satisifies

$$\left(\nabla_j + \frac{1}{k_B T}\nabla_j U(\mathbf{r}^N)\right) P_{\text{eq}} = 0 \,, \tag{3.72}$$

i.e.

$$P_{\text{eq}} = \frac{e^{-\beta U}}{Z} \,, \tag{3.73}$$

where $\beta = 1/k_BT$ - the result given in equation 3.1. Equation 3.70 can also be written in terms of an operator $\mathbf{O}$ as

$$\frac{\partial}{\partial t}P(\mathbf{r}^N;t) = \mathbf{O}P(\mathbf{r}^N;t)\,, \tag{3.74}$$

where

$$\mathbf{O} = \sum_{i,j=1}^{N} \nabla_i \cdot \mathbf{D}_{ij}(\mathbf{r}^N) \cdot \left(\nabla_j + \frac{1}{k_BT}\nabla_j U(\mathbf{r}^N)\right)\,. \tag{3.75}$$

The advantage of writing it in this form is that the formal solution is given by

$$P(\mathbf{r}^N;t) = P(\mathbf{r}^N;0)e^{\mathbf{O}\tau}\,, \tag{3.76}$$

in which the exponential represents an expansion in powers of $\mathbf{O}\tau$.

We now consider the time dependence of a correlation function

$$\left\langle f_1[\mathbf{r}^N(0)]f_2[\mathbf{r}^N(\tau)]\right\rangle \equiv \langle f_1(0)f_2(\tau)\rangle = \int d\mathbf{r}_0^N \int d\mathbf{r}^N f_1[\mathbf{r}^N(0)]f_2[\mathbf{r}^N(\tau)]P(\mathbf{r}^N,\tau;\mathbf{r}_0^N,0)\,, \tag{3.77}$$

where $P(\mathbf{r}^N,\tau;\mathbf{r}_0^N,0)$ is the probability that the particles are in positions $\mathbf{r}_0^N$ at time 0 and positions $\mathbf{r}^N$ at the later time τ. We may rewrite this in terms of the conditional probability $P(\mathbf{r}^N,\tau \mid \mathbf{r}_0^N,0)$ which we define by

$$P(\mathbf{r}^N,\tau;\mathbf{r}_0^N,0) = P(\mathbf{r}^N,\tau \mid \mathbf{r}_0^N,0)P(\mathbf{r}_0^N)\,, \tag{3.78}$$

where $P(\mathbf{r}_0^N)$ is the probability that the particles adopt the position $\mathbf{r}_0^N$, which is simply the equilibrium distribution given in equation 3.73. The conditional probability satisfies the Smoluchowski equation with the initial condition that

$$P(\mathbf{r}^N,0 \mid \mathbf{r}_0^N,0) = \delta(\mathbf{r}^N - \mathbf{r}_0^N)\,. \tag{3.79}$$

Using equations 3.73, 3.76, 3.77, 3.78, 3.79 we obtain

$$\langle f_1(0)f_2(\tau)\rangle = \frac{1}{Z}\int d\mathbf{r}_0^N \int d\mathbf{r}^N f_1[\mathbf{r}_0^N]f_2[\mathbf{r}^N]\exp\left[-\beta U(\mathbf{r}_0^N)\right]e^{\mathbf{O}\tau}\delta(\mathbf{r}^N - \mathbf{r}_0^N)\,. \tag{3.80}$$

The integral may be performed over $\mathbf{r}^N$ to give (see [20] for details)

$$\langle f_1(0)f_2(\tau)\rangle = \left\langle f_1(0)e^{\tilde{\mathbf{O}}\tau}f_2(0)\right\rangle , \tag{3.81}$$

where $\tilde{\mathbf{O}}$ is the adjoint operator given by

$$\tilde{\mathbf{O}} = \sum_{i,j=1}^{N}\left(\nabla_j + \frac{1}{k_BT}\nabla_j U(\mathbf{r}^N)\right).\mathbf{D}_{ij}(\mathbf{r}^N)\cdot\nabla_i . \tag{3.82}$$

Once more the exponential represents a power series:

$$\langle f_1(0)f_2(\tau)\rangle = \langle f_1(0)f_2(0)\rangle + \tau\left\langle f_1(0)\tilde{\mathbf{O}}f_2(0)\right\rangle + \tau^2\left\langle f_1(0)\tilde{\mathbf{O}}\tilde{\mathbf{O}}f_2(0)\right\rangle \ldots \tag{3.83}$$

3.4.1 Mean square displacement and dynamic structure factor

We may use equation 3.81 to find the mean square displacement of colloids both with and without hydrodynamic forces. The derivation involves much tedious algebra and can be found in the work by Tough *et al* [72]. Only the main results will be quoted here.

In one dimension the mean square displacement is given by

$$\begin{aligned}\left\langle \Delta r_i^2(\tau)\right\rangle &= \left\langle [r_i(\tau) - r_i(0)]^2\right\rangle . \\ &= 2\left\langle r^2\right\rangle - 2\langle r(0)r(\tau)\rangle\end{aligned} \tag{3.84}$$

Substituting $f_1 = f_2 = r$ into equation 3.83 and using the results from [72] gives

$$\frac{\langle \Delta r_i^2(\tau)\rangle}{2} = \langle D_{ii}\rangle\tau - \frac{\tau^2}{2}\sum_{j=1}^{N}\sum_{k=1}^{N}\left[\beta\left\langle D_{ij}\frac{\partial^2 U}{\partial r_j\partial r_k}D_{ik}\right\rangle + \left\langle \frac{\partial D_{ik}}{\partial r_j}\frac{\partial D_{ij}}{\partial r_k}\right\rangle\right] + O(\tau^3) , \tag{3.85}$$

which in the absence of hydrodynamics takes the simpler form

$$\frac{\langle \Delta r_i^2(\tau)\rangle}{2} = \tau\frac{k_BT}{\zeta} - \frac{\tau^2}{2}\frac{k_BT}{\zeta^2}\left\langle \frac{\partial^2 U}{\partial r_i^2}\right\rangle + O(\tau^3) . \tag{3.86}$$

ζ is the friction coefficient in the absence of hydrodynamic interactions given in section 2.4. In the absence of particle interactions ($U = 0$), equation 3.86

simplifies to the Stokes Einstein equation for 1-dimension (c.f. equation 2.54):

$$\left\langle \Delta r_i^2(\tau) \right\rangle = 2D_0\tau \ . \tag{3.87}$$

A similar process may be undertaken to find the dynamic structure factor. In this case the appropriate substitutions are

$$f_1 = f_2^* = \frac{1}{\sqrt{N}} \sum_{j=1}^{N} e^{i\mathbf{Q}\cdot\mathbf{r}_j} \ , \tag{3.88}$$

and the solution is

$$f(Q,\tau) = 1 - \frac{1}{S(Q)} \frac{Q^2\tau}{N} \sum_{j,k=1}^{N} < D_{jk} e^{i\mathbf{Q}\cdot(\mathbf{r}_j - \mathbf{r}_k)} > + O(\tau^2) \tag{3.89}$$

$$= 1 - \frac{D_0}{S(Q)} Q^2\tau + O(\tau^2) \ , \tag{3.90}$$

with and without hydrodynamic interactions respectively. $S(Q)$ is the static structure factor introduced in section 2.3.3.

$$S(Q) = \frac{1}{N} \sum_{j=1}^{N} \sum_{k=1}^{N} \left\langle e^{i\mathbf{Q}\cdot(\mathbf{r}_j(t) - \mathbf{r}_k(t))} \right\rangle \ . \tag{3.91}$$

The term of order τ^2 is non-trivial and contains derivatives of both U and D_{jk}. This results in a dynamic structor factor which is significantly non-exponential and, were cumulant analysis applied, it would reveal a diffusion coefficient that was a function of time $D(\tau)$. Of particular interest is the short time diffusion coefficient. As $\tau \longrightarrow 0$ the first cumulant is given by

$$\frac{df(Q,\tau)}{d\tau} = \frac{Q^2}{S(Q)} \frac{1}{N} \sum_{j,k=1}^{N} < D_{jk} e^{i\mathbf{Q}\cdot(\mathbf{r}_j - \mathbf{r}_k)} > \tag{3.92}$$

$$= \frac{D_0 Q^2}{S(Q)} \ , \tag{3.93}$$

with and without hydrodynamics respectively. Note that $\tau \longrightarrow 0$ also includes the proviso $\tau \gg \tau_M$. From these equations we can define a hydrodynamic factor $H(Q)$ such that

$$D_{\text{eff}}^S = D_0 \frac{H(Q)}{S(Q)} \ , \tag{3.94}$$

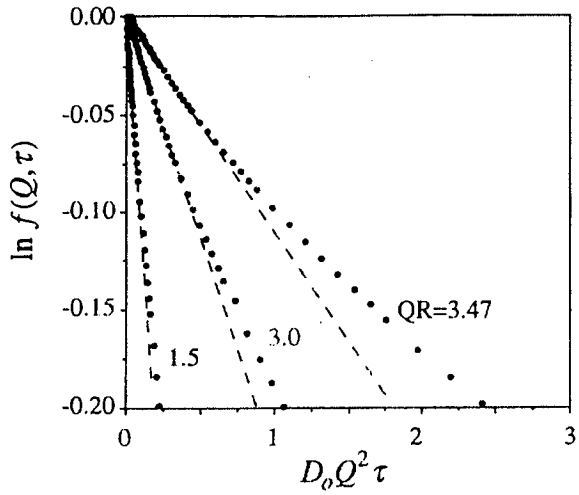

Figure 3.9: TCDLS correlation functions $\ln f(Q,\tau)$ against the normalised decay time $D_0Q^2\tau$ for a concentrated system of hard spheres. Short time diffusion is marked by the dashed line. The peak of the static structure factor is at $QR = 3.47$. The correlation function is clearly not a single exponential. Reproduced from [16].

with

$$H(Q) = \frac{1}{ND_0} \sum_{j,k=1}^{N} < D_{jk} e^{i\mathbf{Q}\cdot(\mathbf{r}_j - \mathbf{r}_k)} > , \tag{3.95}$$

and D_{eff}^S is the effective short time diffusion coefficient.

Segrè *et al.* used two colour dynamic light scattering to study a concentrated (up to $\phi_c = 0.494$) system of PMMA colloids [16]. They found that the dynamic structure factor was significantly non-exponential with the diffusion slowing with time (see figure 3.9). Consider the definition of the dynamic structure factor given by equations 2.40 and 2.41. For a concentrated system this is equivalent to

$$\begin{aligned} f(Q,\tau) &= \frac{1}{NS(Q)} \sum_{j=1}^{N} \sum_{k=1}^{N} \left\langle e^{i\mathbf{Q}\cdot(\mathbf{r}_j(0) - \mathbf{r}_k(\tau))} \right\rangle \\ &= \frac{1}{NS(Q)} \sum_{j=k} \left\langle e^{i\mathbf{Q}\cdot(\mathbf{r}_j(0) - \mathbf{r}_j(\tau))} \right\rangle + \frac{1}{NS(Q)} \sum_{j\neq k} \left\langle e^{i\mathbf{Q}\cdot(\mathbf{r}_j(0) - \mathbf{r}_k(\tau))} \right\rangle . \end{aligned} \tag{3.96}$$

These terms are referred to as self- and distinct-diffusion respectively. In the absence of interactions, positions of different particles are uncorrelated and the

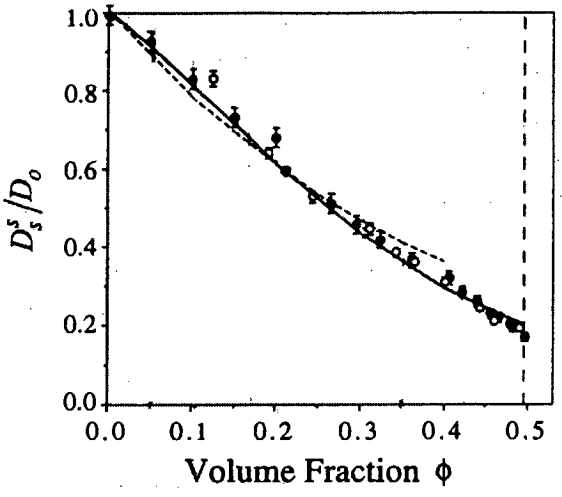

Figure 3.10: Normalised short-time self-diffusion coefficients D^S/D_0. Closed circles represent TCDLS experiments on particles of PMMA, the open circles represent LBE simulations, the dashed line the theoretical predictions of Beenakker and Mazur and the solid lines the theoretical predictions of Tokuyama and Oppenheim. Reproduced from [16].

cross terms vanish. When this occurs, $f(Q,\tau)$ essentially represents the diffusion of a single particle and, since this condition also results in $S(Q) = 1$, it takes the form of $f(Q,\tau)$ derived in equation 2.57. Alternatively, in the limit of taking measurements at high Q, small variations in the relative particle positions $\mathbf{r}_j - \mathbf{r}_k$ cause large variations in the phase factor $\mathbf{Q}\cdot(\mathbf{r}_j - \mathbf{r}_k)$ and the cross-terms once more vanish in the ensemble average. Segrè *et al.* note that by taking measurements at a scattering-vector where $S(Q) = 1$ (which occurs either side of the main peak in $S(Q)$), the cross-terms in equation 3.91 cancel. While this does not guarantee their absence in equation 3.96, he notes that previous work at this scattering vector gives a reasonable description of the self motions. He thus measures the short time self diffusion coefficient and compares it to both the theory of Beenaker and Mazur [73] and simulations based on the fluctuating lattice Boltzmann equation. The agreement is suprisingly good over the whole range of volume fractions studied (figure 3.10).

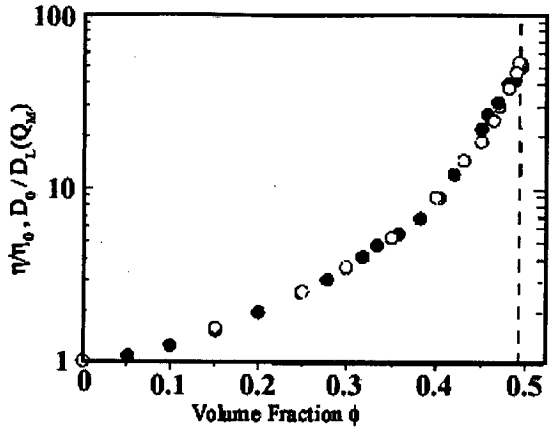

Figure 3.11: Viscosity and inverse structural relaxation rate versus the volume fraction ϕ of suspensions of PMMA spheres. The open circles are the values of η/η_0 and the filled circles represent $D_0/D^L(Q_m)$. The size of the symbols represents the estimated uncertainty in both measurements. Reproduced from [74].

Segrè *et al.* also studied the long time diffusion coefficient D^L [74]. He found that the longer time decays are roughly exponential and fit them with $f(Q, \text{large } \tau) = \exp[-D^L(Q)Q^2\tau]$. From this, and from viscosity studies, he obtained the identity

$$\frac{D_0}{D^L(Q_m)} = \frac{\eta}{\eta_0}, \tag{3.97}$$

where $D^L(Q_m)$ represents the long time diffusion coefficient at wavevector Q_m, corresponding to the peak in the structure factor (see figure 3.11). This diffusion coefficient does not represent self-diffusion. η is the low-shear-rate viscosity of the suspension. D_0 and η_0 represent the low concentration diffusion coefficient and viscosity respectively. This implies that the long time diffusion *at the peak* of the structure factor follows the Stokes-Einstein relation. Segrè notes that there is no theory explaining this identity.

3.4.2 Relevance to colloid-polymer mixtures

Currently the Smoluchowski equation has not been solved for a colloid-polymer mixture. However we may make some tentative predictions based on the above

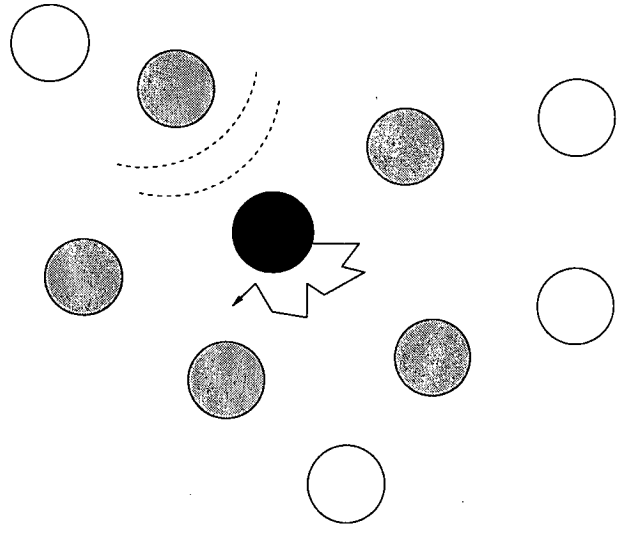

Figure 3.12: Illustration of diffusive modes in a concentrated system of hard spheres. At short times the dominant mode is the self-diffusion of a colloid (black circle) within a cage of other colloids (shaded circles). The only colloid-colloid interactions are hydrodynamic (an example of this interaction is represented by the dotted lines). At longer times the dominant mode is the structural relaxation of the cage.

treatment. The dynamics of systems of concentrated colloids are often explained in terms of a *cage model.* At short times the dominant diffusional mode is that of self-diffusion within a 'cage' of other colloids. The timescale is such that the diffusion of a single colloid has not yet been slowed down by direct interactions with other colloids, and the reduction in the short time diffusion coefficient is entirely due to hydrodynamic interactions. The dominant mechanism at longer times is the structural rearrangement of the cage. This is similar in many ways to the diffusive modes of a Cahn-Hilliard system. Figure 3.12 shows a schematic of this behaviour. The position of the peak of the structure factor represents (in reciprocal space) the spatial size of the cage, and its relaxation is governed by both direct interactions and hydrodynamic effects.

Consider a system of dilute colloids in a polymer solution at concentrations below c^*. At short times the dominant diffusional mode is self-diffusion of a single colloid. On this timescale the diffusion of the colloid will not have been slowed

by direct interactions and we would expect a reduction in the diffusion coefficient from its value in the pure solvent. The reduction would be entirely due to hydrodynamic considerations. The flow of fluid around a polymer coil is extremely complex due to its irregular shape. Experimentally it is found that a single polymer coil acts as though hydrodynamically impermeable - there is a strong cooperative effect in the central parts of the coil, and the liquid moves with the segments [39]. There is, to my knowledge, no calculation similar to that of Beenakker and Mazur [73] for the hydrodynamic reflections from a cage of polymers. A size ratio $\xi < 1$ might imply that the polymer cage is hydrodynamically weaker than a colloid cage, as might the somewhat flexible nature of the coils.

At longer times there should be at least two cooperative relaxations, similar to the modes in the Cahn-Hilliard theory. If we ensure that the number of colloids is significantly less than that of the polymer, at least one of these modes should simply be the relaxation of the polymer cage. On this timescale direct interactions between the colloid and polymer should be important and it seems likely that, at times long compared to this relaxation of the polymer cage, the colloid effectively sees the polymer solution as a continuum. In this case the Stokes-Einstein relation would be expected to hold, though with a viscosity $\eta = \eta_{\text{polymer}}$. We might compare this to the long time relaxation in the system of concentrated colloids, though in our case the structure factor for the colloids in the colloid-polymer mixture is essentially unity throughout.

Based on the Smoluchowski equation, one might expect the following behaviour of the *colloids* in a dilute colloid/less dilute polymer mixture.

- A dynamic structure factor that is significantly non-exponential
- A short time diffusion coefficient[5] that is less than the value in pure solvent

[5]Since dilute, all colloid motion considered is self-diffusion

and with a reduction factor (D^S/D_0) of a similar order to that of the short time self-diffusion in a suspension of colloids at the same total number density.

- An exponential long time diffusion coefficient that scales with the viscosity of the solution.

3.5 Conclusions

In this chapter I have discussed how both direct and solvent-mediated interactions modify the diffusion of the colloid in a colloid-polymer mixture. The Cahn-Hilliard approach gives an insight into the way thermodynamic interactions affect the diffusion. In a closed system it is not possible to assign a separate free energy to the polymer and the colloid, and the chemical potentials couple - a gradient in the chemical potential of one species leads to diffusion in the other. This coupling changes the diffusional modes from pure colloid and pure polymer to a complicated mixture of condensation and demixing. Within this model, spinodal decomposition is driven by demixing. These modes lead to a double-exponential form of the colloid dynamic structure factor with the initial slope independent of the presence of a reservoir. In a system with a reservoir, the reduction in diffusion coefficient due to the depletion interaction is damped out by hydrodynamic interactions.

While the Cahn-Hilliard gives useful insights into the system, it is the Smoluchowski formulation that gives an exact equation for the dynamics of the system. Unfortunately this is currently unsolved for a system of dilute colloids and polymers, however we can make some useful predictions based on both experimental and theoretical results in concentrated systems of hard spheres. We would expect a significantly non-exponential dynamic structure factor with the reduction in the short-time diffusion coefficient only due to hydrodynamic interactions with the

polymer. At long times it would not be suprising if the Stokes-Einstein equation were to hold but with the viscosity replaced by that of the polymer solution.

Chapter 4

Experimental investigation

4.1 Introduction

In this chapter I will present results from preliminary dynamic light scattering experiments performed on a model system over a range of scattering vectors and polymer concentrations. Assuming that the cross-scattering (in which the electric field scattered from one species is correlated with that from the other) is negligible, the colloid dynamic structure factor may be obtained from these experiments. It was found that these dynamic structure factors did not take the simple exponential form given in equation 2.57. In addition, the mean square displacement of the colloid with time $< \Delta r^2(t) >$, as obtained by equation 2.56, appeared to depend on the scattering vector it was measured at. It is proposed that this unphysical result is due to the incorrect assumption of negligible cross-scattering in the analysis of the dynamic light scattering data.

A novel method for both calculating and estimating experimentally the magnitude of the cross scattering was developed for this work. Several methods were considered for reducing its magnitude. Contrast variation, in which the refractive index of the polymer or solvent is changed, was considered but the most suitable

solvent, tetralin, was found to swell the particles[1]. No other solvent/polymer pairs could be found that would reduce the cross-scattering, were safe to use and could be obtained in sufficient quantities for both light scattering and rhelogocial measurements.

Since I was able to calculate the *magnitude* of the cross-scattering, a measurement of its *form* would, in general, allow a correction for its effect to be made. A new experimental procedure was proposed to measure this form but the presence of noise and the polydispersity of the colloidal samples made an accurate measurement impossible.

Instead, a new methodology was derived in which effect of cross-scattering was minimised by eliminating data corrupted by cross-scattering from the analysis. The procedure made use of the scattering vector dependence of the diffusion coefficient to identify this data. Once the dynamic structure factor of the colloid alone was obtained, it could be analysed according to the theories put forward in the previous chapters. This analysis, and the results obtained from it, are discussed towards the end of this chapter.

For clarity, this chapter has not been written from a historical perspective and the emphasis is placed upon those experiments in which the problems associated with cross-scattering had been minimised.

4.2 Preliminary measurements

A large number of dynamic light scattering experiments were performed on colloid-polymer mixtures at various compositions and size ratios. Throughout these experiments it was assumed that cross-scattering was negligible, so that the total dynamic structure factor measured at the correlator $f_T(Q,\tau)$ could be written as

[1]The results of these experiments can be found in Chapter 2.

the weighted sums of the colloid and polymer dynamic structure factors (assuming, as usual, that we may neglect the scattering from the solvent):

$$I_T f_T(Q,\tau) = I_c f_c(Q,\tau) + I_p f_p(Q,\tau) \,, \tag{4.1}$$

where

$$I_T = I_p + I_c \,. \tag{4.2}$$

I_α represents the intensity scattered from component α and the subscripts T, c, p refer to total, colloid and polymer respectively.

To obtain the dynamic structure factor of the colloid alone, the following procedure was followed:

- DLS was performed on the mixture of colloids and polymers to obtain I_T and $f_T(Q,\tau)$.

- The mixture was then centrifuged at high angular velocity. The colloids are denser then the solvent and move to the bottom of the cell forming a close-packed sediment. The polymers are more closely density matched with the solvent and do not sediment under the conditions used here[2]. Measurements of the transmitted intensity were made through the supernatant fluid at regular periods (usually daily) until no change was seen over a period of two days. When this occurs all the colloids are contained within the sediment.

- The DLS experiment was repeated on the supernatant to obtain I_p^s and $f_p^s(Q,\tau)$. Assuming there is no change in the polymer static or dynamic structure factor on removal of the dilute colloid then $I_p^s = I_p$ and $f_p^s(Q,\tau) = f_p(Q,\tau)$.

[2]This has been confirmed by experiment: a polymer solution was centrifuged at high angular velocity for one week and the transmitted laser intensity through the top of the sample measured daily. No change in this intensity was seen throughout the period.

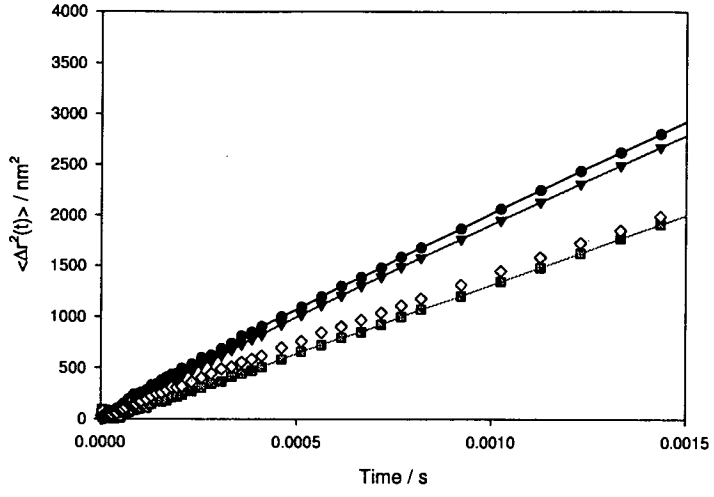

Figure 4.1: Mean square displacement against time for 150nm colloids diffusing in a solution of linear polystyrene in *cis*-decalin. The colloid volume fraction is 0.005 and the effective polymer volume fraction 0.54. The size ratio is 0.87. Data obtained at $30°, 50°, 70°, 90°$ is represented by squares, diamonds, triangles and circles respectively.

Before every measurement of intensity, the intensity of a test sample was measured so that any variation in the intensity of the laser beam before and after the sample was centrifuged could be accounted for.

From equations 4.1 and 4.2, $f_c(Q,\tau)$ may be now calculated. Using equation 2.56, reproduced here for convenience, the mean square displacement of the colloid with time may be obtained[3]:

$$f_c(Q,\tau) = e^{-\frac{Q^2<\Delta r^2(t)>}{6}} . \tag{4.3}$$

Typical results obtained at four angles are shown in figure 4.1. Results obtained at different angles are not co-linear. This would seem to imply that the mean square displacement is a function of the angle used to measure it. Since we are in the dilute colloid limit, all diffusion measured is *self*-diffusion and, assuming we are

[3]Strictly speaking this equation is an approximation. Its validity for describing the motion of a dilute colloid in a polymer solution is discussed later. It will be shown that it is expected to hold for all the experiments in this chapter.

far from the form-factor minimum so that polydispersity effects are negligible, the diffusion coefficient obtained at all angles should be the same. Figure 4.1 cannot be a true, physical representation of the diffusion of the colloid.

It seems logical that the results in figure 4.1 do not represent the self-diffusion of the colloid. If cross-scattering were not negligible then the data would in fact represent the weighted sum of the cross and colloid dynamic structure factors. To proceed further it is necessary to find the magnitude of the cross-scattering in this system to verify whether it is the assumption that it is negligible that is causing these apparently unphysical results.

4.3 Cross scattering

If a light scattering experiment is performed on a suspension containing two scattering species, then the intensity of scattered light may be split into three distinct terms[4] - a 'pure' scattering from each species in which the electric field from each species is correlated with itself, and cross scattering from the correlation of the electric field scattered by the first species with that from the second. Each of the three partial intensities has an associated dynamical part, representing how the intensity is correlated in time. Thus a typical binary system is characterised by six unknown parameters.

4.3.1 Static light scattering

Consider equation 2.23. For two species (1, 2) the electric field scattered at time t and scattering vector Q becomes

$$E_s(\mathbf{Q},t) = \sum_{j\epsilon 1} \delta n(\mathbf{r}_j) e^{i\mathbf{Q}\cdot\mathbf{r}_j(t)} + \sum_{k\epsilon 2} \delta n(\mathbf{r}_k) e^{i\mathbf{Q}\cdot\mathbf{r}_k(t)} \,, \tag{4.4}$$

[4]Assuming again that the scattering from the solvent is negligible.

where $\mathbf{r}_k(t)$ is the position of the k'th scatterer at time t and the other terms retain their meaning from equation 2.23. The ensemble averaged intensity becomes

$$I_T = \underbrace{\left\langle \sum_{j\varepsilon 1}\sum_{k\varepsilon 1} \delta n_1^2 \exp i\mathbf{Q}\cdot(\mathbf{r}_j-\mathbf{r}_k)\right\rangle}_{\text{pure1}} + \underbrace{2\left\langle \sum_{i\varepsilon 1}\sum_{j\varepsilon 2} \delta n_1 \delta n_2 \exp i\mathbf{Q}\cdot(\mathbf{r}_j-\mathbf{r}_k)\right\rangle}_{\text{cross}} + \underbrace{\left\langle \sum_{i\varepsilon 2}\sum_{j\varepsilon 2} \delta n_2^2 \exp i\mathbf{Q}\cdot(\mathbf{r}_j-\mathbf{r}_k)\right\rangle}_{\text{pure2}} . \quad (4.5)$$

Each of these terms may be addressed independently. The pure terms are rewritten as in section 2.3.3 and to obtain

$$I_\alpha = N_\alpha b_\alpha^* b_\alpha \left(1 + \frac{N_\alpha}{V}\int (g_{\alpha\alpha}(r)-1)e^{i\mathbf{Q}.\mathbf{r}}d\mathbf{r}\right) , \quad (4.6)$$

where the $b_\alpha \equiv b_\alpha(\mathbf{Q})$ and so on. $g_{\alpha\alpha}(r)$ represents the self-radial distribution function of species α, with number N_α and particle volume V_α. It is proportional to the probability that, if we fix a particle of species α at $r = 0$, another particle of the same species is found at position r.

An expression for the cross scattering[5] is developed using a similar argument to that used to obtain equation 4.6. We rewrite the position of the j'th scatterer as $\mathbf{r}_j(t) = \mathbf{R}_j^s(t) + \mathbf{r}_j^s$ where $\mathbf{R}_j^s(t)$ is the position at time t of the center of the sphere containing the j'th scatterer and $\mathbf{r}_j^s$ is the position of the scatterer relative to that sphere (see figure 2.9):

$$\begin{aligned} I_x &= \delta n_1 \delta n_2 \left\langle \sum_{j\varepsilon 1}\sum_{k\varepsilon 2} \exp i\mathbf{Q}\cdot(\mathbf{r}_j-\mathbf{r}_k)\right\rangle \\ &= \delta n_1 \delta n_2 \left\langle \sum_{j\varepsilon 1}\sum_{k\varepsilon 2}\sum_{l\varepsilon 1}\sum_{m\varepsilon 2} \exp i\mathbf{Q}\cdot(\mathbf{R}_s^j-\mathbf{R}_s^k)\exp i\mathbf{Q}\cdot(\mathbf{r}_s^l-\mathbf{r}_s^m)\right\rangle \\ &= b_1^* b_2 \left\langle \sum_{j\varepsilon 1}\sum_{k\varepsilon 2} \exp i\mathbf{Q}\cdot(\mathbf{R}_s^j-\mathbf{R}_s^k)\right\rangle \\ &= b_1^* b_2 \frac{N_1 N_2}{V}\int d\mathbf{r}(g_{12}(r)-1)e^{i\mathbf{Q}.\mathbf{r}} , \end{aligned} \quad (4.7)$$

where $g_{12}(r)$ is defined as $\left\langle \delta(r-R_s^j)\delta(\bar{r}-R_s^k)\right\rangle / V^2$ with $j\varepsilon 1$ and $k\varepsilon 2$. In this case there is no $j = k$ cancellation as for the pure terms.

[5]Strictly speaking this means 'scattering associated with the cross term'.

4.3.2 Obtaining the static structure factors - the approximate radial distribution function route

The integrals in equations 4.6 and 4.7 may be evaluated on selection of suitable radial distribution functions. For a system of dilute colloid in a polymer solution, we may assume that the colloids are far enough separated that they do not interact via the depletion potential. The self-radial distribution function for the colloid may therefore be written as

$$g_{cc}(r) = \begin{cases} 0 & r < 2R_c \\ 1 & r \geq 2R_c = \sigma_c \end{cases} \tag{4.8}$$

with R_c the radius of a colloidal particle. Physically this means that all colloid-colloid separations with no overlap are equally likely. Performing the Fourier transform gives the integral of equation 4.6 as:

$$\int (g_{cc}(r) - 1) e^{i\mathbf{Q}.\mathbf{r}} d\mathbf{r} = -\frac{4\pi}{Q^3} (\sin Q\sigma_c - Q\sigma_c \cos Q\sigma_c) \ . \tag{4.9}$$

Thus bracketed term in equation 4.6 becomes

$$S_{cc} = 1 - \frac{24\phi_c}{(Q\sigma_c)^3} (\sin Q\sigma_c - Q\sigma_c \cos Q\sigma_c) \ , \tag{4.10}$$

where ϕ_c is the colloid volume fraction.

In this system, the simplest approximation to the cross-radial distribution function takes the form

$$g_{cp}(r) = \begin{cases} 0 & r < \sigma_x = \sigma_c(1+\xi)/2 \\ 1 & r \geq \sigma_x \end{cases} \tag{4.11}$$

allowing us to rewrite equation 4.7 as

$$\begin{aligned} I_x &= b_c^* b_p \frac{N_c N_p}{V} \int d\mathbf{r} (g_{cp}(r) - 1) e^{i\mathbf{Q}.\mathbf{r}} \\ &= b_c^* b_p \sqrt{N_c N_p} S_{cp} \ , \end{aligned} \tag{4.12}$$

where

$$\begin{aligned} S_{cp} &= \sqrt{\rho_c \rho_p}\frac{4\pi}{Q^3}\left(\sin Q\sigma_x - Q\sigma_x \cos Q\sigma_x\right) \\ &= \frac{3}{(Q\sigma_x)^3}\sqrt{\phi_c \phi_p}\,\xi^{-3/2}(1+\xi)^3\left(\sin Q\sigma_x - Q\sigma_x \cos Q\sigma_x\right) . \end{aligned} \quad (4.13)$$

ϕ_p is the volume fraction of polymer.

Finally we need an expression for the polymer self-radial distribution function. Although the polymer is assumed to act as an ideal gas, the presence of the colloid limits the possible spatial configurations of the polymer centres of mass. Warren *et al.* [63] have suggested, and confirmed by simulations, that a suitable form might be

$$g_{pp}(r) = \frac{1}{\alpha}e^{-r/R_c} , \quad (4.14)$$

where α is the free volume factor. Performing the Fourier transform gives

$$\int (g_{pp}(r) - 1)e^{i\mathbf{Q}.\mathbf{r}}d\mathbf{r} = 8\pi\left(\frac{1}{\alpha} - 1\right)\frac{R_c^3}{(1+(QR_c)^2)^2} , \quad (4.15)$$

so the bracketed term of equation 4.6 becomes

$$S_{pp} = 1 + \frac{6\phi_p}{\xi^3}\left(\frac{1}{\alpha} - 1\right)\frac{1}{(1+(QR_c)^2)^2} . \quad (4.16)$$

4.3.3 Obtaining the static structure factors - the intuitive route

The previous method for obtaining the structure factor required a 'guess' of the radial distribution function, and the accuracy depends on how well we have modelled reality. Another method for obtaining the structure factors, with fewer sources of uncertainty, works by relating each of the partial structure factors to the colloid self-structure factor. This may be formulated in terms of an 'intuitive' method, developed by me, or by using integral equations, as formulated by Louis *et al.*

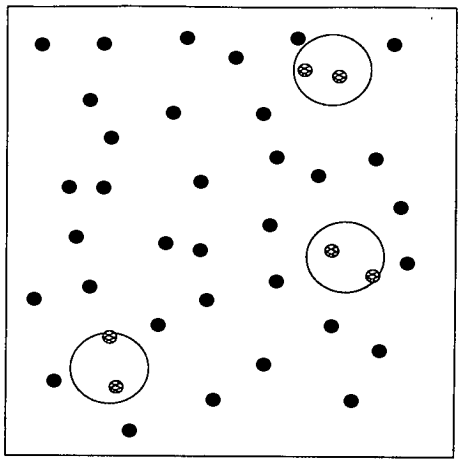

Figure 4.2: Schematic showing the recalculation of the polymer scattering. The system acts like a homogeneous gas of polymers (small circles) with the scattering from the polymers that would be within the depleted region (large circles) subtracted.

Consider the polymer-polymer scattering. We can rewrite the total electric field scattered by the polymers as that from a homogenous system of polymers $\mathbf{E}_h$ minus that from the polymer present within the depleted region $\mathbf{E}_d$ (see figure 4.2). The depleted region is the volume from which the centre of mass of a polymer is excluded, i.e. a sphere of radius $R_C(1+\xi)$ centred on the colloid.

$$\begin{aligned}
\mathbf{E}_p &= \mathbf{E}_h - \mathbf{E}_d \\
\Rightarrow I_p &= \left\langle \mathbf{E}_p^*(\mathbf{Q}).\mathbf{E}_p(\mathbf{Q}) \right\rangle \\
&= \left\langle (\mathbf{E}_h^*(\mathbf{Q}) - \mathbf{E}_d^*(\mathbf{Q})).(\mathbf{E}_h(\mathbf{Q}) - \mathbf{E}_d(\mathbf{Q})) \right\rangle \\
&= \left\langle \sum_{j\epsilon h}\sum_{k\epsilon h} \delta n(\mathbf{r}_j)\delta n(\mathbf{r}_k) \exp i\mathbf{Q}\cdot(\mathbf{r}_j - \mathbf{r}_k) \right\rangle \\
&- 2\left\langle \sum_{j\epsilon d}\sum_{k\epsilon h} \delta n(\mathbf{r}_j)\delta n(\mathbf{r}_k) \exp i\mathbf{Q}\cdot(\mathbf{r}_j - \mathbf{r}_k) \right\rangle \\
&+ \left\langle \sum_{j\epsilon d}\sum_{k\epsilon d} \delta n(\mathbf{r}_j)\delta n(\mathbf{r}_k) \exp i\mathbf{Q}\cdot(\mathbf{r}_j - \mathbf{r}_k) \right\rangle . \qquad (4.17)
\end{aligned}$$

The first part is trivial to solve - it is the scattering from a homogenous system of polymers (which are ideal gas-like). By substituting $g(r) = 1 \; \forall \; r$ into equation 4.6 we may write this term as $N_p b_p^* b_p$.

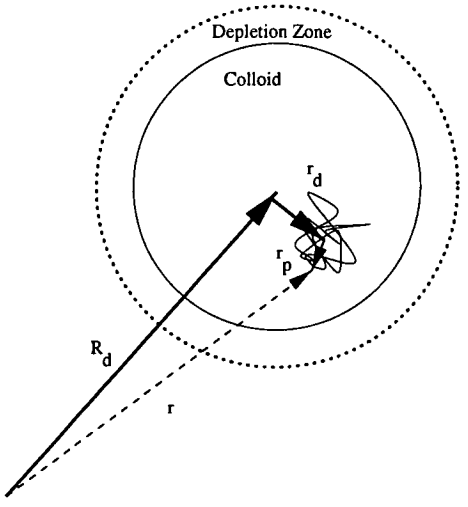

Figure 4.3: Schematic illustrating the redefinition of the position r of the j'th scatterer. R_d is the vector to the centre of mass of the colloid, r_d the vector connecting the centre of the colloid and that of the polymer and r_p the position of the scatterer relative to the centre of the polymer

The second term relates the correlation of the polymer in a depleted region with an ideal gas of polymers. Again $g(r) = 1$ everywhere, but there are significantly fewer terms in the sum in equation 4.17. The depleted regions contain $N_p(1-\alpha)$ polymers. Again assuming that the depletion zones do not overlap, the total number of polymers in a single depleted region may be written $N_p\frac{V_d}{V}$ where V_d is the volume of a single depleted region. Thus the second term of equation 4.17 may be written as $2N_p\frac{V_d}{V}b_p^*b_p$. Note that for a dilute colloid $\frac{V_d}{V} \ll 1$.

The final term of equation 4.17 expresses the correlation of a polymer within a single depleted region with other polymers within its own and other depleted regions. We rewrite the position of the j'th scatterer $\mathbf{r}_j$ as $\mathbf{R}_d^j + \mathbf{r}_d^j + \mathbf{r}_p^j$ where $\mathbf{R}_d$ is the vector to the centre of a depleted region (which is also the centre of the colloidal sphere), $\mathbf{r}_d$ is the vector to the centre of the polymer within the depleted region, and $\mathbf{r}_p$ is the vector to the polymer scattering volume (see figure 4.3). As before we can break up the sum as these three vectors are uncorrelated:

$$I_{dd} = \left\langle \sum_{j\epsilon d}\sum_{k\epsilon d} \delta n(\mathbf{r}_j)\delta n(\mathbf{r}_k) \exp i\mathbf{Q}\cdot(\mathbf{r}_j - \mathbf{r}_k) \right\rangle$$

$$= \delta n_p^2 \left\langle \sum_{j,k}^{N_d} \sum_{l,m}^{N_p(d)} \sum_{n,q}^{\infty} \exp i\mathbf{Q}\cdot(\mathbf{R}_d^j - \mathbf{R}_d^k) \exp i\mathbf{Q}\cdot(\mathbf{r}_d^l - \mathbf{r}_d^m) \exp i\mathbf{Q}\cdot(\mathbf{r}_p^n - \mathbf{r}_p^q) \right\rangle$$

$$= b_p^* b_p \left\langle \sum_{j,k}^{N_d} \sum_{l,m}^{N_p(d)} \exp i\mathbf{Q}\cdot(\mathbf{R}_d^j - \mathbf{R}_d^k) \exp i\mathbf{Q}\cdot(\mathbf{r}_d^l - \mathbf{r}_d^m) \right\rangle .$$

The sum over n, q was solved in the usual way to obtain the polymer form factor. The sum over l, m correlates the positions of a polymer within a single depleted region with other polymers within the same depleted region. The polymers may be anywhere in the depleted region, but there are only $N_p \frac{V_d}{V}$ within each region. This sum therefore gives the form factor of a sphere of radius $R_d = R_p + R_c$ i.e.

$$I_{dd} = b_p^* b_p B_d^* B_d \left(N_p \frac{V_d}{V}\right)^2 \left\langle \sum_{i,j}^{N_d} \exp i\mathbf{Q}\cdot(\mathbf{R}_d^i - \mathbf{R}_d^j) \right\rangle$$

$$= b_p^* b_p \beta_d^* \beta_d \frac{N_p^2 N_c}{V^2} S_{cc} , \tag{4.18}$$

where

$$B_d = \frac{1}{V_d} \int_0^{2\pi} d\phi \int_0^{\pi} d\theta \int_0^{R_d} dr \exp(iQr\cos\theta) , \tag{4.19}$$

$\beta_d = B_d V_d$ and the sum over i and j is identified as the structure factor of the colloids - $S_{cc} = \frac{1}{N_c} \left\langle \sum_{i,j}^{N_c} \exp i\mathbf{Q}\cdot(\mathbf{R}_s^i - \mathbf{R}_s^j) \right\rangle$. Equation 4.17 thus becomes:

$$I_p = N_p b_p^* b_p \left(1 - \underbrace{2\frac{V_d}{V}}_{\approx 0} + \rho_p \rho_c \beta_d^* \beta_d S_{cc} \right) , \tag{4.20}$$

where ρ_c, ρ_p are the number densities of the colloids and polymers respectively.

The relationship between the cross-term and the colloid term is derived in a similar fashion. Using the same convention as in the previous section we obtain:

$$\mathbf{E}_p = \mathbf{E}_h - \mathbf{E}_d \tag{4.21}$$

$$\Rightarrow I_x = 2\langle \mathbf{E}_c^*(\mathbf{Q}).\mathbf{E}_p(\mathbf{Q}) \rangle$$

$$= 2\langle \mathbf{E}_c^*.(\mathbf{E}_h(\mathbf{Q}) - \mathbf{E}_d(\mathbf{Q})) \rangle$$

$$= 2\left\langle \sum_{j\epsilon c} \sum_{k\epsilon h} \delta n(\mathbf{r}_j)\delta n(\mathbf{r}_k) \exp i\mathbf{Q}\cdot(\mathbf{r}_i - \mathbf{r}_j) \right\rangle$$

$$- \left\langle \sum_{j\epsilon c} \sum_{k\epsilon d} \delta n(\mathbf{r}_j)\delta n(\mathbf{r}_k) \exp i\mathbf{Q}\cdot(\mathbf{r}_j - \mathbf{r}_k) \right\rangle . \tag{4.22}$$

Here $\mathbf{E}_c$ refers to the electric field scattered by the colloids. Once more we treat each term individually. The first represents the correlation between the colloids and an ideal gas of polymers. The radial distribution function for such a system is given by $g_{cp}(r) = 1 \; \forall \; r$ and so using equation 4.7 we set this term to zero. The second term represents the correlation between a polymer within the depleted region and the colloids (which are themselves centred on the depleted region). We rewrite the position of the colloid scatterer as $\mathbf{r}_j = \mathbf{R}_s^j + \mathbf{r}_s^j$ (figure 2.9) and that of the polymer scatterer as $\mathbf{r}_k = \mathbf{R}_d^k + \mathbf{r}_d^k + \mathbf{r}_p^k$ (figure 4.3). Noting that $\mathbf{R}_d \equiv \mathbf{R}_s$, we obtain:

$$\begin{aligned} I_x &= -2\delta n_p \delta n_c \left\langle \sum_{j,k}^{N_d} \sum_{l}^{N_p(d)} \sum_{m,n}^{\infty} \exp i\mathbf{Q}\cdot(\mathbf{R}_d^j - \mathbf{R}_d^k) \exp i\mathbf{Q}\cdot\mathbf{r}_d^l \exp i\mathbf{Q}\cdot(\mathbf{r}_p^m - \mathbf{r}_s^n) \right\rangle \\ &= -2b_c^* b_p \left\langle \sum_{j,k}^{N_d} \sum_{l}^{N_p(d)} \exp i\mathbf{Q}\cdot(\mathbf{R}_d^j - \mathbf{R}_d^k) \exp i\mathbf{Q}\cdot\mathbf{r}_d^l \right\rangle \\ &= -2N_p N_c b_c^* b_p B_d \frac{V_d}{V} S_{cc} \,. \end{aligned} \tag{4.23}$$

Using equation 4.5, 4.20 and 4.23 we can now write down the total scattering from a colloid-polymer mixture:

$$\begin{aligned} I_T &= N_c b_c^* b_c S_{cc} - N_c \rho_p b_c^* b_p \beta_d S_{cc} + N_p b_p^* b_p (1 + \rho_p \rho_c \beta_d^* \beta_d S_{cc}) \\ &= N_c S_{cc} \left(\bar{P}_c(Q) - 2\sqrt{\bar{P}_c(Q)\bar{P}_p(Q)}\rho_p \beta_d(Q) + \bar{P}_p(Q)\frac{N_p}{N_c}[\frac{1}{S_{cc}} + \rho_p \rho_c \beta_d^*(Q)\beta_d(Q)] \right) \,, \end{aligned} \tag{4.24}$$

where $\bar{P}_c(Q) = b_c^*(Q)b_c(Q)$ represents the scattering power of the colloids respectively, $\bar{P}_p(Q) = b_p^*(Q)b_p(Q)$ represents the scattering power of the polymers and the Q dependence has been explicitly written in. Using these equations we only need estimate one structure factor, from which the others may be derived.

4.3.4 Obtaining the static structure factors - the integral equation route

A similar result to that obtained by the intuitive method may be derived using integral equations. The binary mixture is characterised by three total and three

direct correlation functions, $h_{jk}(r) = g_{jk}(r) - 1$ and $c_{jk}(r)$ respectively. Ornstein and Zernike formulated a way of relating these quantities in reciprocal space [75]:

$$\hat{h}_{jk}(Q) = \hat{c}_{jk}(Q) + \sum_l \rho_l \hat{c}_{jl}(Q)\hat{h}_{lk}(Q) \ . \tag{4.25}$$

Percus and Yevick suggested a form for the direct correlation function for short range interactions (see [45]):

$$c_{jk}(r) = [1 - \exp(\beta U_{jk}(r))]g_{jk}(r) \ , \tag{4.26}$$

where $U_{jk}(r)$ is interparticle potential for species j and k. In the Asakura Oosawa model the pair correlation functions are:

$$g_{jk} = 0 \quad r < R_{jk} \ , \tag{4.27}$$

where $R_{jk} = R_c$ for the colloids, $R_c(1+\xi)$ for the cross-term and 0 for the polymers. Under these criteria the second and third equations of 4.25 become:

$$\begin{aligned} S_{cp}(Q) &= \sqrt{\rho_1\rho_2}\hat{h}_{12}(Q) = \sqrt{\rho_1\rho_2}\hat{c}_{cp}(Q)S_{cc}(Q) \\ S_{pp}(Q) &= 1 + \rho_2\hat{h}_{22}(Q) = 1 + \rho_1\rho_2\hat{c}^2_{cp}(Q)S_{cc}(Q) \ , \end{aligned} \tag{4.28}$$

where $\hat{c}_{cp}(Q)$ is the Fourier transform of $c_{cp}(r)$ which, from the Percus-Yevick closure relation, must take the form

$$c_{cp}(r) = 0 \quad r > \sigma_x = R_c(1+\xi) \ . \tag{4.29}$$

We may compare the Ornstein-Zernike result (equation 4.28) with that obtained by the intuitive method (equation 4.24). $\beta(r)$, which is a step function, is clearly the low density limit of $c_{cp}(r)$, which can take any form for $r < R_c(1+\xi)$. Figure 4.4 compares the two quantities. The exact form of $c_{cp}(r)$ and therefore the partial structure factors can be found by solving the first of the Ornstein-Zernike relations. Louis *et al.* [32] found that no analytic result existed, but solved the equations numerically to obtain the three partial structure factors.

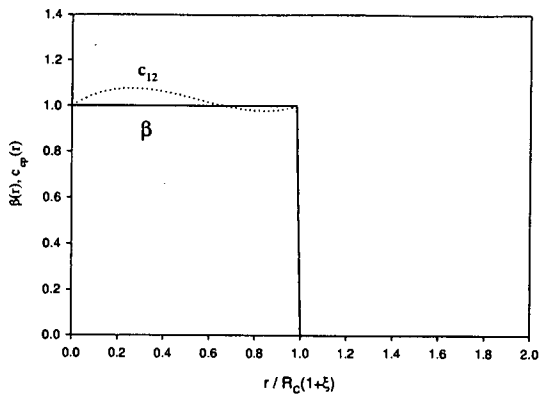

Figure 4.4: Schematic of $c_{cp}(r)$ and $\beta(r)$. Both are confined to be zero at distances greater than $R_c(1+\xi)$, but the direct correlation function may be non-unity at lower distances. β is the low density limit of c_{cp}.

4.3.5 Obtaining the static structure factors - comparison of results

The results from the three methods are shown in figure 4.5 for a typical colloid volume fraction and polymer concentration used in my experiments. For the intuitive approach I used S_{cc}, as given by equation 4.10, as the partial structure factor from which the others were calculated. S_{cc} calculated this way gives a value within 5% of the 'exact' value calculated by Louis. This in turn leads to a 5% error in the magnitude of S_{cp} as calculated by the intuitive approach compared to the Louis result. The value obtained by Fourier transforming g_{cp} is within 1% of the 'exact' result, implying that our model for g_{cp} is close to reality. This model assumed that there was no correlation between the positions of the polymer and colloid except that the polymer cannot enter the depleted region. Long range correlations therefore do not exist between the colloid and the polymer.

The error in S_{pp} as obtained by the radial distribution function route is large: the deviation from unity is more than 350% greater than both the intuitive and integral equation approach. The form of g_{pp} is thus poor. In their paper [63],

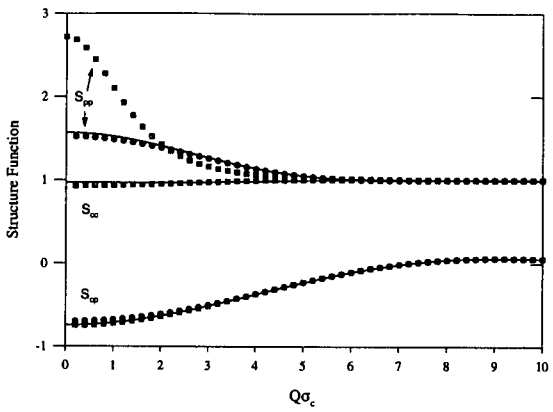

Figure 4.5: Comparison of three methods for finding the partial structure factors of a colloid-polymer mixture. The squares represent the results obtained by Fourier transforming estimates for the radial distribution function. The circles are the cross and polymer structure factors obtained by relating these quantities to the colloid structure factor, and the lines represent the 'exact' result found by solving the Ornstein-Zernike relation within a Percus-Yevick approximation.

Warren *et al.* found from simulations that g_{pp} is expected to decay from $1/\alpha$ to 1, and has a finite, negative slope at $r = 0$. The actual form of g_{pp} given is an approximation that fits these constraints. From this work it is clear that this approximation is not a good one. The intuitive and integral equation methods agree within 5%.

The close agreement between my and Louis's values imply that the direct correlation function c_{cp} does not significantly differ from the β-factor introduced in my work. Equation 4.24 appears to be an accurate way of describing the total scattering, at least at these low colloid volume fractions.

4.4 Dynamic structure factor

The total dynamic structure factor scattered from a colloid-polymer mixture $f_T(Q,\tau)$ may be expressed in terms of the partial dynamic structure factors

weighted by the relative intensities:

$$\begin{aligned} I_T f_T(Q,\tau) &= \langle E_T^*(0)E_T(\tau)\rangle = \left\langle \left(E_c^*(0)+E_p^*(0)\right)\left(E_c(\tau)+E_p(\tau)\right)\right\rangle \\ &= \langle E_c^*(0)E_c(\tau)\rangle + 2\langle E_c^*(0)E_p(\tau)\rangle + \left\langle E_p^*(0)E_p(\tau)\right\rangle \\ &= I_c f_c(Q,\tau) + 2I_x f_x(Q,\tau) + I_p f_p(Q,\tau)\ , \end{aligned} \tag{4.30}$$

where I_α is the intensity scattered by component α, the magnitude of which was given in the previous section. In general the *measured* dynamic structure factor contains contributions from both the polymer, colloid and cross dynamic structure factors. The relative weights of these contributions are given by the partial intensities (I_α/I_T). These may be obtained either experimentally or theoretically using equation 4.24. The weight of the cross scattering W_x compared to that of the colloid is given by

$$W_x = 2\sqrt{\frac{\bar{P}_p(Q)}{\bar{P}_c(Q)}}\rho_p\beta_d(Q)\ , \tag{4.31}$$

and that of the polymer is

$$W_p = \frac{\bar{P}_p(Q)}{\bar{P}_c(Q)}\frac{N_p}{N_c}\left[\frac{1}{S_{cc}} + \rho_p\rho_c\beta_d^*(Q)\beta_d(Q)\right]\ . \tag{4.32}$$

These equations represent the total scattering of the polymer and cross terms compared to the colloid, so the full expression for the scattering power must be used. A polymer coil of radius of gyration R contains significantly fewer scatterers than a colloid of the same radius. Using equations 2.16, 2.21 and 2.22, we obtain the following form for the scattering power of a colloid and polymer:

$$\bar{P}_p(Q) = \frac{I_o}{r^2}\frac{4\pi^2 n_s^2}{\lambda_0^4}\left(\frac{dn}{dc}\right)^2\frac{M_W^2}{N_A^2}P_p(QR_g) \tag{4.33}$$

$$\bar{P}_c(Q) = \frac{I_o}{r^2}\frac{4\pi^2 n_s^2 \delta n^2 v_c^2}{\lambda_0^4}P_c(QR_c)\ , \tag{4.34}$$

where I_o is the input intensity, r the distance from the scattering volume to the detector, λ_0 the wavelength of laser light, n_s the solvent refractive index, v_c the volume of the colloid and the other symbols take their meaning from equations

2.21 and 2.22. P_c, P_p are the normalised form factors derived in equations 2.27 and 2.28. Values of dn/dc can be found in the literature for common polymers and solvents [29].

Another method for obtaining the relative magnitude of the cross and polymer scattering is by experiment; though the simplest method, described here, does make some incorrect assumptions which must be accounted for. The total intensity I_T of a colloid-polymer mixture is measured over a range of angles. The sample cell is then centrifuged until the colloids have sedimented and do not contribute to the scattering (see section 4.2). The intensity measured through the supernatant $I_{\rm ac}$ now represents I_p/S_{pp}. To make any further progress we assume (incorrectly) that the intensity scattered by the colloids alone is given by

$$I_c = I_T - I_{\rm ac} S_{pp} \; . \tag{4.35}$$

The relative weight of the polymer scattering is then given by

$$W_p = \frac{I_{\rm ac} S_{pp}}{I_T - I_{\rm ac} S_{pp}} \; . \tag{4.36}$$

Rewriting the intensity of the cross scattering (equation 4.12) as

$$I_x = 2\sqrt{I_c(Q) I_p(Q)} \frac{S_{cp}(Q)}{S_{cc}(Q) S_{pp}(Q)} \; , \tag{4.37}$$

the relative weight of the cross scattering can be written as

$$I_x = 2\sqrt{(I_T - I_{\rm ac} S_{pp}) I_{\rm ac} S_{pp}} \frac{S_{cp}(Q)}{S_{cc}(Q) S_{pp}(Q)} \; . \tag{4.38}$$

We thus need two measurements of intensities and an estimate for S_{cc}, S_{cp} and S_{pp} for which we use the results of section 4.3.3. Equation 4.35 clearly overestimates the value of I_c and the magnitude of the cross and polymer scattering are both underestimated by W_x. It is interesting to note that, from equation 4.37 and figure 4.5, I_x is negative for $QR_c < 4.49/(1+\xi)$. The concept of a negative intensity is clearly a difficult one, but the intensity of the cross scattering is not a

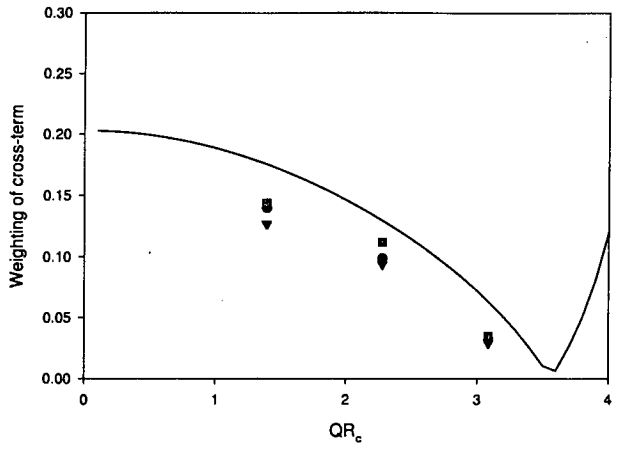

Figure 4.6: Plot of the relative magnitude of the cross scattering (I_x/I_c) against QR_c for a polymer concentration of $0.44c^*$. The line represents the theoretical result of equation 4.31 and the symbols are the experimental results at colloid volume fractions of 0.09% (circles), 0.23% (triangles) and 0.69% (squares). The size ratio is 0.261.

measurable intensity separate from those of the colloid and polymer. It is a quirk of the manner in which we have chosen to divide up the total intensity that gives this apparently unphysical result.

Figure 4.6 shows the theoretical and experimental magnitude of the cross-term for a high effective polymer volume fraction ($c/c^* = 0.44$) and three different colloid volume fractions. The two methods give similar results, and the experimental results confirm that the magnitude of the cross-term is independent of the colloid volume fraction. As Q is increased, the magnitude of the cross-term falls (until $QR_c(1+\xi) = 4.49$) whereas the magnitude of the polymer term increases (figure 4.7). The relative magnitude of the polymer term is, as expected, highly dependent on the colloid volume fraction.

4.5 Obtaining the colloid dynamic structure factor

The data from a dynamic light scattering experiment contains information on three partial intensities coupled with three partial dynamic structure factors. To

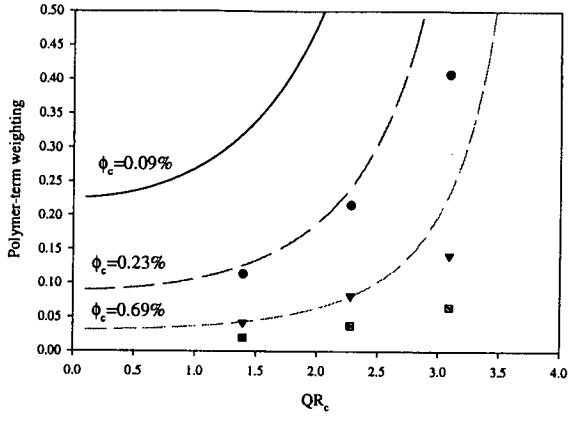

Figure 4.7: Plot of the relative magnitude of the polymer scattering (I_p/I_c) against QR_c for a polymer concentration of $0.44c^*$. The lines represents the theoretical result of equation 4.32 or three colloid volume fractions, and the symbols are the experimental results at colloid volume fractions of 0.09% (circles), 0.23% (triangles) and 0.69% (squares). The size ratio is 0.261.

obtain information about the scattering from one species only (colloid, polymer, cross) we must have some prior knowledge about the other two terms. Either we must know (or be able to measure) their form and magnitude, or we must know that two of the three partial intensities are sufficiently small as to be neglected. In practice the former option is difficult since both $f_x(Q,\tau)$ and $f_c(Q,\tau)$ are unknown. It is therefore desirable to be able to minimise the partial intensity of any two of the colloid, polymer and cross scattering so that the data represents the dynamic structure factor of a single species. Experimentally this may be performed in several ways.

4.5.1 Contrast variation

The magnitude of the scattering from a particular species is dependent on refractive index difference between that species and the background solvent. By changing the refractive index of the solvent n_s, we can adjust the relative scat-

Solvent	n_i	T_θ/°C
Dodecane	1.4216	?
Cyclohexane	1.4267	34.5
Tetralin	1.5413	?
cis-decalin	1.4810	12.5
trans-decalin	1.4695	20.4

Table 4.1: Good solvents for polystyrene and PHSA and bad solvents for PMMA, together with their refractive index n_i and their theta temperature T_θ. A question mark (?) indicates no experimental data on the theta point. Data from [29].

tering. The dependencies are:

$$\begin{aligned} I_c &\propto (n_c - n_s)^2 \\ I_x &\propto |\,(n_c - n_s)(n_p - n_s)\,| \\ I_p &\propto (n_p - n_s)^2\,, \end{aligned} \tag{4.39}$$

where n_p, n_c represent the refractive index of the polymer and colloid respectively. If there were a solvent such that $(n_p - n_s) = 0$ then both the polymer and cross scattering would vanish as desired.

The refractive index of a solvent may be changed by either mixing with another solvent or by changing the solvent. For both methods, the resulting solvent would have to be a good solvent for polystyrene (and ideally have an experimentally accessible theta temperature 10°C$< T_\theta <$ 40°C) and for PHSA, and a poor solvent for PMMA. As can be imagined this places some severe restraints on the choice of solvent. Table 4.1 lists the more common solvents that satisfy these conditions, along with their theta temperature for polystyrene. The solvent suitable for index matching the polymer is tetralin but, as shown in Chapter 2, this solvent enters the PMMA particles, swelling them and changing their refractive index profile. The exact timescale for this behaviour seems to be different for each particle and the subsequent internal rearrangement of tetralin is complicated. This makes

using tetralin as the solvent extremely challenging.

Instead of trying to remove the scattering from one species, we could increase the scattering from the other; for example if *trans*-decalin is used instead of *cis*-decalin then the magnitude of the colloid scattering increases by a factor of 2.6, whereas that from the polymer only by 1.2 (and the cross-term therefore increases by a factor 1.8). We must, however, be careful that the refractive index difference is not so large that multiple scattering becomes significant even at these low concentrations. This condition effectively excludes both dodecane and cyclohexane from consideration.

An alternative to changing the solvent is to use a mixture of solvents. Indeed, intensity measurements on a binary mixture suspended in three different solvent mixtures with different refractive indices would allow a calculation of the constants of proportionality in equations 4.39. The technique of using a 'contrast series' is common in neutron scattering. However, in our case changing the composition of the mixture would change the theta temperature for polystyrene and therefore its size. This could be accounted for by performing the intensity measurements at different solvent temperatures, so that the Fixman parameter remains constant. Unfortunately there is little information in the literature on the theta point of mixtures of suitable solvents.

Clearly the only suitable solvents for this system are *cis*-decalin or *trans*-decalin, with the latter favoured when we wish to increase the scattering from the colloid. Since changing the solvent is not particularly easy, another option to consider is to use a polymer with a more suitable refractive index. There is only one polymer currently available that has a suitable refractive index and for which *cis*-decalin is a good solvent (within the experimentally accessible temperature range) - poly(butadiene). For the majority of the time spent on this research this was unavailable at sufficiently high molecular weights.

Another option to consider is to change both the polymer and the solvent. This opens up the possibilities for a close refractive index match between solvent and polymer and an accessible theta temperature; however the new solvent would also have to be a good solvent for PHSA and a poor solvent for PMMA so that the colloids retain their hard-sphere inter-particle potential. No such solvents are readily available.

4.5.2 Scattering vector dependence

The scattering power of the colloids is Q-dependent (equation 4.34) and shows a minimum at the experimentally accessible value of $Q_{\min}R_c = 4.49$. As $Q_{\min}$ is approached, the colloid term becomes small twice as quickly as the cross-term (which contains a $\sqrt{P_c(QR_c)}$ dependence). This property can be exploited to obtain measurements of the cross dynamic structure factor. As $Q_{\min}$ is approached, the colloid term becomes negligible. When this occurs equation 4.30 becomes:

$$I_t f_t(Q,\tau) = I_x f_x(Q,\tau) + I_p f_p(Q,\tau) \; . \tag{4.40}$$

The intensity and dynamic structure factor of the polymer can then be measured by centrifuging the mixture until all the colloid has sedimented and performing DLS on the supernatant. Thus $f_x(Q,\tau)$ can be calculated. In practice many measurements are made as $Q_{\min}$ is approached until $I_t f_T(Q,\tau) - I_p f_p(Q,\tau)$ no longer changes. At this point the scattering by the colloid may be neglected.

This experiment was performed on colloids of radius 175nm in *cis*-decalin (not *trans*-decalin, as we wished to minimise the colloid scattering). These show a form factor minimum at 90.3°. The polymer had a radius of gyration at 20.0°C of 86.5nm. Figure 4.8 shows plots of $\varrho f_c(Q,\tau) + (1-\varrho) f_x(Q,\tau)$, where $\varrho = I_c/(I_c + I_x)$, against $Q^2\tau$ for various angles. The data at different angles seem to roughly have the same slope and there is no obvious trend on increasing the

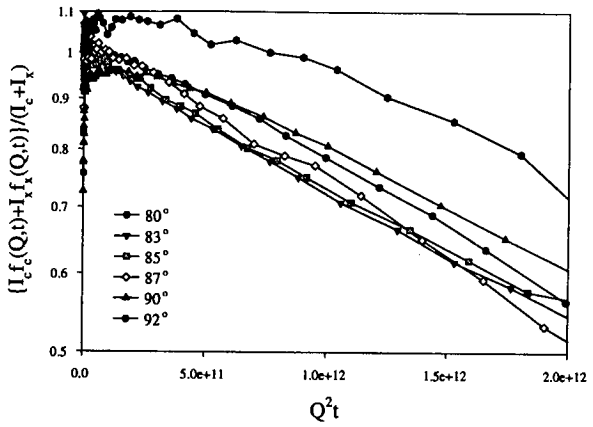

Figure 4.8: Plot of $\varrho f_c(Q,\tau)+(1-\varrho)f_x(Q,\tau)$, where $\varrho = I_c/(I_c+I_x)$, against $Q^2\tau$ for various angles. The colloid volume fraction is 0.11% and the polymer concentration is $0.327c^*$.

detection angle. Since we are measuring near the minimum of the particle form factor, noise from background scattering is not negligible.

This data represents the weighted sum of the colloid and the cross dynamic structure factor. A form for the cross dynamic structure factor is not known, but as a first guess one might assume that it decays as a simple exponential with a diffusion coefficient that is the average of the polymer and colloid diffusion coefficients in the pure solvent, i.e. $(D_c^0 + D_p^0)/2$. In this example, this would result in a cross dynamic structure factor that decayed roughly 1.5 times as fast as that of the colloid. As the relative proportions of the colloid and cross scattering change, this difference in diffusion coefficients should result in a trend in the first cumulant. Assuming that the form factor of the colloid is given by the ideal form of equation 2.27, the scattering from the colloid should decrease over the range 80° to 90° (QR = 4.07 to 4.47) by 32%. The scattering from the cross term therefore decreases by 16%. This results in a change in the first cumulant of

$$\begin{aligned} \frac{\Gamma_f}{\Gamma_i} &= \frac{\varrho^f D_c + (1-\varrho^f)D_x}{\varrho^i D_c + (1-\varrho^i)D_x} \\ &= \frac{0.64 + 1.94\nu + 1.26\nu^2}{0.64 + 1.86\nu + 1.26\nu^2}, \end{aligned} \tag{4.41}$$

where ν is the ratio of cross to colloid scattering at 80°. For $\nu \lesssim 0.1$ the change in the first cumulant due to the increased cross scattering roughly equals ν. In this experiment the first cumulants obtained at all angles lie randomly within the range $(3.0 \pm 0.2) \times 10^{-13}$ m^{2}s^{-1}, implying that ν is less than 6%.

This treatment assumes an ideal form for the colloid form factor; however, real colloidal suspensions are never monodisperse and the scattering never goes identically to zero as the form factor minimum is approached (see, for example, figure 2.10). The colloid scattering might not decrease as much as predicted by the simple treatment given above and the change in the weighting of the cross dynamic structure factor given in equation 4.30 might be too small to allow detection of a trend in the first cumulant. Another factor to consider is the noise in the data: as the colloid scattering is reduced the intensity of the polymer term dominates over that of the cross-term. Table 4.2 shows the relative magnitudes of I_T and I_p as the minimum is approached. The absolute error in $f_x(Q,\tau)$ due to noise in $f_T(Q,\tau), f_p(Q,\tau), I_T$ and I_p is therefore large. The dominant source of noise in these quantities is scattering from the solvent ($I_{\text{solvent}}/I_T \sim 0.1$). It is possible that the change in the first cumulants is not evident above the noise.

Work on different mixtures of colloids and polymers did not give significantly different results and it became obvious that a reliable measurement of $f_x(Q,\tau)$ could not be made by this method.

4.5.3 Increasing the number of colloids

Based on equations 4.6 and 4.12 one might assume that as the number density of colloids is increased, the ratio of cross-scattering to colloid-scattering would be reduced by a factor of $\sqrt{N_c}$, where N_c is the number of colloids. However this does not take into account the dependence of S_{cp} on colloid number density. The correct form is given in equation 4.31. Suprisingly the ratio of cross to

Angle	I_p/I_T
80	0.568
83	0.565
85	0.650
87	0.723
90	0.784
92	0.848

Table 4.2: Relative magnitudes of polymer to total scattering as the colloid form factor minimum is approached. I_p denotes the polymer intensity and I_T the total intensity scattered.

colloid scattering is independent of the number of colloids present, as can be seen experimentally in figure 4.6. This counter-intuitive result stems from the lack of a $(i = j)$ term in the cross static structure factor (equation 4.7). Physically, the static structure factor of the colloids contains a correlation between light scattered in a single colloid with light scattered from that same colloid, and similarly for the polymer. While the shape information is contained within the form factor $P(QR)$, the magnitude of this scattered light is independent of the presence of other colloids. The higher the total number of colloids, the higher this 'self' scattering is. This is the origin of the N_c dependence of the colloid scattering.

For the cross scattering, there is no 'self' scattering and the first order term in the static structure factor is between a colloid and the nearest polymer. This clearly will be dependent on both the number of colloids and the number of polymers. This explains the N_cN_p dependence of the cross scattering. Since the colloid and cross scattering both have the same dependence on N_c, increasing the number of colloids makes no difference to the magnitude of the relative scattering.

The same is not true for the ratio of polymer to colloid scattering which decreases like $C + 1/N_c$, where C is a constant, as the colloid number density is increased.

The constant comes from the higher order correlations between the positions of polymers due to the presence of the colloids.

4.5.4 A new methodology

In this work, I would like to obtain the dynamic structure factor of the colloid alone. Since the dynamics of the cross scattering cannot be easily measured it is necessary to minimise the magnitude of this scattering until negligible. For simplicity the magnitude of the polymer scattering is also reduced until negligible. This is done by increasing the colloid volume fraction until further addition of colloid results in no change in the measured dynamic structure factor. Adding colloid has no effect on the magnitude of the cross scattering, and this is minimised by using *trans*-decalin as the solvent and choosing a suitable range of scattering vectors for the measurements.

There is a very neat way of exploiting the Q-dependence of $f_c(Q,\tau)$ to check whether the polymer or cross scattering is significant. As the colloid is dilute, $f_c(Q,\tau)$ represents *self*-diffusion and should take the form derived in equation 2.56, though with a diffusion coefficient that may be time dependent. The scattering vector dependence is given by:

$$\ln f(Q,\tau) \propto -Q^2 \,. \tag{4.42}$$

Strictly speaking this is an approximation. van Megen and Underwood [76] investigated the deviation from Gaussian behaviour using concentrated systems of hard spheres. They defined the deviation from Gaussian behaviour by a factor $\alpha_2(t)$ given by

$$f(Q,\tau) = \exp\left(-Q^2 w(t)\right)\left[1 + \frac{\alpha_2(t)(Q^2 w(t))^2}{2} + \ldots\right] \tag{4.43}$$

They found that for colloid volume fractions lower than $\phi_c^L = 0.266$, $\alpha_2(t)$ was effectively zero but increased to 0.15 for $\phi_c^U = 0.361$. In these experiments the

colloid volume fraction is lower than ϕ_c^L but the *total* volume fraction of colloids and polymers may be greater than ϕ_c^U. The accuracy of the Gaussian approximation in such a system is unknown. As will be shown in section 4.7.3 this approximation appears valid for polymer concentrations up to $0.5c^*$.

If the total dynamic structure factor $f_T(Q,\tau)$ represents colloid diffusion only it should show Q^2-scaling. If, on the other hand, $f_T(Q,\tau)$ is a weighted sum of the dynamic structure factor of more than one species (colloid and cross or polymer) then this proportionality will not hold. We incorporate this result into the previous experimental method - the colloid concentration is increased until this Q^2 dependence is seen, at which point the total structure factor represents only the colloid-term. Any persistant deviation from Q^2-scaling must be due to the cross scattering. Figure 4.6 showed that the magnitude of the cross-term falls as Q is increased (within a certain range). It is likely that, for a particular experiment, there will be a range of Q for which the total dynamic structure factor scales with Q^2, and it is within this range that the cross-term may be neglected.

This method forms the basis of my experimental technique for obtaining the dynamic structure factor of the colloid in a colloid-polymer mixture. The range of polymer concentration for which we may perform this experiment is limited by the presence of phase boundaries. At high polymer concentrations, the depletion force induces phase separation in even dilute suspensions of colloids. If this occurs before the polymer scattering is negligible with respect to the colloid scattering, then this method cannot be used to obtain the colloid dynamic structure factor.

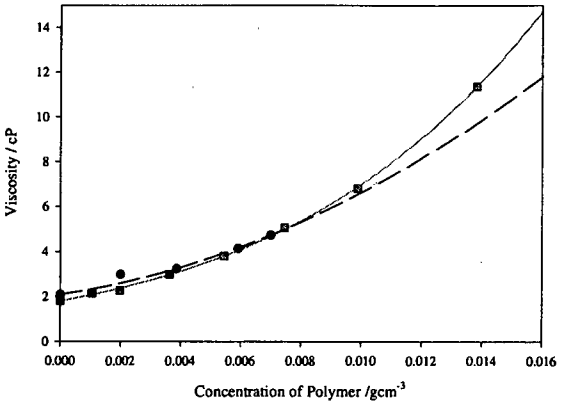

Figure 4.9: Plot of viscosity of polymer solutions in *trans*-decalin at 20.4°C (circles) and 28.6°C (squares) against concentration. Lines have been added to guide the eye. Typical errors in the measurement of the viscosity are 0.01%.

4.6 Results obtained by DLS and TCDLS

4.6.1 Sample description

The colloid was characterised by both DLS and SLS to give a radius of 150 ± 3nm and a polydispersity less than 6%. Two stock solution were made up in *cis*-decalin at volume fractions differing by a factor of about 10.

The polymer was linear polystyrene with a molecular weight of 1.95×10^6 AMU as measured by the suppliers, suspended in *trans*-decalin. The theta point for this system is $T_\theta = 20.4$°C ($R_p = 39.2$nm, $c^* = 12.9$mgcm^{-3}) and measurements were performed at this temperature and also at 28.6°C ($R_p = 42.8$nm, $c^* = 9.84$mgcm^{-3}). The viscosity of these solutions were measured at both temperatures using the Ubbelohde viscometer and the results are shown in figure 4.9.

The colloid was added dropwise to 1g of polymer solution and shaken well. No more than 4 drops of either stock solution were added in total, typically resulting in an increase of total mass of about 6%. Using this method, volume fractions

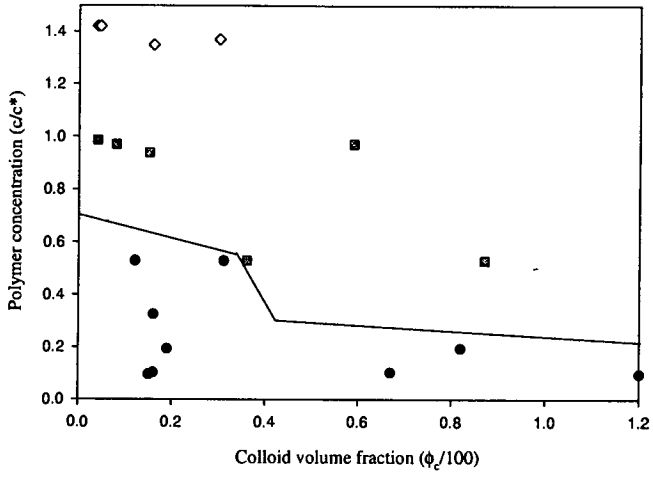

Figure 4.10: Part of the phase diagram for a colloid-polymer mixture with a size ratio of 0.285. Circles represent fluid, squares are fluid/crystal coexistence and diamonds are gels. The lines are added to guide the eye.

could be explored as low as 0.04% up to 0.9%. Since the colloid starts in a different solvent, there is a slight refractive index change on mixing but this amounted to less than 0.05% and as such is negligible. The viscosity of the polymer might also be expected to change on addition of the colloid due to both a diluting effect, and changing the quality of the solvent. The former effect is easily accounted for by a simple recalculation, whereas the magnitude of the latter effect can only be found by experiment. The change due to the solvent quality was found to cause a maximum difference of 0.62% in the viscosity.

The relevant part of the phase diagram for the mixture at 28.6°C is shown in figure 4.10 and at this temperature (and the theta temperature) phase transitions limited the range of polymer concentrations that could be investigated by this technique to $0 < c_p/c^* < 0.5$. The phase separation is hard to characterise (e.g. fluid-crystal, gel etc.) as only a small amount of the sedimented phase exists. Several times the presence of a phase boundary could only be detected by studying the transmission of the sample. When phase separation occured, the transmission decreased noticeably over a period of 2-6 hours after mixing due to the increased

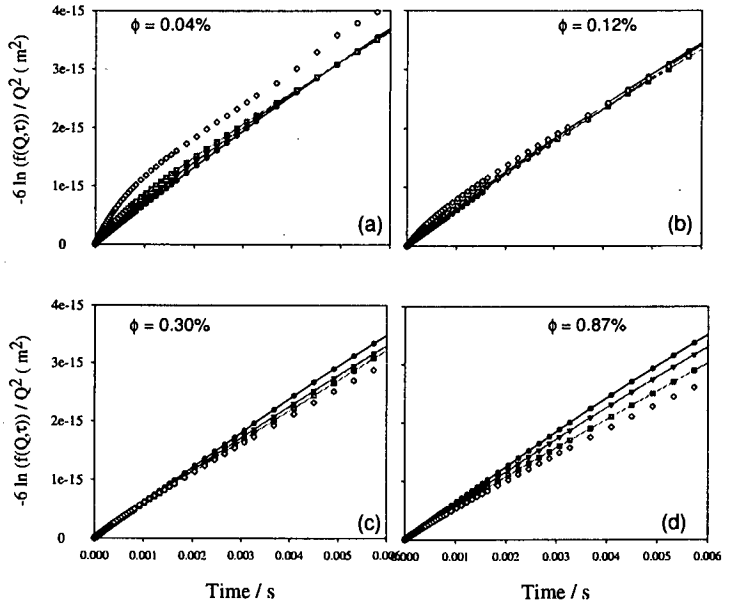

Figure 4.11: Plot of $\langle \Delta r^2(t) \rangle = -6 \ln f_T(Q,\tau)/Q^2$ against time for four different colloid volume fractions and at four different angles. 30°, 50°, 70° and 90° are represented by circles, triangles, squares and diamonds respectively with lines to guide the eye. The effective polymer volume fraction is 0.35, and the size ratio 0.285.

scattering at small angles of the aggregates, and then increased to a higher value than initially.

Dynamic light scattering was performed on the mixtures with polymer concentrations within the above range at four angles, 30°, 50°, 70° and 90°, corresponding to $QR_c = 1.40, 2.29, 3.11$ and 3.84. From equation 4.31 the relative weight of the cross scattering should decrease by a factor of roughly 4 over this range.

4.6.2 Form of results

The mean square displacement as a function of time was obtained from the measured dynamic structure factor using equation 2.56. It should be noted that unless the measured dynamic structure factor represents self-diffusion of the colloid, then $< \Delta r^2(t) >$ as obtained by this method has no physical meaning. Figure 4.11 shows a typical set of results for four different colloid volume fractions. At low

colloid volume fractions (figure 4.11a) the data obtained at lower angles decay slower than those obtained at higher angles[6] As the colloid volume fraction is increased the positive deviation is lost and data from all angles scales with Q^2 (figure 4.11b). This is as expected if the cross and polymer terms are now negligible. However, when the volume fraction is increased still further, the scaling is broken and negative deviation is seen (figure 4.11c,d). The origin of the deviation cannot be due to scattering from either the cross-term (which remains constant as the colloid volume fraction is increased), nor the polymer-term (which should decrease as the colloid volume fraction increases). It must therefore be related to some other aspect of dynamic light scattering from higher volume fraction mixtures.

Although the absolute volume fraction is low, the contrast between the solvent and the colloid is high and multiple scattering effects may be significant. Segrè *et al.* [51] found that multiple scattering can cause the correlation functions to decay quicker (for $QR < 3.3$) or slower (for $QR > 3.3$) than expected. This would explain the negative deviation seen in figures 4.11c,d. To confirm this hypothesis, experiments were performed using TCDLS which effectively suppresses the effect of multiple scattering and the results are shown in figure 4.12. At the lower two concentrations (figures 4.12a,b) the result obtained by TCDLS is in good agreement with that obtained by DLS indicating that multiple scattering is not significant. At higher concentrations (figures 4.12c,d) however, negative deviation is seen in the DLS result, whereas Q^2-scaling is not broken in the TCDLS data. This is good evidence that the breaking of Q^2-scaling is due to multiple scattering.

It is preferable to perform experiments on simple DLS as opposed to TCDLS for two reasons: firstly the TCDLS set-up is extremely time-consuming to align

[6]From the slowest decaying to the faster decaying the order is $30°, 50°, 70°, 90°$. This will be referred to as a 'positive deviation from Q^2-scaling'. The reverse order will be referred to as a 'negative deviation'.

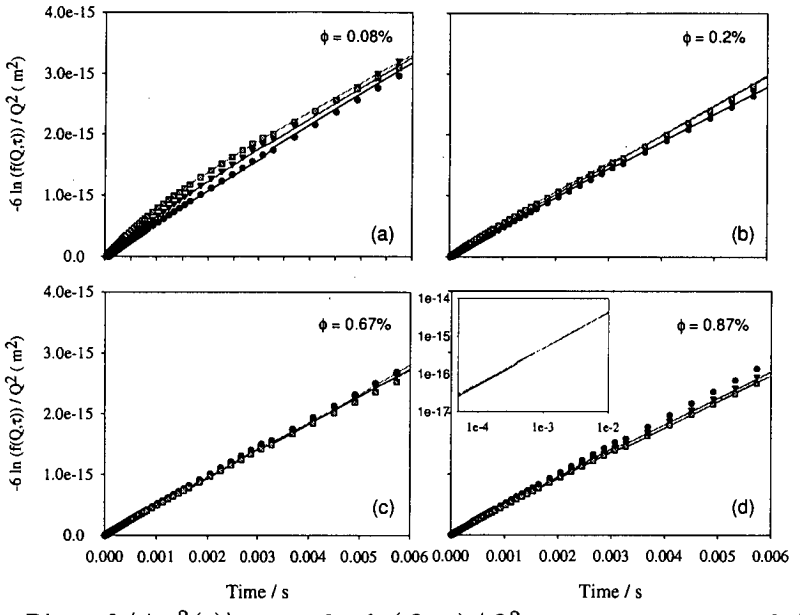

Figure 4.12: Plot of $\langle \Delta r^2(t) \rangle = -6 \ln f_T(Q,\tau)/Q^2$ as obtained by DLS (points) and TCDLS (lines) against time for four different colloid volume fractions and at three different angles. The circles, triangles and squares represent DLS results obtained at $30°, 50°$ and $70°$ respectively. The effective polymer volume fraction is 0.30, and the size ratio 0.261. The inset of figure d is a log-log representation of the TCDLS result. As can be seen, the Q^2-scaling occurs over all timescales.

and needs frequent, minor adjustment. Secondly, there is much competition for experimental time on the equipment. From figure 4.11 it would appear that Q^2-scaling is reached at a lower colloid volume fraction than multiple scattering becomes significant. It is however conceivable that there is a cancelling effect between multiple scattering, leading to a negative deviation, and polymer scattering, leading to a positive deviation, that causes the Q^2-scaling seen in figure 4.11b. Several experiments on samples showing Q^2-scaling by DLS were repeated on TCDLS to remove the effect of multiple scattering. No difference between the two methods was observed implying that neither polymer nor multiple scattering is significant when Q^2-scaling first appears.

At the highest polymer concentrations studied, although the results at 50°, 70° and 90° showed Q^2-scaling, the dynamic structure factor obtained at 30° did not fit onto the Q^2-scaling master curve, decaying slightly too slowly. This is likely

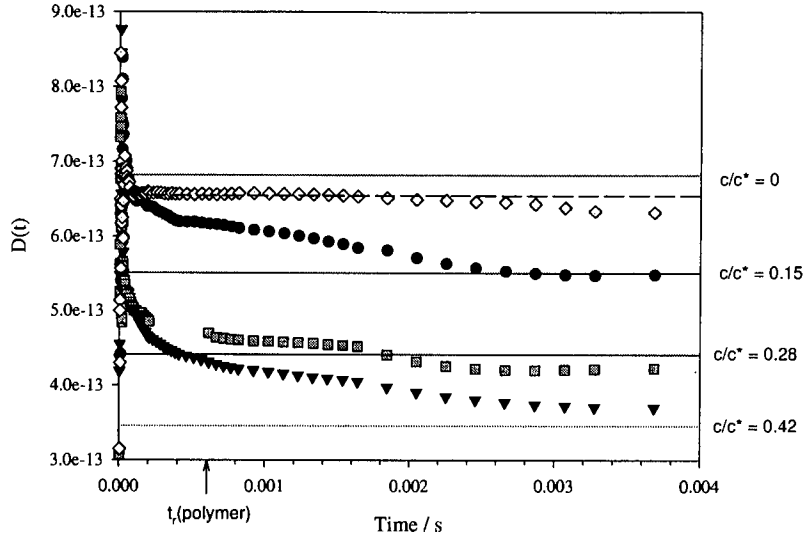

Figure 4.13: Plot of the colloid diffusion coefficient (as obtained by cumulant analysis) as a function of time for three different volume fractions of polymer. The symbols represent the data, with diamonds representing diffusion in pure solvent and circles, squares and triangles representing diffusion in polymer concentrations of 0.15, 0.20, 0.42 respectively (measured in terms of the overlap concentration). Measurements were made at 20.4°C. The lines indicate the Stokes-Einstein result with the viscosity set as that measured for the polymer solution. The error in this measurement is about 4%, the magnitude of which is shown by the dotted line for the pure solvent. Also marked on the plot is the relaxation time of a single polymer coil t_r(polymer).

to be due to the increased magnitude of the cross-term at this angle and the data was excluded from the analysis.

I have presented a method for obtaining the colloid dynamic structure factor from a colloid polymer mixture by DLS. The colloid volume fraction is increased until Q^2-scaling is first seen. At this point the contribution from both the polymer and cross-terms may be ignored, and the effect of multiple scattering can be neglected.

4.6.3 Short and long time behaviour

The dynamic structure factor of the colloids was analysed by both a continuous numerical differential and a stepped series of cumulant fits to obtain the diffusion

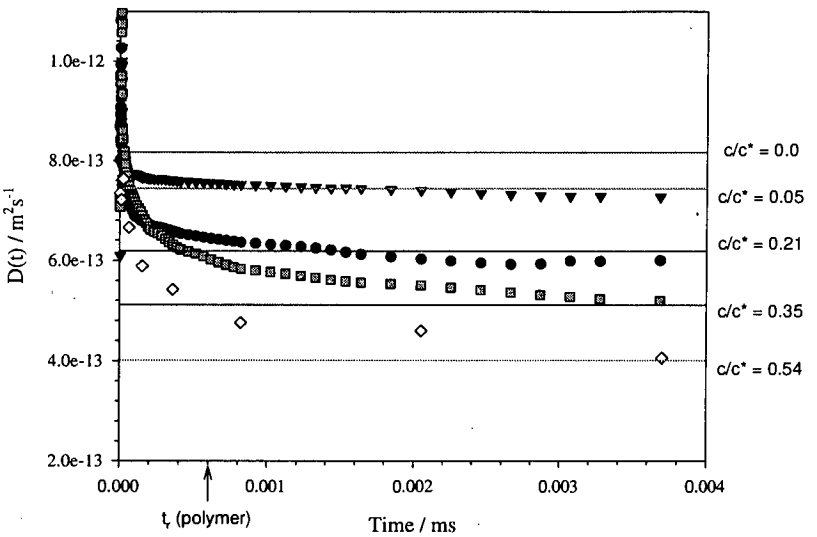

Figure 4.14: Plot of the colloid diffusion coefficient (as obtained by cumulant analysis) as a function of time for four different volume fractions of polymer. The symbols represent the data, with triangles, circles, squares and diamonds representing diffusion in polymer concentrations of 0.05, 0.21, 0.35 and 0.54 respectively (measured in terms of the overlap concentration). Measurements were made at 28.6°C. The lines indicate the Stokes-Einstein result with the viscosity set as that measured for the polymer solution. The uppermost line is the Stokes-Einstein result with the viscosity set to be that of the pure solvent. The error in the lines is about 4%. Also marked on the plot is the relaxation time of a single polymer coil $t_r(\text{polymer})$.

coefficient as a function of time, both methods giving identical results. Figure 4.13 shows the results for three different polymer concentrations. The relaxation time of a single polymer in *trans*-decalin at the theta point is $t_r(\text{polymer}) \sim 0.6$ ms (equation 1.2). At times long compared to this time the colloid diffusion coefficient approaches that predicted from the Stokes-Einstein equation, with a viscosity equal to that of the polymer solution η_p i.e.

$$D(t > t_r(\text{polymer})) = \frac{k_B T}{6\pi\eta_p R_c} \tag{4.44}$$

At short times the diffusion coefficient is higher and the initial diffusion $D(t \longrightarrow 0)$ is slightly below free diffusion in the solvent. This would seem to support the hypothesis that at short times the diffusion of the colloid is slowed only by weak

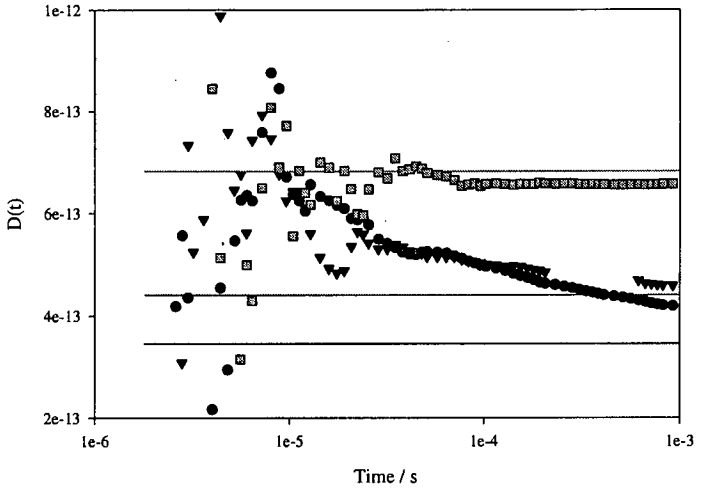

Figure 4.15: A plot showing the noise present in the short time diffusion coefficient. The true value is obtained by extrapolating through the noise to zero time. The symbols represent the data, with squares representing diffusion in pure solvent and circles and triangles representing diffusion in polymer concentrations of 0.15 and 0.20 respectively (measured in terms of the overlap concentration). The lines indicate the Stokes-Einstein result with the viscosity set as that measured for the polymer solution. The error in this measurement is about 4%.

hydrodynamic interactions with a cage of polymers i.e.

$$D(t \longrightarrow 0) \equiv D(0) = H(c_p)\frac{k_B T}{6\pi\eta_s R_c} \tag{4.45}$$

where $H(c_p)$ is a hydrodynamic factor associated with the cage of polymers.

The results shown in figure 4.14 were obtained at a slightly higher temperature (28.6°C instead of 20.4°C), which has the effect of changing the solvent quality from theta to good. There is no qualitative difference between the two sets of results: the diffusion slows as time increases approaching a value given by equation 4.44. Clearly the long time behaviour is not affected by any change in the static structure factor of the polymers, nor by the change in the size ratio of the mixture as we leave the theta point.

These plots show substantial noise at short times due to the fitting process, (see

figure 4.15). At short times, $f(Q,\tau)$ has not decayed significantly and the results obtained by the differentiation routine are acutely sensitive to small amounts of noise in the data. The short time diffusion coefficient is obtained by extrapolating through the noise to the zero time diffusion coefficient.

4.7 Discussion of results

4.7.1 Hydrodynamic factor for a polymer cage

The form of the colloid dynamic structure factor is as predicted in Chapter 3. At long times, the diffusion coefficient is given by a continuum description of the polymer solution whereas, at shorter times, the colloid diffuses faster. The hydrodynamic factor for a system of hard spheres has been determined both theoretically and experimentally [16]. It is interesting to see how this factor changes when the caging colloids are effectively replaced with polymer coils.

Polymer coils are known to be hydrodynamically impermeable, i.e. no solvent passes through the coils [39]. The hydrodynamic interaction is characterised by a *hydrodynamic radius* which, in the Zimm model, is related to the radius of gyration by $R_g = 1.51R_H$. We may therefore convert the effective polymer volume fraction, given in terms of c^*, into an effective *hydrodynamic* volume fraction - c_p/c_H^*. The hydrodynamic factor associated with a cage of polymers at a particular effective hydrodynamic volume fraction can be compared to that associated with a cage of hard spheres (figure 4.16).

The hydrodynamic drag appears less for the cage of polymers than for the colloids. The dotted line in figure 4.16 represents the linear best fit through all sets of data points. It does not appear that the hydrodynamic factor is dependent on the size ratio between the colloid and polymer, at least for these two experiments. To a

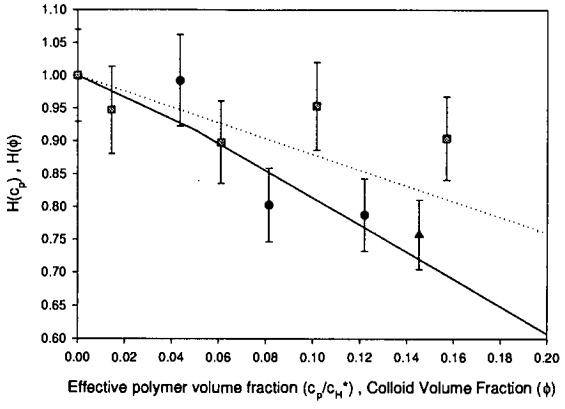

Figure 4.16: Plot showing the hydrodynamic factor for the short time self-diffusion of colloids within a polymer cage. The circles represent the results for a theta solvent and the squares are results for a good solvent. The effective polymer volume fraction is calculated using the hydrodynamic radius of gyration. The triangle is the result obtained from diffusion through PBD (see section 4.7.3). The dotted line represents a linear best fit line through all the data points. The solid line represents the results for a concentrated system of hard spheres, reproduced from [16].

first approximation $H(\phi)$ may be considered linear in colloid or polymer volume fraction:

$$H(\phi) = 1 - a\phi \,. \tag{4.46}$$

For the colloid the factor a is approximately 2.0, whereas for the polymer it is approximately 1.2. Since changing the size of the caging particles appears not to affect $H(c_p)$, the difference between the hydrodynamic factors of the polymer and colloid cages is likely to be the structure of the cage constituents. As the concentration is increased, polymers in the free volume do not significantly change their structure from an ideal gas. Suspensions of colloids, on the other hand, develop a preferred spacing, seen as a strong peak in their static structure function, eventually leading to crystal formation upon crossing the phase boundary.

There must also be another qualitative difference between the hydrodynamics of the two cages. As the polymer concentration is increased overlap occurs (at an effective hydrodynamic volume fraction of 0.296). The hydrodynamics retardation

of a polymer mesh might differ strongly from a cage of free polymer coils.

It would seem that the quantity $H(c_p)$ might be calculable if one assumes that the polymers act as hard spheres at a size ratio of 1, and the structure of the cage constituents is allowed to vary. Such a study is beyond the scope of this thesis, but might reveal some physical insights into the hydrodynamics of a colloidal cage.

4.7.2 Errors

In this chapter I have proposed an experimental method for obtaining the colloid dynamic structure factor from a colloid-polymer mixture. The relative magnitude of the polymer scattering is roughly inversely propotional to the colloid volume fraction and, by increasing the latter, the polymer term in the dynamic light scattering equation may be neglected. The magnitude of the polymer scattering is strongly Q-dependent, and data obtained at higher Q values will contain the largest proportion of polymer scattering. Data should not be taken close to $QR_c = 4.49$ at which point the form factor of the colloid term has a minimum.

The removal of the cross scattering is more difficult and, while certain measures can be taken to minimise it, we are perhaps fortunate that it can be reduced to a negligible level in this system. The relative magnitude of the cross-term falls with increasing Q, until $QR_C(1+\xi) = 4.49$, and it is desirable to take data near this point.

The magnitudes of the cross and polymer scattering are further reduced by only accepting data that scales with Q^2 over a range of Q. When this occurs the total dynamic structure factor $f_T(Q,\tau)$ represents diffusion due to the colloid alone. The relative magnitude of the cross and polymer scattering when scaling occurs may be estimated by the following procedure. The data obtained at 90° contains

the largest proportion of polymer scattering and so is the last to collapse on the Q^2-scaling master curve (figure 4.11b). The magnitude of the polymer scattering when it finally does collapse is, by theory and experiment, 7%.[7] Similarly the data at 30° contains the largest proportion of cross scattering. As the effective polymer volume fraction is increased, we find that the data at this angle no longer collapses onto the master curve. The calculated magnitude of the cross-term at the point when first it fails to collapse is around 8%.

These two terms lead to an error in the measured value of $D(t)$ for the colloid, though the magnitude of this error is dependent on the exact form of $f_{x,p}(Q,\tau)$. A first estimate would assume that both take the dependence

$$f_\alpha(Q,\tau) = e^{-D_\alpha Q^2 \tau} \tag{4.47}$$

with D_α the diffusion coefficient of either the polymer and cross species. Figure 4.17 shows the Q-dependence, and the concentration dependence, of the polymer scattering. Data obtained at the higher angles (50° and above) and over a range of concentrations fall roughly on the same line, however equation 4.47 manifestly does not hold. The deviation at 30° is probably due to dust in the sample which would be expected to scatter more at small angles. The further lack of a Q-dependence is due to the relatively low values of QR_p investigated (up to $QR_p = 1.2$) meaning that light scattering is revealing information on the whole coil and not a portion of it [77].

The non-exponentiality of $f_P(Q,\tau)$ is not suprising: the polymer concentration is high enough for the Stokes-Einstein equation to be invalid and interactions between polymers are likely. An investigation into the exact form of the diffusion coefficient for a system of polymers is beyond the scope of this work; however, the departure from $\ln f(Q,\tau) = -Q^2 D_p t$ may be safely neglected for calculation of the error in $D_c(t)$. The data is fit with $D_p = (3.9 \pm 0.1) \times 10^{-12}\mathrm{m}^2\mathrm{s}^{-1}$.

[7] This result is based on two measurements at polymer concentrations of $0.1c^*$ and $0.44c^*$.

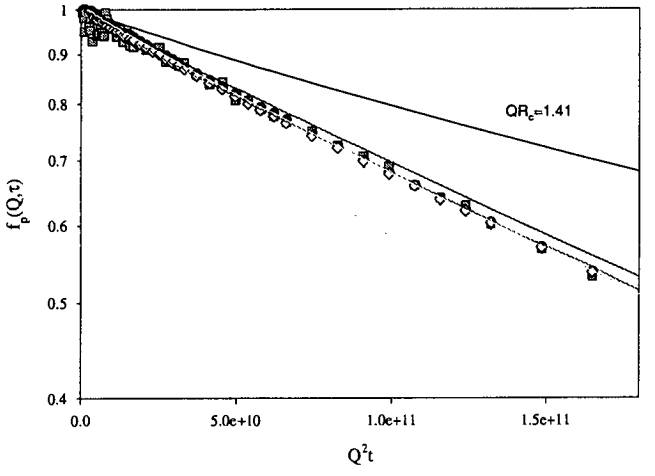

Figure 4.17: The dynamic structure factor of various concentrations of polymer solutions. The symbols represent plots at $QR_c = 3.8$ and concentrations of $0.05c^*$ (squares), $0.11c^*$ (triangles), $0.21c^*$ (circles) and $0.35c^*$ (diamonds). The lines are data obtained at different scattering vectors corresponding to $QR_c = 1.4, 2.3, 4.1, 3.8$. All but the data obtained at $QR_C = 1.4$ (marked) lie roughly on the same line.

The largest error in $D_c(t)$ due to cross and polymer scattering will be as $t \longrightarrow 0$, since the higher diffusion coefficient of the polymer implies that both $f_{p,x}(Q,\tau)$ decay quicker than $f_c(Q,\tau)$ (by a factor of approximately 4 and 2 respectively). The error in $D_c(0)$ is given by

$$\frac{\Delta D_c(0)}{D_c(0)} = \mu_x \frac{D_x}{D_c(0)} + \mu_p \frac{D_p}{D_c(0)} \tag{4.48}$$

where $\mu_{x,p}$ is the relative magnitude of the cross and polymer scattering. Substituting in $\mu_x = 0.08, \mu_p = 0.07$ and $D_x = (D_p + D_c)/2$ gives a typical maximum error of 44%, large enough to account for the deviation of $D_c(t)$ from the Stokes-Einstein equation! In reality the error is not this large as we have failed to take into account that when the cross-scattering is at its maximum accepted value, the polymer scattering is small, and vice versa. Furthermore, the partial intensity of the cross scattering is negative for scattering vectors lower than $Q_- = R_c/(1+\xi)$ so that the cross and polymer terms in the full dynamic structure factor equation have different signs. This leads to some cancellation in the systematic error of

$D_c(0)$. The total error due to neglect of the cross and polymer scattering therefore fluctuates between roughly $-\mu_x D_x/D_c(0)$ at the lower angles and $\mu_p D_p/D_c(0)$ at the higher angles. This means that the errors in the data at different angles may be taken as random, and averaging this data results in a typical maximum error of 6%.

4.7.3 Experiments on poly(butadiene)

At the end of this work, a small amount of high molecular weight 1,4-poly(butadiene) was kindly donated to me by J. Allgaier[8]. The refractive index of PBD is 1.51 [29] making it practically invisible in *cis*-decalin. The cross-scattering is therefore expected to be minimal. An experiment could now be performed to confirm that cross-scattering was correctly removed in the previous experiments.

The polymer was characterised at 20°C in cyclohexane as measurements in *cis*-decalin are difficult due to the close contrast match. The molecular mass was 856×10^3 AMU, obtained by a Zimm plot, and its nominal radius of gyration $R_g = 51.8$nm [78]. The closeness of the radius in cyclohexane to that in *cis*-decalin depends strongly on the difference in the theta temperature between the two solvents. The colloid used was 175nm giving a size ratio of $\xi = 0.296$. This is similar to size ratios used in polystrene polymer / PMMA colloids used previously.

Measurements were performed using both DLS and TCDLS at three scattering angles: $30°, 50°$ and $70°$. The form factor of the colloid exhibits a minimum at an angle of 90.3° and the effect of background scattering became significant at angles greater than about 80°. The polymer concentration was fixed at $0.50c^*$ and three colloid volume fractions were used: $\phi_c = 0.01\%$, $\phi_c = 0.4\%$, $\phi_c = 0.9\%$. At these volume fractions the structure factor for the colloids should be essentially unity, and multiple scattering is not expected to be significant.

[8]Forschungzentrum Jülich, Germany

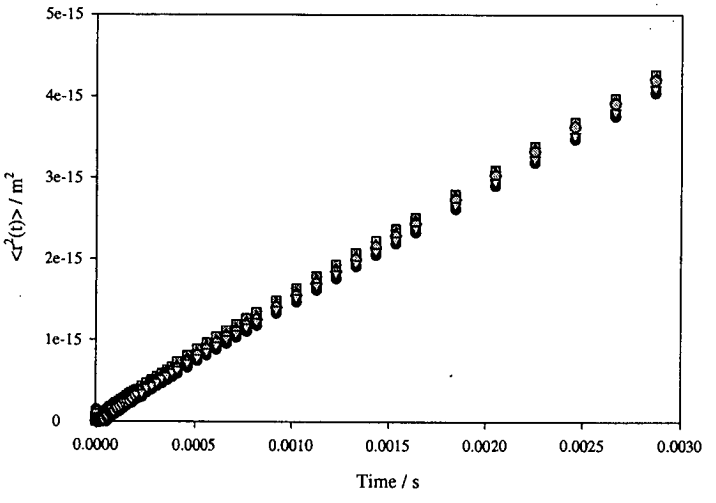

Figure 4.18: Data obtained by DLS on trace quantities of colloid diffusing through a solution of poly(butadiene). The concentration of the PBD is roughly $0.5c^*$, and results obtained for three colloid concentrations ($\phi_c = 0.01\%$, 0.4%, 0.9%) and three angles ($\theta = 30°, 50°, 70°$) are shown. Data obtained at all angles and all concentrations are coincident implying that cross and polymer scattering are negligible.

The polymer is not expected to scatter much due to the close contrast match between it and the solvent. The dark count for this experiment was 0.077kHz, the scattering from *cis*-decalin was 0.10kHz and the scattering from the polymer solution 0.15kHz at all angles. Assuming additivity of intensities, the polymer scattering is roughly 0.05kHz. At 70° the scattering from the most dilute colloid was 2kHz, some 40 times more. The sample with the highest concentration of colloid scattered roughly 10 times more than this. Thus cross and polymer scattering are not expected to be significant in this experiment.

Figure 4.18 shows the DLS results obtained at all angles and all concentrations. There is no concentration dependence implying that, as expected, polymer scattering is negligible. Data from all angles give the same $< \Delta r^2(t) >$, calculated using equation 2.56, implying that cross scattering, which from figure 4.6 is expected to show Q-dependence, is also negligible. TCDLS on these samples revealed that at these low colloid concentrations multiple scattering effects are not

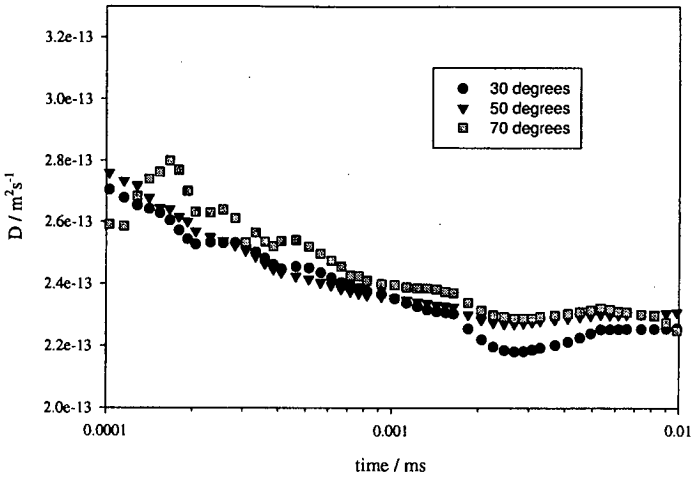

Figure 4.19: Plot showing the diffusion coefficient of colloid in a solution of poly(butadiene) as a function of time. The polymer concentration is roughly $0.5c^*$ and results obtained from three colloid concentrations have been averaged. Results obtained at each angle are shown separately. The diffusion coefficient for 175nm diffusing through pure *cis*-decalin is $3.63 \times 10^{-13}\mathrm{m}^2\mathrm{s}^{-1}$.

significant.

A cumulant analysis on the data showed that the data did not fit a single exponential and a continuous numerical differential approach was used, the results of which are shown in figure 4.19. The diffusion coefficient is clearly a function of time. At short times the diffusion coefficient D^S is lower than that expected for a colloid diffusing through pure *cis*-decalin ($D_0 = 3.63 \times 10^{-13}\mathrm{m}^2\mathrm{s}^{-1}$), and at long times the diffusion coefficient approaches some final value D^L.

Since possessing only a minimal amount of PBD, viscosity measurements could not be undertaken with the Ubbelohde viscometer and only a single measurement on a Carrimed rheometer was possible. This gave a final viscosity of 5.7 ± 0.1 cP, though the Carrimed is known to give results as much as 10% in error. The expected final diffusion coefficient is thus $(2.2 \pm 0.2) \times 10^{-13}\mathrm{m}^2\mathrm{s}^{-1}$ which agrees with the value of D^L obtained earlier.

These results confirm those presented earlier in this chapter. At long times the colloid sees the polymer solution as a continuum and the Stokes-Einstein equation may be used. At shorter times the colloid diffuses faster, though is slowed by hydrodynamic interactions with a cage of polymers. The hydrodynamic factor for this system is shown in figure 4.16. The slight difference between this point and the best fit line is likely to be due to the difference in the theta temperatures between *cis*-decalin and cyclohexane, leading to an incorrect value for the effective hydrodynamic volume fraction.

This experiment confirms that the cross and polymer scattering were correctly removed in the previous set of experiments. The presence of Q^2-scaling implies that the Gaussian approximation (equation 4.42) made throughout this chapter is valid, at least for polymer concentrations up to $0.5c^*$. Furthermore, this experiment shows that the colloid diffusion is indifferent to the exact chemical details of the polymer, as might be expected.

4.8 Conclusions

In this chapter I have detailed an experimental investigation into the self-diffusion of colloids though a polymer solution. Results from initial experiments showed an unphysical scaling with scattering vector which was identified to be due to the neglect of cross-scattering in the data analysis. A novel method for obtaining the magnitude of this cross-scattering both theoretically and experimentally has been proposed. A methodology was suggested that would measure the form of the cross-scattering, though both experimental noise and polydispersity in the colloidal samples made an accurate measurement difficult.

A new methodology was then proposed to measure the diffusion coefficient of the colloid alone. It used the dependence of the dynamic structure factor on scatter-

ing vector to identify data significantly corrupted by cross-scattering. This data could then be removed from the analysis. Contrast variation was also used to minimise the cross and polymer scattering, though this led to multiple scattering effects becoming significant. Experiments using two colour dynamic light scattering effectively removed this multiple scattering and data was thus obtained that represented the diffusion of the colloids alone. A further experiment using poly(butadiene), which is nearly iso-refractive with *cis*-decalin confirmed that both the polymer and cross-scattering had been correctly removed in the previous experiments.

The data was analysed according to both a stepped cumulant and continual differential analysis. The diffusion coefficient was shown to be a function of time and at long times the 'polymer solution as a continuum' assumption appeared valid. In this regime the Stokes-Einstein equation could be used to find the diffusion coefficient. At shorter times, the diffusion was slowed by hydrodynamic interactions with a cage of polymers. This hydrodynamic slowing was less than for diffusion in a concentrated system of hard spheres. It was proposed that this was due to the differing structures of the caging particles.

The size ratio of the caging polymers to the colloid was changed by a modest change in the solvent temperature. No difference was observed in the magnitude of the hydrodynamic factor between the two cases. Using poly(butadiene) instead of polystyrene also resulted in no change in the colloid diffusion coefficient, implying that the diffusion is insensitive to the exact chemical composition of the polymer.

Chapter 5

Literature review

5.1 Introduction

The study of the diffusion of trace quantities of colloid through a polymer solution is not a new topic. However, despite considerable effort, no clear model has emerged and much of the literature appears contradictory. In this chapter I will provide a summary of the work and address the apparent disparities. In particular, attention will be paid to results which support or contradict those presented in the previous chapter.

One of the main aims of previous work has been to investigate the behaviour of the colloid diffusion coefficient as a function of polymer concentration [2–8] with particular attention being paid to polymer concentrations above that where overlap occurs. The colloid diffusion coefficient is invariably obtained by dynamic light scattering, with a variety of analysis techniques being used to fit the data. Any time dependence of the colloid diffusion coefficient is usually neglected, an assumption equivalent to treating the polymer solution as a continuum. The accuracy of this assumption has been discussed by Won *et al.* [5]. They note that for this to be valid the colloid should have moved many times its own radius

during the time scale of the measurement, and that motion of the colloid on a length scale of the radius of the polymer R_p may result in deviations from the Stokes-Einstein equation. Ye and Tong [6] also comment on the polymer as a continuum assumption, stating that 'when the relevant length scale becomes comparable to or smaller than ξ[1], the polymer solution cannot be treated as a continuum any more and its local viscosity η_c may change with the length scale at which it is probed'.

The importance of the relative size of the colloid and a mesh of polymers at concentrations above c^* has been confirmed by experiments on the sedimentation of trace colloids through a polymer network [6]. It was found that as the mesh size of the network was decreased, the effective local viscosity for a sedimenting colloid increased. While our experiments are performed below the overlap concentration, it is expected that the relative size of the colloid and cage of polymers will affect the observed behaviour. Working from a similar premise as Ye *et al.* [6], Donath *et al.* [7] calculated the magnitude of the local viscosity change for a polymer cage by solving the Stokes-Einstein equation for a two step viscosity profile, i.e. $\eta = \eta_d$ for $R_c < r < R_c + R_p$ and $\eta = \eta_p$ for $r > R_c + R_p$, where R_c, R_p are the radii of the colloid and polymer respectively. They have reasoned that such a profile must always exist due to the depletion layer surrounding the colloid in which the momomer segment density is less than in the bulk. Furthermore, they have argued that the monomer segment density within the depletion zone takes some time to reach its equilibrium distribution and should the colloid diffusion be sufficiently fast then this distribution may not be reached.

Were the Stokes-Einstein equation to hold, then we would expect the quantity $D\eta$, where D is the diffusion coefficient of the tracer spheres and η the viscosity of the polymer solution, to be constant. Won [5] defines a positive deviation from Stokes-Einstein as $D\eta/D_0\eta_s > 1$, where D_0 and η_s refer to the diffusion coefficient

[1]The correlation length of the polymer network

and viscosity in the zero polymer concentration limit. Negative deviation is thus when $D\eta/D_0\eta_s < 1$. Both positive deviations from [10,13,14], negative deviations from [9–12] and adherence [4,12,79–81] to the Stokes-Einstein relation have been reported. Won *et al.* [5] report a study in which they find an increasing positive deviation for polymer concentrations up to approximately twice c^* but then a return to Stokes-Einstein behaviour.

There have been complications in previous studies that have led to the large spread of reported behaviour. Several studies used polystrene colloids diffusing through aqueous (hydroxypropyl)cellulose (HPC) [12, 82–85]. Russo *et al.* [12] showed that the HPC adsorbed onto the surface of the polystrene latex causing bridging flocculations. They demonstrated that the addition of a small amount of surfactant suppressed this adsorption. Phillies *et al.* [3] studied the polystyrene/HPC/surfactant/water system but note: 'It should be recognised that (hydroxypropyl)cellulose/water is a relatively complicated chemical system, whose properties may be significantly sensitive to the presence of small amounts of surfactant.' Streletzky and Phillies [2] have also studied this system using dynamic light scattering. They found that the dynamic structure factor could not be fitted with a single exponential so instead they fit their data with the following functional forms

$$\begin{aligned} f(Q,\tau) &= \exp(-\theta\tau^{\beta}) \\ &= A_f \exp(-\theta_f\tau) + (1-A_f)\exp(-\theta\tau^{\beta}) \\ &= A_f \exp(-\theta_f\tau^{\beta_f}) + (1-A_f)\exp(-\theta\tau^{\beta}) \\ &= A_f \exp(-\theta_f\tau^{\beta_f}) + (1-A_f)\exp(-\theta\tau) \end{aligned}$$

where $\theta, \theta_f, \beta, \beta_f, A_f$ are fitting parameters. The choice of fitting function was determined by its stability. They correctly state that these forms '..(do not) necessarily follow directly from a correct physical model'. It is therefore difficult to ascribe any physical meaning to these fits, or the results obtained from them.

Several other studies have used water as the dispersing fluid for charge stabilised spheres diffusing through hydrophilic polymer solutions, including poly(ethylene oxide) [9, 86], poly(acrylic acid) [10, 11, 14, 81, 82] and polylysine [79]. These systems are not ideal for a study of the validity of the Stokes-Einstein equation due to the complicated nature of the interactions between the various components.

The idea that the diffusion coefficient of the colloid may have an explicit time-dependence which could be measured in a light scattering experiment was first discussed by Donath *et al.* [8]. They suggest that '..in the range of the dynamical reduction of the depletion effect, the fluctuations of the diffusion coefficient of the particle, due to the polymer interaction, become important. This would certainly introduce a change of the shape of the autocorrelation function in light scattering experiments.' Before this work, no author has ever claimed to see a time dependence in the colloid diffusion coefficient in a colloid-polymer mixture, and no attempt has been made to measure such a dependence.

In this thesis, I have shown that the diffusion coefficient can be strongly time dependent with the long time behaviour following the Stokes-Einstein equation. Neglecting this time-dependence could lead to an incorrect diffusion coefficient being obtained, and this is perhaps another reason for spread of reported results. In the rest of this chapter I will limit myself to discussions of the literature on 'model' systems, consisting of uncharged, spherical colloids diffusing through non-adsorbing polymer solutions in a non-aqueous solvent.

5.2 Polystyrene spheres and linear polystyrene in DMF

Onyenemezu *et al.* studied cross-linked polystyrene spheres of radius $R_c = 0.19 \pm 0.02\mu$m diffusing through large molecular weight linear polystyrene suspended in

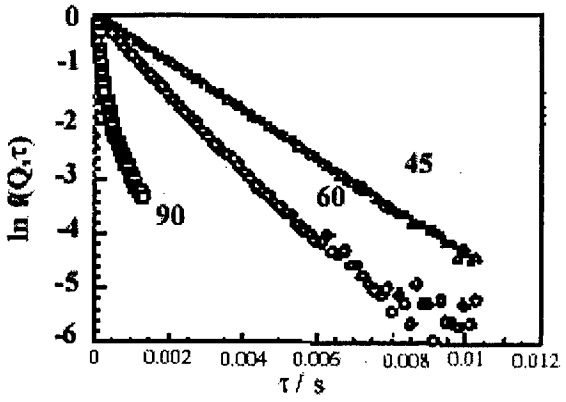

Figure 5.1: Dynamic structure factors for polystyrene spheres diffusing through linear polystrene in DMF at 45°,60° and 90°. The polymer concentration was 0.00117g/ml PS1100K and the colloid concentration was approximately 10^{-5} g/ml. Reproduced from [4].

N,N-dimethylformamide (DMF) [4]. This system is not expected to be charged and DMF is a good solvent for polystyrene at 25° C, indicating that absorption of the polymer onto the spheres is unlikely.

The system was studied using dynamic light scattering at polymer concentrations up to approximately $5c^*$ and at two size ratios: $\xi = 0.09$ and 0.206. Typical results are shown in figure 5.1. The diffusion coefficient was calculated using data obtained by a second order cumulant fit. They found that the data at 45° ($QR_c = 2.27$) was well described by a single exponential decay, though at higher angles ($QR_c = 2.96, 4.19$) there was some curvature. The data showing curvature was fitted using a CONTIN analysis which is a constrained inverse Laplace transform routine, used frequently in the literature (for example [87]). Figure 5.2 shows the comparison between the CONTIN results and the cumulant fit. Although similar, there are differences of up to a factor of two between results obtained at different angles. The average diffusion coefficient was found to obey the Stokes-Einstein equation (figure 5.3).

The authors suggest that the curvature in the dynamic structure factors is caused

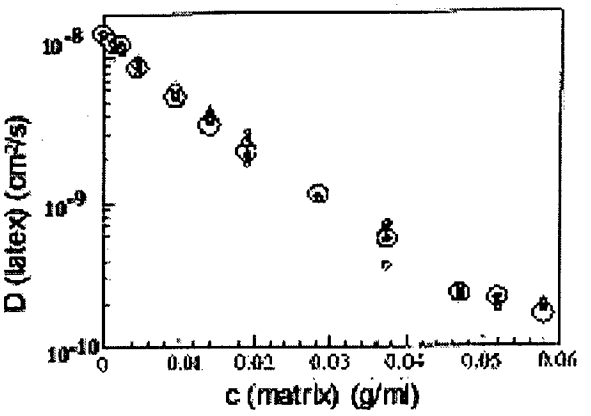

Figure 5.2: Comparison of diffusion coefficients determined from cumulant fit (large open circles) with those deduced from CONTIN analysis (all other symbols) in the presence of PS1100K in DMF. At each linear polystyrene concentration there were multiple runs at 45°,60° and 90°. Reproduced from [4].

by scattering from the polymer and note that the magnitude of the polymer scattering is 'order of magnitudes lower' than the colloid. It is possible to calculate the relative magnitude of the polymer to the colloid scattering. Since both are made from polystyrene, the scattering power of each species is identical and the relative intensities depend only on the molecular weight M, the concentration c and the shape of each species. Using equations 2.21 and 4.33 and assuming no correlation in the positions of the colloids or the polymers, we obtain:

$$\frac{I_p}{I_c} = \frac{c_p M_p P_p(Q)}{c_c M_c P_c(Q)}, \tag{5.1}$$

where I_p/I_c is the relative intensity of polymer to colloid scattering, $P(Q)$ the form factor and the subscript p, c refer to polymer and colloid respectively. For the samples used to obtain figure 5.1, this results in a ratio of 0.02, 0.06 and 3 at angles of 45°, 60° and 90° respectively. The high value at 90° is due to the form factor minimum of the colloid at $\theta = 98.5°$.

While for most angles the ratio of polymer to colloid scattering is low, the ratio of cross scattering to colloid scattering is given by $I_x/I_c = 2\sqrt{I_p/I_c}S_{cp}$, where I have assumed that the colloid and polymer structure factor are approximately

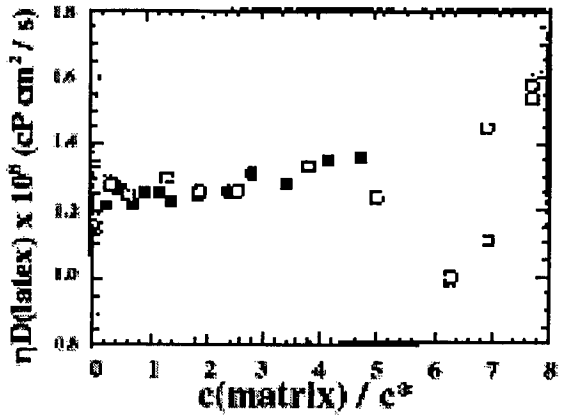

Figure 5.3: Test of Stokes-Einstein equation as a function of the reduced concentration. The points represent two different polymers. Theoretically $D\eta = (1.1 \pm 0.1) \times 10^8 cPcm^2s^{-1}$, whereas experimentally $D\eta = (1.26 \pm 0.17) \times 10^8 cPcm^2s^{-1}$. Reproduced from [4].

unity. The magnitude of S_{cp} - the cross structure factor, is hard to estimate, but certainly values up to 0.5 are not unusual. This puts an upper bound on the magnitude of the cross-scattering of 15%, 25% and 170% at angles of 45°, 60° and 90° respectively. I would suggest that the curvature seen in the dynamic structure factors is due to either polymer or cross scattering. This is supported by the lack of Q^2-scaling as seen in figure 5.2. Intepretation of data obtained in this experiment is therefore difficult and it is perhaps surprising that the average of the CONTIN obtained diffusion coefficients with those obtained by cumulant analysis does appear to follow the Stokes-Einstein equation.

5.3 A return to Stokes-Einstein behaviour

As discussed earlier, positive deviation from Stokes-Einstein ($D\eta/D_0\eta_s > 1$), negative deviation and adherence have all been reported, but mainly in complicated systems. Won *et al.* [5] report a study on a 'model' system, namely cross-linked polystyrene latex spheres diffusing through poly(vinyl methyl ether) (PVME)

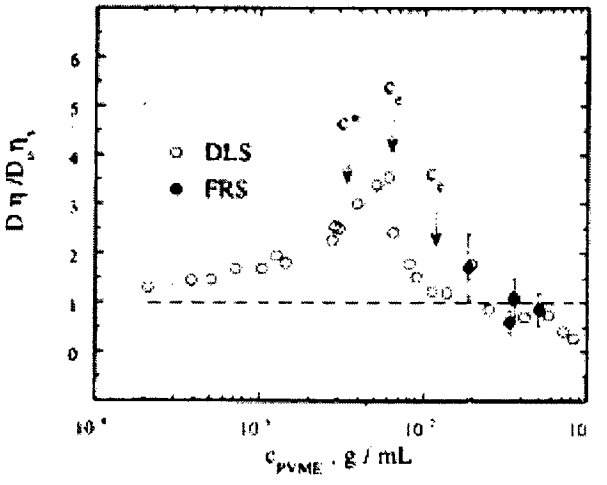

Figure 5.4: Product of the sphere diffusivity and the solution viscosity normalised by the corresponding values at infinite dilution, as a function of polymer concentration. The dashed line corresponds to the Stokes-Einstein equation. Reproduced from [5].

dissolved in toluene. They found an increasing positive deviation for polymer concentrations up to approximately twice c^* but then a return to Stokes-Einstein behaviour (figure 5.4).

The system under study is not expected to be charged, nor is absorption of the PVME onto the colloid expected. The light scattering data was fitted with a second order cumulant fit and the diffusion coefficients obtained scaled well with Q^2. The second cumulant was typically 0.1, though increased to 0.2 as the polymer concentration increased. The data was also analysed using the CONTIN transformation which consistently gave a diffusion coefficient 25% larger than that from cumulant analysis.

PVME is nearly isorefractive with toluene and Won *et al.* performed static light scattering on the spheres, both with and without polymer present, and found no difference in the intensity. It is therefore unlikely that cross or polymer scattering was significant in this experiment. However, the high value of the second cumulant reveals that the correlation function is not a single exponential. Consider a

dynamic structure factor given by the weighted sum of two exponentials:

$$f(Q,\tau) = a_1 e^{\Gamma_1 \tau} + a_2 e^{\Gamma_2 \tau} \; . \tag{5.2}$$

The cumulants for such a system are given by:

$$\begin{aligned} \bar{\Gamma} &= a_1\Gamma_1 + a_2\Gamma_2 \\ \frac{\mu_2}{\bar{\Gamma}^2} &= a_1 a_2 \frac{(\Gamma_1 - \Gamma_2)^2}{\bar{\Gamma}^2} \; , \end{aligned} \tag{5.3}$$

where $\mu_2/\bar{\Gamma}^2$ is the second cumulant. For the experiments in the previous chapter, an estimate for these values might be $a_2 = 0.5$ and $\Gamma_2 \sim 0.75\ \Gamma_1$ which gives a second cumulant of 0.02. The second cumulant obtained by Won *et al.* could therefore indicate a time-dependent diffusion coefficient.

The diffusion coefficient obtained by cumulant analysis is the short time diffusion coefficient which, although slowed somewhat by hydrodynamic interactions with the cage of polymers, would still give a ratio $D\eta$ that was higher than expected by the Stokes-Einstein. It is therefore tenable that the positive deviation observed by Won et al. is the faster local diffusion within the cage of polymers. As the polymer concentration increases, the size of the cage decreases until the colloid is effectively trapped in a mesh of polymers. When this occurs, local diffusion within a cage cannot occur and we might expect the dynamic structure factor to return to a single exponential. The return to Stokes-Einstein, as seen by Won *et al.* is an indication that this is occuring.

5.4 Sedimentation and light scattering

Sedimentation experiments can provide useful insights into the behaviour of a colloidal probe in a polymer solution as the rate of sedimentation depends on the solution viscosity. Sedimentation is typically measured over minutes and hours and so provides information on the long-time motion of the colloid. In a dilute

suspension the sedimentation viscosity v_{sed} is given by:

$$v_{\text{sed}} = \frac{2R_c^2 \delta\rho\, g}{9\eta_p}\,, \tag{5.4}$$

where R_c is the radius of the colloid, $\delta\rho$ is the density difference between the colloid and solvent, g is the acceleration due to gravity and η_p is the viscosity of the polymer solution.

Ye *et al.* [6] studied a system of calcium carbonate colloids with an adsorbed monolayer of a randomly branched calcium alkylbenzenesulfonate surfactant diffusing through either hydrogenated polyisoprene (PIP) or its end-functionalised derivative amine-PIP, both suspended in decane. Decane is a good solvent for both the colloids and the polymers. The amine-PIP is known to absorb onto the colloid surface within one month.

Equation 5.4 was tested by measurements on the colloid with the end-absorbed amine PIP and complete adherence was found up to approximately $6c^*$. The ratio of the sedimentation velocity at polymer concentration c_p with its value at infinite dilution, $v_{\text{sed}}(c_p)/v_{\text{sed}}(0)$, therefore equates to the viscosity ratio η_p/η_0 between the polymer solution viscosity η_p and its infinite dilution limit η_0. Light scattering measurements were also performed on this system and Q^2-scaling was seen at all polymer concentrations. The diffusion coefficient was extracted using a second order cumulant analysis. An identity was found between the ratio $D(c_p)/D(0)$ of the diffusion coefficient at some polymer concentration c_p compared with the infinite dilution limit and $v_{\text{sed}}(c_p)/v_{\text{sed}}(0)$, indicating that the Stokes-Einstein equation was obeyed (figure 5.5).

The lack of a Q^2-dependent diffusion coefficient indicates that cross or polymer scattering was probably not significant in this experiment. The apparent adherence to the Stokes-Einstein equation can be explained in terms of the relative sizes of the colloid and polymer cage. Each colloid has on average one amine-PIP chain absorbed onto it. The first measurement made by Ye *at al.* is at a polymer

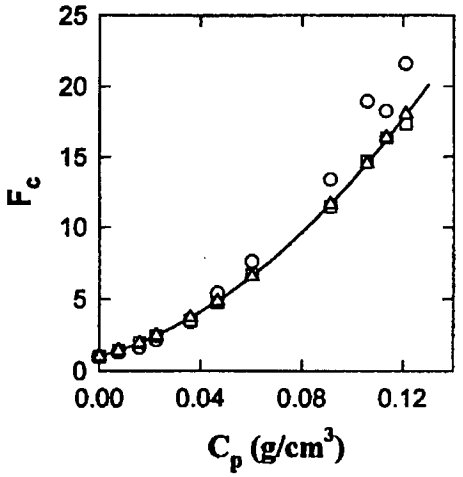

Figure 5.5: Measured $F_c = \eta_p/\eta_0$ as a function of polymer concentration for colloid diffusing in amine-PIP solutions. The squares are obtained from sedimentation measurements, the circles from light scattering measurements with a second order cumulant fit and the triangles from light scattering measurements with a triple exponential fit. The solid curve shows the viscosity of the polymer solution. The deviation of the circles at higher polymer concentrations is probably due to the increased fraction of polymer scattering. Reproduced from [6].

concentration of roughly $0.5c^*$. At this point the centres of the polymer chains are roughly $1.26R_g$ apart, where R_g is the radius of gyration of the polymer. The size ratio in this system is 1.6, meaning that the colloid/polymer structure is roughly $1.63R_g$ in radius. As in the previous section, the colloid/polymer structure is effectively trapped within a mesh of polymer, and even at short times direct interactions are significant. As before, the Stokes-Einstein equation is obeyed for such a system.

5.5 Effect of depletion on the Stokes friction coefficient

An interesting approach to the problem of colloids diffusing in polymer solutions is provided by Donath *et al.* [7, 8]. When determining the static properties of

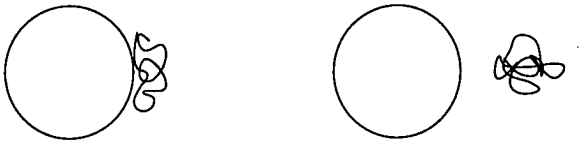

Figure 5.6: Schematic showing available polymer conformations close to ($r < R_c + R_p$) and far from ($r > R_c + R_p$) a colloid, where R_c is the radius of the colloid and R_p the radius of gyration of the polymer. There are considerably fewer configurations available to the polymer when close, making it entropically less favourable than the latter arrangement.

a colloid-polymer mixture, the effect of the polymer is often integrated out and replaced with an effective colloidal inter-particle potential. On average it is entropically unfavourable for a polymer centre of mass to come within $R_c + R_p$ of the colloid centre of mass, as the number of conformations available to it is severly reduced (see figure 5.6). As a result the local polymer segment density within this zone is reduced compared to the bulk. It is entropically favourable for two such depleted regions to overlap, as it increases the volume available to the polymers.

Donath *et al.* considered the effect of this depletion zone on the diffusion of a colloid. They treated the polymer solution as a continuum, but with a viscosity dependent on the distance from the centre of mass of the colloid $\eta(r) = \eta_p f(r)$. By solving the Navier-Stokes equation for such a profile they found that the Stokes-Einstein equation should be modified to

$$D_c = \frac{k_B T}{\alpha \pi \eta_p R_c} , \tag{5.5}$$

where

$$\begin{aligned} \alpha &= 6\left(\frac{1+2\frac{\eta_p K}{R_c}}{1+3\frac{\eta_p K}{R_c}}\right) \\ K &= \frac{1}{\eta_p}\int_0^\infty \left(\frac{1}{f(r)} - 1\right) dr , \end{aligned} \tag{5.6}$$

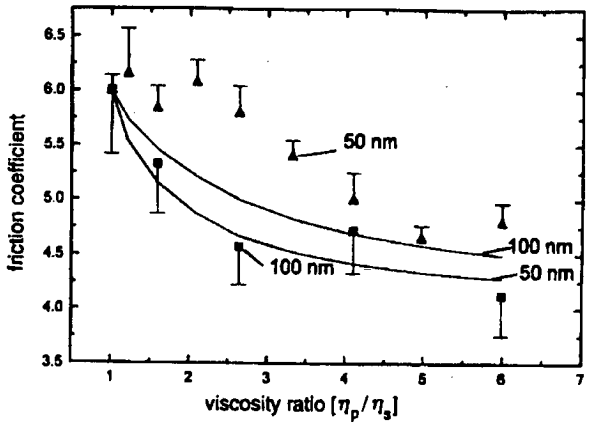

Figure 5.7: Friction coefficient as a function of the viscosity ratio η_p/η_0. The solid lines are theoretical plots according to a single step profile with a characteristic thickness of depletion layer $\lambda = 10$nm. Particle radii are 100nm and 50 nm. The solid points are experimental results from dynamic light scattering on liposomes from L-α-lecithin, containing 20% phosphatidylserine in 10mM KCl electrolyte solution. The dextran solutions with the appropriate concentrations were prepared and some liposome stock solution was added for a good scatter signal. Triangular points correspond to liposomes prepared with a nucleopore filter of 50nm pore size. The square points represent liposomes prepared with 100nm pore size. Error bars are the standard deviations. Reproduced from [7].

and the other symbols take their usual meanings. The two limits for α are clearly 4 ($K \longrightarrow \infty$) corresponding to complete slip, and 6 ($K \longrightarrow 0$) corresponding to stick boundary conditions.

Clearly a model is needed for $f(r)$ and, based on previous work on electrophoretic measurements on charged liposomes diffusing through aqueous dextran [88], Donath *et al.* suggest a double step and an exponential profile. Light scattering measurements are also reported and the measured diffusion coefficient is found to decrease with increasing polymer concentration, though not according to the predicted theoretical form (figure 5.7).

The model put forward in this thesis shares similar ideas to that of Donath *et al.* They predict a different local viscosity from the bulk viscosity, though not that the colloid can sample both. The motion described is of a 'meta-particle'

consisting of a colloid and a fixed depletion zone. In our model, this would be equivalent to the 'cage' of polymers remaining at fixed distances from the colloid. In reality, however, as the colloid diffuses the depletion zone does not necessarily move with it. This issue has been addressed by Donath *et al.* [8]. They formulated the problem in terms of the time taken for the polymer segment density in the depletion zone to equal the equilibrium distribution, τ_d. If the time taken for the colloid to diffuse over a distance equal to the depletion layer thickness is smaller than this equilibrium time, then the depletion zone is not considered to be fixed to the particle.

In order to estimate τ_d they predict that it is equal to the time necessary to 'measure' the entropy of the polymer layer in a hydrodynamically homogeneous region at the particle interface. The latter quantity is bound by the decay time of the individual polymer molecule correlation function τ_{corr} (i.e. the characteristic time taken for a single polymer to explore its own configurations) and the time τ_{ent} taken for a molecule to diffuse over a sufficiently large number of configurations in the available configuration space. Thus in a linear approximation one could write

$$\tau_d = \tau_{\text{ent}} - (\tau_{\text{ent}} - \tau_{\text{corr}})\frac{n-1}{n+n_{\text{crit}}-1}\,, \tag{5.7}$$

where n is the number of molecules in the hydrodynamically homogeneous region of the depletion layer and n_{crit} a parameter characterising the relative weight of τ_{corr} in the calculation of τ_d.

Having estimated τ_d, the magnitude of the depletion effect is calculated from

$$\varepsilon = \left(1 - \frac{\tau_d}{\tau_d + \tau_c}\right)\,, \tag{5.8}$$

in which $\varepsilon = 1$ indicates a stationary colloid and $\varepsilon = 0$ indicates no depletion layer. The authors found τ_d by Brownian dynamics simulations, and thence calculated the magnitude of ε for various size ratios. They found that increasing the polymer concentration led to an increase in the depletion effect.

Whilst the exact physical meaning of τ_{ent} and its relation to τ_d is not immediately obvious, the results obtained by Donath *et al.* appear to be predictions for the long-time diffusion of the colloid. They find that the Stokes-Einstein equation should not necessarily be obeyed. Unfortunately the rather approximate nature of their calculations make direct comparison with our system problematic; however it is clear that their model echos that put forward in this thesis: the colloid diffuses faster than the polymer cage can rearrange itself, and so the colloid samples a range of viscosities.

5.6 Conclusions

A study has been made of the current literature on colloid diffusing through polymer solutions. The main topic of interest has been the validity of the Stokes-Einstein equation as the polymer concentration is increased. Many studies used chemically and physically complicated systems to test this equation and, as a result, their conclusions are difficult to interpret. Work performed on 'model' systems provides many contradictory results with both adherence and concentration dependent deviation seen. The origins of these contradictions would appear to be twofold - the neglect of cross and polymer scattering has led to incorrect data being obtained, and the neglect of any time-dependence has led to incorrect data analysis.

While a time-dependence of the colloid diffusion coefficient has been predicted before, no in depth study has been made into this phenomemon. Although some studies show evidence of time-dependence in the data, others do not. The latter have been explained in terms of the size ratio of the diffusing and polymer cage. There is no study that conclusively contradicts the results put forward in this paper.

The validity of the Stokes-Einstein equation for describing the long-time diffusion coefficient has been challenged and while the relation appeared to be obeyed in this study, further work is needed to establish whether this is always the case.

Chapter 6

Conclusions

This work was prompted by a simple question: is the Stokes-Einstein equation followed for colloids diffusing in a polymer solution? Answering this question required a detailed look at the theory behind diffusion in colloid-polymer mixtures, a critical analysis of the literature and a suprisingly complicated experimental investigation. In this section I will draw together these different strands and try to present a final picture of the nature of the diffusion and the complications involved in finding this out. While it is my belief that the answers presented in this thesis are complete, the field of colloid-polymer diffusion is by no means a closed book and there are several avenues of investigation that would provide useful information on this field.

6.1 Summary of results

The Stokes-Einstein equation is the governing equation for colloids of infinite dilution diffusing through a continuum. A polymer has a similar size and relaxation timescale as the colloids and therefore a polymer solution cannot be treated as a continuum. I have shown, using a simple Cahn-Hilliard treatment,

that interactions between particles mean that the diffusion in a colloid-polymer mixture cannot be treated as N particles diffusing independently; density fluctuations decay through collective diffusional modes, one mode being present for each species with a fixed number density. In a closed system the two modes are condensation dominated, in which fluctuations are in the total density, and demixing dominated, in which the fluctuations are in species density.

Including hydrodynamics into the Cahn-Hilliard treatment is difficult and a different formalisation is required. The accuracy of the Smoluchowski formalisation for describing diffusion in a concentrated systems of hard spheres is well established and I have shown how parallels may be drawn between this system and a system of dilute colloid diffusing in a polymer solution. It was predicted that the dominant diffusional mode at short times would be self-diffusion of the colloid within a cage of polymers. The motion is hindered by hydrodynamic interactions with the polymers. At long times the dominant mode is the relaxation of the cage structure and the diffusion of the colloid over longer distances.

An experimental investigation made use of dynamic light scattering to measure the diffusion coefficient as a function of time. The theoretical predictions were confirmed. The hydrodynamic drag provided by the cage of polymers was found to be slightly less than that from a cage of colloids. This was explained in terms of the structural differences between the two systems. A colloidal cage has a well defined inter-particle spacing, whereas a polymer cage is effectively a 'snapshot' of an ideal gas. At long times the diffusion followed that predicted by Stokes-Einstein equation for motion through a solvent with a viscosity equal to that of the polymer solution.

The key parameters in this theory are the size ratio of the species and the timescale of the polymer relaxation. The behaviour should be indifferent to the exact chemical details of the polymer and colloid. This was confirmed by measurements using two different polymers. No quantitative difference between the

two was found.

If the solvent quality is changed then the size ratio also varies. The effect of a modest change in size ratio (10%) was investigated but no qualitative difference found.

6.1.1 Complications

The measurement of the diffusion coefficient of the colloids in a colloid-polymer mixture is not a trivial affair, as witnessed by the wide variety of contradictory results in the literature. The neglect of cross scattering, in which the light scattered by a polymer is correlated with that from a colloid, can lead to incorrect data analysis. In this work I have given a method for calculating the magnitude of the cross scattering based on a simple model for the static structure factors of a colloid-polymer system. An attempt to measure the cross dynamic structure factor was made, but with limited success.

Cross scattering is experimentally challenging to remove. The magnitude of the cross scattering is independent of the number of colloids in the system and can only be detected by the comparison of results obtained at different scattering angles: if Q^2-scaling is seen then the cross scattering is negligible. The easiest way to reduce cross scattering is to change the refractive index of the solvent to contrast match the polymer.

A further complication found in the literature is the use of systems with complex interactions. This was resolved in these experiments by using a well characterised model system in a non-aqueous solvent.

6.2 Suggestions for further work

Apart from the dynamics of more concentrated mixtures of colloids and polymer, there are several more aspects of the diffusion of dilute colloids through polymer solutions that could be investigated. So far only concentrations up to about half the overlap concentration have been studied. As the polymer concentration increases the size of the cage decreases. It would be very interesting to see what happens as the cage size approaches the size of the colloid. It is possible that a return to Stokes-Einstein behaviour would be seen for long and short timescales.

As the polymer concentration is increased beyond the overlap concentration, an extended network, or mesh, is formed. The diffusion of dilute colloid in such a mesh is not a trivial affair, due to the viscoelastic behaviour of the mesh. At short times the mesh would appear elastic, whereas at longer times the polymer network has a chance to break and reform. There are theories suggesting that two viscous modes are possible, depending on whether the solvent moves relative to the polymer mesh or not. The importance of these modes could be investigated by dynamic light scattering.

For both of these studies, new methodologies will have to be invented to cope with the increased scattering from the polymers and to prevent phase separation but the results should give another aspect on this fascinating topic.

Bibliography

[1] H.N.W. Lekkerkerker, W.C.K. Poon, P.N. Pusey, A. Stroobants, and P.B. Warren. Phase behaviour of colloid plus polymer mixtures. *Eur. Phys. Letts.*, 20:559–564, 1992.

[2] K.A. Streletzky and G.D.J Phillies. Translational diffusion of small and large mesoscopic probes in hydroxypropylcellulose-water in the solutionlike regime. *J. Chem. Phys.*, 108:2975–2988, 1998.

[3] G.D.J. Phillies and D. Clomenil. Probe diffusion in polymer solutions under theta and good conditions. *Macromol.*, 26:167–170, 1993.

[4] C.N. Onyenemezu, D. Gold, M. Roman, and W.G. Miller. Diffusion of polystyrene latex spheres in linear polystyrene nonaqueous solutions. *Macromol.*, 26:3833–3837, 1993.

[5] J. Won, C. Onyenemezu, W.G. Miller, and T.P. Lodge. Diffusion of spheres in entangled polymer solutions - a return to Stokes-Einstein behavior. *Macromol.*, 27:7389–7396, 1994.

[6] X. Ye, P. Tong, and L.J. Fetters. Transport of probe particles in semidilute polymer solutions. *Macromol.*, 31:5785–5793, 1998.

[7] E. Donath, A. Krabi, M. Nirschl, V.M. Shilov, M.I. Zharkikh, and B. Vincent. Stokes friction coefficient of spherical particles in the presence of poly-

mer depletion layers - analytical and numerical calculations, comparison with experimental data. *Chem. Soc. Faraday Trans.*, 93:115–119, 1997.

[8] E. Donath, D. Walther, A. Krabi, G.C. Allan, and B. Vincent. A new relaxation effect with polymer depletion layers. *Langmuir*, 12:6263–6269, 1996.

[9] E.C. Cooper, P. Johnson, and A.M. Donald. Probe diffusion in polymer solutions in the dilute semidilute crossover regime. 1: Poly(ethylene oxide). *Polymer*, 32:2815–2822, 1991.

[10] T.H. Lin and G.D.J. Phillies. Probe diffusion in poly(acrylic acid) water - effect of probe size. *Macromol.*, 17:1686–1691, 1984.

[11] T.H. Lin and G.D.J. Phillies. Translational diffusion coefficient of a macroparticulate probe species in salt-free poly(acrylic acid) water. *J. Chem. Phys.*, 86:4073–4077, 1982.

[12] P.S. Russo, M. Mustafa, T. Cao, and L.K. Stephens. Interactions between polystyrene latex spheres and a semiflexible polymer, hydroxypropylcellulose. *J. Colloid Interface Sci.*, 122:120–137, 1988.

[13] R. Furukawa, J.L. Arauzlara, and B.R. Ware. Self-diffusion and probe diffusion in dilute and semidilute aqueous solutions of dextran. *Macromol.*, 24:599–605, 1991.

[14] T.-H. Lin and G.D.J. Phillies. Probe diffusion in polyacrylic-acid water - effect of polymer molecular weight. *J. Colloid Interface Sci.*, 100:82–95, 1984.

[15] S. Asakura and F. Oosawa. Interaction between particles suspended in solutions of macromolecules. *J. Polymer Sci.*, 33:183–192, 1958.

[16] P.N. Segrè, O.P. Behrend, and P.N. Pusey. Short-time Brownian motion in colloidal suspensions: Experiment and simulation. *Phys. Rev. E*, 52:5070–5083, 1995.

[17] I. Bodnar and J.K.G. Dhont. Strong critical enhancement of the shear viscosity of colloidal systems. *Phys. Rev. Letts.*, 77:5304–5307, 1996.

[18] W.C.K. Poon, L. Starrs, S.P. Meeker, A. Moussaïd, R.M.L. Evans, P.N. Pusey, and M.M. Robins. Delayed sedimentation of transient gels in colloid-polymer mixtures: dark field observations, rheology and dynamic light scattering studies. *Faraday Discuss.*, 112:143–154, 1999.

[19] W.C.K. Poon and P.N. Pusey. In M. Baus et al., editors, *Observation, Prediction and Simulation of Phase Transitions in Complex Fluids*, chapter 1. Kluwer, Dordrecht, 1995.

[20] P.N. Pusey. Colloidal suspensions. In J.-P. Hansen, D. Levesque, and J. Zinn-Justin, editors, *Liquids, Freezing and the Glass Transition*, chapter 10. Elsevier, Amsterdam, 1991.

[21] D.J. Fairhurst. *Polydispersity in Colloidal Phase Transitions.* PhD thesis, University of Edinburgh, 1999.

[22] M. Doi and S. Edwards. *The Theory of Polymer Dynamics.* Oxford Science Publications, Oxford, 1986.

[23] A.Y. Grosberg and A.R. Khokhlov. *Statistical Physics of Macromolecules.* American Institute of Physics, New York, 1994.

[24] L. Antl, J.W. Goodwin, R.D. Hill, R.H. Ottewill, S.M. Owens, and S. Papworth. The prepration of poly(methyl methacrylate) latices in non-aqueous media. *Coll. Surf.*, 17:67–78, 1986.

[25] W.B. Russel, D.A. Saville, and W.R. Schowalter. *Colloidal Dispersions.* Cambridge University Press, Cambridge, 1948.

[26] R.J.R. Cairns, W. van Megen, and R.H. Ottewill. A comparison between theoretically computed and experimentally measured pressures for interacting sterically stabilized particles. *J. Colloid Interface Sci.*, 79:511–517, 1981.

[27] S-E. Phan, W.B. Russel, Z. Cheng, J. Zhu, P.M. Chaikin, J.H. Dunsmuir, and R.H. Ottewill. Phase transition, equation of state, and limiting shear viscosities of hard sphere dispersions. *Phys. Rev. E.*, 54:6633–6644, 1996.

[28] P.N. Pusey and W. van Megen. Phase-behaviour of concentrated suspensions of nearly hard spheres. *Nature*, 320:340–342, 1986.

[29] J. Brandrup and E.H. Immergut, editors. *The Polymer Handbook.* Wiley, New York, Chichester, 1989.

[30] R.C. Weast, editor. *CRC handbook of Chemistry and Physics.* CRC Press, Baton Rouge, Florida, 1988.

[31] S. P. Meeker. *Low-shear Rheology and Delayed Sedimentation of Colloidal Systems.* PhD thesis, University of Edinburgh, 1997.

[32] A.A. Louis, R. Finken, and J.-P. Hansen. The structure of colloid-polymer mixtures. *Eur. Phys. Letts.*, 46:741–747, 1999.

[33] W. Schaertl and H. Sillescu. Brownian dynamics of polydisperse colloidal hard spheres: Equilibrium structures and random close packings. *J. Stat. Phys*, 77:1007–1025, 1994.

[34] W.G. Hoover and F.H. Ree. Melting transition and communal entropy for hard spheres. *J. Chem. Phys.*, 49:3609–3617, 1968.

[35] S.E. Paulin and B.J. Ackerson. Observation of a phase transition in the sedimentation velocity of hard spheres. *Phys. Rev. Letts.*, 64:2663–2666, 1990.

[36] J.L. Barrat and J.P. Hansen. On the stability of polydisperse colloidal crystals. *J. Physique*, 47:1547–1553, 1986.

[37] R. McRae and A.D.J. Haymet. Freezing of polydisperse hard spheres. *J. Chem. Phys.*, 88:1114–1124, 1988.

[38] G.C. Berry. Thermodynamic and conformational properties of polystyrene I - Light-scattering studies on dilute solutions of linear polystyrenes. *J. Chem. Phys.*, 44:4550–4564, 1966.

[39] P. Munk. *Introduction to Macromolecular Science.* Wiley, New York, Chichester, 1989.

[40] R.W. Whorlow. *Rheological Techniques.* Horwood, New York, 1992.

[41] G. Maret. Diffusing wave spectroscopy. *Curr. Op. Colloid Interface Sci.*, 2:251–257, 1997.

[42] B.J. Berne and R. Pecora. *Dynamic Light Scattering.* Wiley, New York, 1976.

[43] J.K.G. Dhont. *An Introduction to the Dynamics of Colloids.* Elsevier, Amsterdam, 1996.

[44] J. Buffle and H.P. van Leeuwen, editors. *Environmental Particles.* Lewis, Boca Raton, 1993.

[45] J.-P. Hansen and I.R. McDonald. *Theory of Simple Liquids.* Academic Press, London, 1976.

[46] N. Dingenouts and M. Ballauff. Small-angle X-ray analysis of latex particles using contrast variation. *Acta Polymerica*, 44:178–183, 1993.

[47] D.J. Fairhurst. Private Communication.

[48] P.N. Pusey and W. van Megen. Detection of small polydispersities by photon correlation spectroscopy. *J. Chem. Phys*, 80:3513–3519, 1984.

[49] D.J. Fairhurst. Unpublished.

[50] Lord Rayleigh. *Phil.Mag.*, 10:73, 1880.

[51] P.N. Segrè, W. van Megen, P.N. Pusey, K. Schätzel, and W. Peters. Two-colour dynamic light scattering. *J. Mod. Opts.*, 42:1929–1952, 1995.

[52] R. Pecora, editor. *Dynamic Light Scattering.* Plenum Press, New York and London, 1985.

[53] A. Moussaïd. Private Communication.

[54] G.K. Batchelor. *An Introduction to Fluid Dynamics.* C.U.P., Cambridge, 1994.

[55] J.C. Brown, P.N. Pusey, and R. Deitz. Photon correlation study of polydisperse samples of polystyrene in cyclohexane. *J. Chem. Phys.*, 62:1136–1144, 1975.

[56] V. Manoharan. Swelling of P.M.M.A. by tetralin. Report for Princeton Materials Institute.

[57] V. Martelozzo. Private Communication.

[58] R.J. Lavery, W. C. K. Poon, and J. Crain. Dynamics of solvent-coated colloids. *In preparation.*

[59] W.C.K. Poon and P.B. Warren. Unpublished.

[60] F. Mandl. *Statistical Physics - second edition.* John Wiley and Sons, Chichester, 1988.

[61] F. H. Ree and W. G. Hoover. Fifth and sixth virial coefficients for hard sphere and disks. *J. Chem. Phys.*, 40:939–950, 1964.

[62] N.F. Carnahan and K.E. Starling. Equation of state for nonattracting rigid spheres. *J. Chem. Phys.*, 51:635–636, 1969.

[63] P.B. Warren, S.M. Ilett, and W.C.K. Poon. Effect of polymer non-ideality in a colloid-polymer mixture. *Phys. Rev. E*, 52:5205–5213, 1995.

[64] H.N.W. Lekkerkerker. Osmotic equilibrium treatment of the phase separation in colloidal dispersions containing non-adsorbing polymer molecules. *Coll. Surf.*, 51:419–426, 1990.

[65] E.J. Meijer and D. Frenkel. Colloids dispersed in polymer solutions - a computer simulation study. *J. Chem. Phys.*, 100:6873–6887, 1994.

[66] J.K.G. Dhont, A.F.H. Duyndam, and B.J. Ackerson. A Smoluchowski approach to the spinodal instability and initial decomposition kinetics in colloidal systems. *Physica A*, 189:503–531, 1992.

[67] P.N. Pusey, H.M. Fijnaut, and A. Vrij. Mode amplitudes in dynamic light scattering by concentrated liquid suspensions of polydisperse hard spheres. *J. Chem. Phys.*, 77:4270–4280, 1982.

[68] L.D. Landau and E.M. Lifshitz. *Statistical Physics (part 1).* Pergamin, Oxford, 1993.

[69] B.U. Felderhof. Diffusion of interacting Brownian particles. *J. Phys. A*, 11:929–937, 1978.

[70] S.M. Ilett, A. Orrock, W.C.K. Poon, and P.N. Pusey. Phase behaviour of a model colloid-polymer mixture. *Phys. Rev. E*, 51:1344–1352, 1995.

[71] R. Klein. Statistical mechanics of colloidal suspensions. Unpublished lecture notes.

[72] R.J.A. Tough, P.N. Pusey, H.N.W. Lekkerkerker, and C. van der Broeck. Stochastic descriptions of the dynamics of interacting Brownian particles. *Mol. Phys.*, 59:595–619, 1986.

[73] C.W.J. Beenakker and P. Mazur. Diffusion of spheres in a concentrated suspension, 2. *Physica A*, 126:349–370, 1984.

[74] P.N. Segrè, S.P. Meeker, P.N. Pusey, and W.C.K. Poon. Viscosity and structural relaxation in suspensions of hard-sphere colloids. *Phys. Rev. Letts.*, 75:958–961, 1995.

[75] L.S. Ornstein and F. Zernike. *Proc. Akad. Sci. (Amsterdam)*, 17:793, 1914.

[76] W. van Megen and S.M. Underwood. Tracer diffusion in concentrated colloidal dispersions. 2: Non-Gaussian effects. *J. Chem. Phys.*, 88:7841–7846, 1988.

[77] P.-G. de Gennes. *Scaling concepts in polymer physics.* Cornell University Press, Ithaca, 1979.

[78] J. Stellbrink. Private Communication.

[79] O.A. Nehme, P. Johnson, and A.M. Donald. Probe diffusion in poly-L-lysine solution. *Macromol.*, 22:4326–4333, 1989.

[80] G.D.J. Phillies, J.J. Gong, L.Y. Li, A. Rau, K. Zhang, L.P. Yu, and J. Rollings. Macroparticle diffusion in dextran solutions. *J. Chem. Phys.*, 93:6219–6223, 1989.

[81] G.D.J. Phillies, C. Malone, K. Ullmann, G.S. Ullmann, J. Rollings, and L.P. Yu. Probe diffusion in solutions of long-chain polyelectrolytes. *Macromol.*, 20:2280–2289, 1987.

[82] W. Brown and R. Rymden. Diffusion of polystyrene latex spheres in polymer solutions studied by dynamic light scattering. *Macromol.*, 19:2942–2952, 1986.

[83] W. Brown and R. Rymden. Comparison of the translational diffusion of large spheres and high molecular-weight coils in polymer solutions. *Macromol.*, 21:840–846, 1988.

[84] T. Yang and A.M. Jamieson. Diffusion of latex spheres through solutions of hydroxypropylcellulose in water. *J. Colloid Interface Sci.*, 126:220–230, 1988.

[85] M. Mustafa and P.S. Russo. Nature and effects of nonexponential correlation-functions in probe diffusion experiments by quasielastic light scattering. *J. Colloid Interface Sci.*, 129:240–253, 1989.

[86] G.S. Ullmann, K. Ullmann, R.M. Lindner, and G.D.J. Phillies. Probe diffusion of polystyrene latex spheres in poly(ethylene oxide)-water. *J. Chem. Phys.*, 89:692–700, 1985.

[87] R.T.C. Ju, W.F. Curtis, and A.P. Gast. CONTIN analysis of colloidal aggregates. *Langmuir*, 8:2165–2171, 1992.

[88] E. Donath, A. Krabi, G. Allan, and B. Vincent. A study of polymer depletion layers by electrophoresis: the influence of viscosity profiles and the non-linearity of the Poisson-Boltzman equation. *Langmuir*, 12:3425–3430, 1996.